Efficient likelihood approximation via Gaussian processes: with an application to an existing *Plasmodium vivax* malaria model

Jacob Cumming

Student ID: 995682

Master of Science (Mathematics and Statistics)

June 2024

Faculty of Science

School of Mathematics and Statistics

Submitted in partial fulfillment for the degree of Master of Science (Mathematics and Statistics)

Acknowledgments

To my primary supervisors Eamon Conway at WEHI and Jennifer Flegg at the University of Melbourne, thanks for all the feedback and encouragement you've provided me over the last year and a half. It has been a blast and I have learnt more than I ever thought I would.

To Ivo Mueller, and the Mueller lab at WEHI, thanks for being willing to take on a Master by coursework student, I know it's a bit out of the ordinary, but you were very willing to make it work, and I appreciated that.

To my beautiful wife Laura, thanks for putting up with my long hours studying on weekends whilst pregnant, and for being completely supportive along the way.

To my unborn child, if you're ever reading this, it's not too late to stop now...

Finally, thanks to God, who I believe gave us mathematics to discover. Soli Deo gloria.

Contents

List of Tables

List of Figures

List of Algorithms

Chapter 1

Introduction

Malaria is an infectious disease that poses a significant global health challenge. In 2022, the World Health Organisation estimated that malaria caused over 600,000 deaths, most of which were in children under five (World Health Organization 2022). The majority of malaria-related deaths are attributable to the *Plasmodium falciparum* species of the parasite. For this reason, it has been the primary focus of most malaria research. However, with declining *P. falciparum* cases, other malaria species, such as *P. vivax*, have gained more attention (Price et al. 2020). The literature is increasingly recognising that the amount of death and severe disease attributable to the *Plasmodium vivax* species has traditionally been underestimated.

Various countries with endemic malaria have undertaken significant efforts to reduce the burden of or eradicate malaria. Mathematical disease models are increasingly aiding these efforts by helping to understand the spread of the disease and estimate the effectiveness of possible interventions. Malaria models are complex due to the many staged lifecycle, as the parasite needs both vertebrate and mosquito hosts. Since malaria is transmitted to humans through mosquitos, the transmission of malaria within a country is highly heterogeneous. Forest workers and those who spend time in areas with high mosquito density are more likely to contract the disease and may bring it back to their local community. *P. vivax* has a dormant liver stage that is absent in *P. falciparum* and can cause relapses, further complicating *P. vivax* models.

To simulate different scenarios using models, modellers must first calibrate the model parameters to approximate observed disease dynamics. Calibration is done by measuring data such as case counts or current prevalence surveys. Standard techniques to calibrate parameters include maximum likelihood estimation and sampling from a posterior distribution, which both require a likelihood function. As models become increasingly complicated, analytic forms for the likelihood may not exist, or calculating the likelihood may be very computationally burdensome. Some researchers calibrate compartmental models by relying on their deterministic counterparts, which is questionable, as the deterministic model sometimes behaves differently from the stochastic model.

Modern likelihood-free techniques, such as approximate Bayesian computation, have been designed to facilitate a principled parameter calibration method. Various forms of approximate Bayesian computation have been widely adopted. However, all forms require large numbers of model runs, which may be unfeasible or undesirable.

Non-parametric regression techniques such as Gaussian process regression have been developed for a long time and used in statistical modelling for decades (see Diggle, Liang, and Zeger 1994), However, their uses in disease modelling have yet to be fully explored. Gaussian processes place a

prior distribution over a function space. Observations from the true function can create a posterior distribution over the same function space, inherently accounting for uncertainty for unobserved values.

Drawing on concepts from approximate Bayesian computation, we aim to improve parameter calibration in malaria models, addressing a recognised need for improvement. We do this by training a Gaussian process to predict how close a model run will be to observed data. The Gaussian process approximation can then be used to extract a synthetic likelihood which approximates the true unknown likelihood. This allows for the use of frequentist and Bayesian parameter inference.

The thesis follows the following outline: The literature review in Part I discusses fundamental concepts of epidemiological modelling, covering deterministic ordinary differential equation models, stochastic models, and their simulation methods. It then examines and reviews various malaria models to assess how *P. vivax* is modelled in the current literature. Part I further surveys parameter inference techniques for disease and other models, comparing frequentist and Bayesian approaches, and ends with discussing likelihood-free techniques, particularly approximate Bayesian computation. Approximate Bayesian computation then motivates the use of Gaussian processes regression, which enables the development of a synthetic likelihood. The synthetic likelihood can be used instead of the unknown true likelihood to use the traditional parameter calibration techniques in complex models. Finally, Part I discusses using Bayesian acquisition functions to efficiently train the Gaussian process regression.

Part II applies and extends this methodology by calibrating parameters specific to a *P. vivax* model using synthetic observed data. The results and discussion section validates the method and demonstrates that the parameters that produced the observed data are recoverable. Finally, the thesis concludes with a discussion of the findings and outlines avenues for future research.

Part I

Literature Review

Chapter 2

Epidemiological Modelling

Researchers have developed compartmental epidemiological models to study the behaviour and characteristics of disease spread and eradication. Compartmental models simplify the dynamics of a disease down to a mathematically representable form. By determining the parameters within a model, it is possible to facilitate an understanding of how the modelled disease spreads and assess the effectiveness of differing disease interventions (such as treatments or vaccinations) without large long-term trials. Models can also simulate various scenarios, such as increases or decreases in viral transmission.

Simple compartmental disease models assume individuals can only be in one of a finite number of states (which are called compartments). These compartments usually correspond to a state of disease. A standard compartmental model may include:

- S - Susceptible: at risk of contracting the disease
- E - Exposed: contracted the disease but not infecting other individuals
- I - Infectious (also called Infected): at risk of infecting others with the disease
- R - Recovered: no longer infectious and incapable of being reinfected.

The number of people in each compartment at time t is a (possibly non-deterministic) function of time t, which we indicate as a subscript t (e.g., S_t is the number of susceptibles at time t). Models are typically described by the compartments they contain. The SIS model depicted in Figure 2.1a consists of a susceptible compartment S and an infectious compartment I. In this model, individuals who recover from infection are immediately susceptible to reinfection, as is the case with most sexually transmitted diseases (Keeling and Rohani 2008, p. 56). Movement between the two compartments is determined by the force of infection λ_t and rate of recovery γ.

The SI with demography model depicted in Figure 2.1b is used to model diseases that infect the individual until death, such as bovine spongiform encephalopathy (BSE), commonly known as mad cow disease (Hagenaars, Donnelly, and Ferguson 2006). In addition to the rates in the SIS model, μ and ν are birth and death rates, respectively. γ becomes the rate of disease-induced mortality.

The $SEIR$ model in Figure 2.1c includes the exposed compartment E and recovered compartment R. The additional parameter σ is the rate at which exposed individuals become infectious. Childhood diseases such as varicella (chickenpox), which give lifetime immunity after infection, can

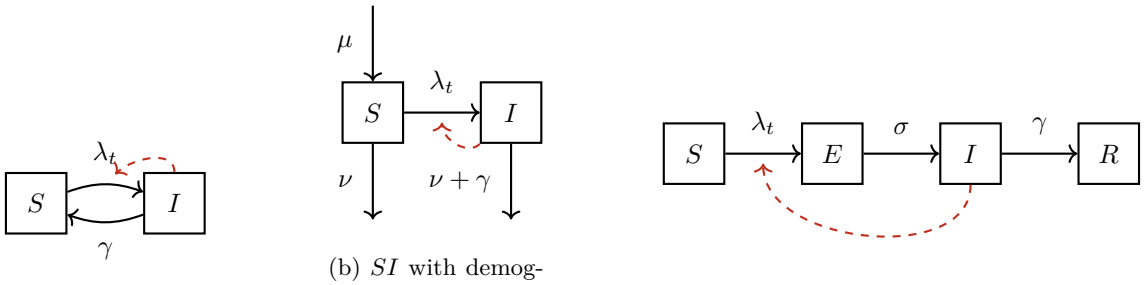

(a) SIS model

(b) SI with demography model

(c) $SEIR$ model

Figure 2.1: Some simple model schematics with varying numbers of compartments: S (susceptible), E (exposed), I (infectious) and R (recovered). The force of infection λ_t is usually a function of I_t, depicted by the dashed red lines. μ and ν are natural birth and death rates, respectively. γ is the rate of progression out of the infectious state. In each of these models, the physical interpretation differs slightly. In the SIS and $SEIR$ models, it is the rate at which individuals move from infectious to susceptible again or into lifelong immunity, whereas, in the SI with demography model, it can be interpreted as the increase in the death rate attributable to disease-induced mortality. σ is the rate of progression from a state of latent infection to becoming infectious.

be modelled using an $SEIR$ model (see Figure), mainly when modelling a local outbreak setting. For example, an $SEIR$ model was used in Zha et al. 2020 for a school outbreak of varicella.

Omitting demography is usually appropriate when disease-induced mortality is low, or the timescale of interest is short compared to the population's lifespan. The number of compartments in a model can be increased to incorporate states such as vaccinated or quarantined that change the disease dynamics. For example, the COVID-19 model described in Acuña-Zegarra et al. 2021 includes a vaccinated compartment and two infectious compartments for symptomatic and asymptomatic individuals. By convention, N_t (often simply N in models with a closed population) is the total number of individuals in the model - the sum of all compartments.

2.1 Deterministic Ordinary Differential Equation Models

Infectious diseases are often simulated as deterministic ordinary differential equations (ODEs). Let the force of infection λ_t be proportional to the number of people in I, such that $\lambda_t := \beta\frac{I_t}{N_t}$. β can be interpreted as the average number of people that an individual interacts with per day in a way such that disease would be spread in that interaction per unit of time t. Since $\frac{I_t}{N_t}$ is the probability that a randomly selected individual is infectious, $\beta\frac{I_t}{N_t}$ can be interpreted as the average number of people that a person interacts with each day who are infectious multiplied by the probability that an infection occurs during that contact. In different diseases, β varies dramatically. β is low for diseases that need prolonged exposure or sexual contact to transmit, whereas β is very high for highly transmittable diseases, such as measles. Implicitly, there is an assumption of complete, uniformly random mixing of people. Uniform mixing is often a poor assumption since, in reality, people see people regularly with varying probabilities and do not mix randomly with the people in a population. Therefore, the infection status of a group of friends or a household is likely to be highly correlated. One solution is to include contact networks in the model (such as Kerr et al. 2021). However, we do not consider these models in this thesis. For this thesis, we assume that β is frequency-dependent instead of density-dependent; that is, a person interacts with the same number of individuals regardless of population size. A density-dependent contact rate assumes

that the number of individuals a person interacts with grows proportionally to population size. In the density-dependent case, the force of infection has the form $\lambda_t := \beta I_t$.

The ODEs that govern the SIS model are

$$\frac{\mathrm{d}S_t}{\mathrm{d}t} = -\lambda S_t + \gamma I_t = -\beta \frac{I_t}{N} S_t + \gamma I_t \tag{2.1}$$

$$\frac{\mathrm{d}I_t}{\mathrm{d}t} = \lambda S_t - \gamma I_t = \beta \frac{I_t}{N} S_t - \gamma I_t. \tag{2.2}$$

Given initial conditions S_0 and I_0, Equation 2.1 (or 2.2) fully describes the model.

The system of ODEs that describe the SI with demography model is

$$\frac{\mathrm{d}S_t}{\mathrm{d}t} = \mu N_t - \lambda_t S_t - \nu I_t = \mu N_t - \beta \frac{I_t}{N_t} S_t - \nu I_t \tag{2.3}$$

$$\frac{\mathrm{d}I_t}{\mathrm{d}t} = \lambda_t S_t - (\gamma + \nu) I_t = \beta \frac{I_t}{N_t} S_t - (\gamma + \nu) I_t. \tag{2.4}$$

Unlike the SIS and $SEIR$ models, N_t is not constant in this model.

Finally, the system of ODEs that describe the $SEIR$ model is

$$\frac{\mathrm{d}S_t}{\mathrm{d}t} = -\lambda_t S_t - \nu I_t = -\beta \frac{I_t}{N} S_t + \gamma I_t \tag{2.5}$$

$$\frac{\mathrm{d}E_t}{\mathrm{d}t} = \lambda_t S_t - \omega E_t = \beta \frac{I_t}{N} S_t - \omega I_t \tag{2.6}$$

$$\frac{\mathrm{d}I_t}{\mathrm{d}t} = \omega E_t - \gamma I_t \tag{2.7}$$

$$\frac{\mathrm{d}R_t}{\mathrm{d}t} = \gamma I_t. \tag{2.8}$$

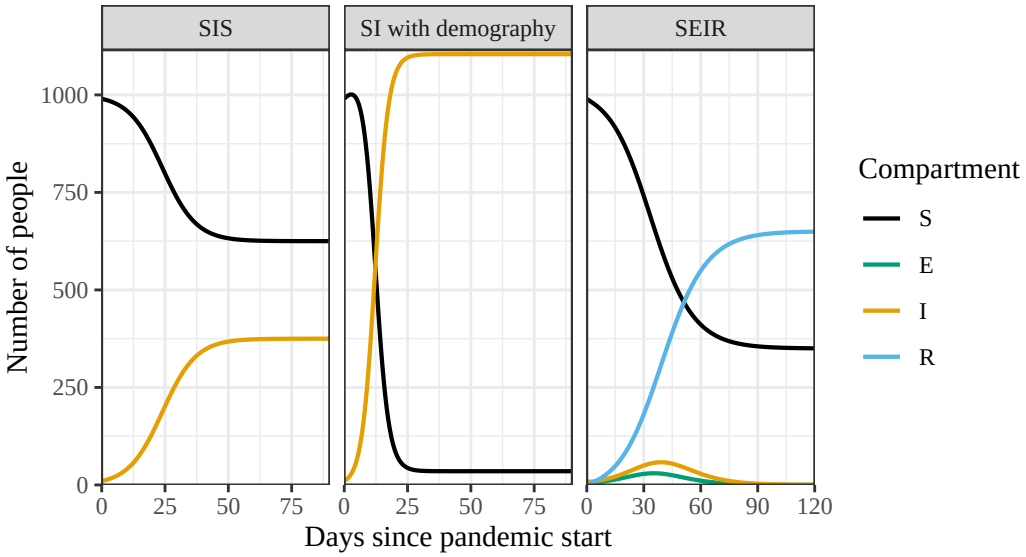

Figure 2.2: Solutions to the ODEs describing the models depicted in Figure 2.1. The initial infectious population was $I_0 = 10$, with $S_0 = 990$. In the $SEIR$ model, $E_0 = R_0 = 0$. For all models, $\beta = 0.4$. For the SIS and SI model with demography, $\gamma = 1/4$. For the SI model with demography, $\mu = 0.012$ and $\nu = 0.0012$. For the $SEIR$ model, $\gamma = 1/90$ and $\sigma = 1/2$.

After specifying the initial conditions S_0, I_0, and so forth, the ODEs can be numerically solved. Figure 2.2 shows solutions to the three models introduced so far for an initial population $N_0 = 1000$, with an initial infectious population $I_0 = 10$. Under the models without demography, N_t remains constant. The disease is eradicated for the $SEIR$ model after a small case spike. The disease reaches a steady state equilibrium for the SIS and SI with demography model, with a much higher number of infected individuals in the SI with demography model, since once an individual acquires the disease, they have it until they die.

2.2 Stochastic Models

Motivating the Form of the Stochastic Model

Deterministic ODE models can be appropriate to study infectious diseases when the disease is near equilibrium and the numbers in each compartment are large. At the start of an epidemic, when the number of infected individuals is small, the behaviour of the epidemic may vary significantly. When case numbers are small, there is a non-zero probability that the disease may die out, but under the right conditions, such as a large gathering of people in a small space, the outbreak may become a pandemic. In these cases, a deterministic model is inadequate in emulating real-world behaviour. For this reason, we consider stochastic models of disease. A natural stochastic analogue for a deterministic model can be constructed considering Poisson point processes and their properties.

Definition 2.1 (Poisson Point Process)**.** $\{\mathcal{N}(t)\}_{t\geq 0}$ *is a* **(stationary) Poisson point process** *with intensity* κ *if*

1. $\mathcal{N}(0) = 0$
2. $\mathcal{N}(t_1) - \mathcal{N}(t_0), \mathcal{N}(t_2) - \mathcal{N}(t_1), \ldots, \mathcal{N}(t_n) - \mathcal{N}(t_{n-1})$ *are independent for* $0 \leq t_0 < t_1 < \cdots < t_{n-1} < t_n$
3. $\mathcal{N}(t_2) - \mathcal{N}(t_1) \sim \text{Pois}(\kappa(t_2 - t_1)), 0 \leq t_1 < t_2$.

To demonstrate how Poisson point processes aid us in creating a natural analogue of the deterministic model, we construct two Poisson processes that, when combined, have the the same instantaneous average behaviour as the deterministic ODE model.

Consider the deterministic SIS model described by Equations 2.1 and 2.2 at time t^*. The instantaneous rate at which S_t is decreasing is $\beta \frac{I_{t^*}}{N} S_{t^*}$. In other words, at time t^*, an individual leaves the susceptible compartment every $\beta \frac{I_{t^*}}{N} S_{t^*}$ units of time.

Now consider a Poisson point process $\{\mathcal{N}_1(t - t^*)\}_{t\geq t^*}$ with intensity $\beta \frac{I_{t^*}}{N} S_{t^*}$ corresponding to the count of the number of individuals who have left S and entered I t units of time since t^*. The average rate at which an individual leaves S is then

$$\begin{aligned}
\frac{\mathrm{d}\mathbb{E}(\mathcal{N}_1(t^*))}{\mathrm{d}t^*} &= \lim_{\delta \to 0} \frac{\mathbb{E}\left(\mathcal{N}(t^* + \delta) - \mathcal{N}(t^*)\right)}{\delta} \\
&\qquad \text{(Since the mean of a Poisson random variable is its intensity)} \\
&= \frac{\beta \frac{I_{t^*}}{N} S_{t^*} (t^* + \delta - t^*) \beta \frac{I_{t^*}}{N} S_{t^*}}{\delta} \\
&= \beta \frac{I_{t^*}}{N} S_{t^*},
\end{aligned}$$

the same rate as the ODE model.

Under the same deterministic ODE formulation of the SIS model, the instantaneous rate into S at time t^* is γI_{t^*}. Also, as above, we construct a Poisson point process $\{\mathcal{N}_2(t-t^*)\}_{t\geq t^*}$ with mean rate γI_{t^*} describing the number of recoveries from I to S since

$$\frac{\mathrm{d}\mathbb{E}(\mathcal{N}_2(t^*))}{\mathrm{d}t^*} = \gamma I_{t^*}.$$

Combining the two processes, we can see that the rate of change in the average number of people in S is

$$\frac{\mathrm{d}\mathbb{E}(\mathcal{N}_2(t^*) - \mathcal{N}_1(t^*))}{\mathrm{d}t^*} = \frac{\mathrm{d}\mathbb{E}(\mathcal{N}_2(t^*)) - \mathrm{d}\mathbb{E}(\mathcal{N}_1(t^*))}{\mathrm{d}t^*} = -\beta\frac{I_t}{N}S_t + \gamma I = \frac{\mathrm{d}S_t}{\mathrm{d}t}.$$

We can model each transition as a Poisson point process for an arbitrary number of compartments and transitions

Therefore, we construct a stochastic analogue for the ODEs in the following way. Let the stochastic model be a random vector $\{\mathbf{C}_t\}_{t\geq 0} = \{C_1(t), C_2(t), \ldots, C_n(t)\}_{t\geq 0}$ where $C_i : \mathbb{R} \to \mathbb{N}\cup\{0\}$, is the number of people in compartment C_i, and for any fixed t, $\{C_1(t), C_2(t), \ldots, C_n(t)\}$ is a random variable describing the state of the model. For example, the SI with demography model can be represented as $\{\mathbf{C}_t\}_{t\geq 0} := \{S_t, I_t\}_{t\geq 0}$.

If the model is in state $\{S_t, I_t\}$, after the next transition at time t^*, the next possible states are:

1. $\{S_{t^*}, I_{t^*}\} = \{S_t + 1, I_t\}$
2. $\{S_{t^*}, I_{t^*}\} = \{S_t - 1, I_t\}$
3. $\{S_{t^*}, I_{t^*}\} = \{S_t - 1, I_t + 1\}$
4. $\{S_{t^*}, I_{t^*}\} = \{S_t, I_t - 1\}$.

Each of these transitions behaves like Poisson processes at time t. We think of these processes in the following way:

- $\{\mathcal{E}_1(t^*)\}_{t^*\geq 0}$: the number of births into S after time t with intensity μN_t
- $\{\mathcal{E}_2(t^*)\}_{t^*\geq 0}$: the number of deaths in S after time t with intensity νS_t
- $\{\mathcal{E}_3(t^*)\}_{t^*\geq 0}$: the number of infections after time t with intensity $\beta\frac{I_t}{N_t}S_t$
- $\{\mathcal{E}_4(t^*)\}_{t^*\geq 0}$: the number of deaths from I after time t with intensity $(\nu+\gamma)I_t$.

Since the sum of two Poisson point processes is a Poisson point process (see Theorem A.1), the time between events in a Poisson process is exponentially distributed (see Theorem A.2) then

$$\{\mathcal{E}(t)\}_{t\geq 0} := \{\mathcal{E}_1(t) + \mathcal{E}_2(t) + \mathcal{E}_3(t) + \mathcal{E}_4(t)\}_{t\geq 0}$$

is a Poisson point process with intensity

$$\mu N_{t^*} + \nu S_{t^*} + \beta\frac{I_{t^*}}{N_{t^*}}S_{t^*} + (\nu+\gamma)I_{t^*}.$$

The time until the next transition is exponentially distributed

$$\text{Exp}(\mu N_{t^*} + \nu S_{t^*} + \beta \frac{I_{t^*}}{N_{t^*}} S_{t^*} + (\nu + \gamma) I_{t^*}).$$

Therefore, simulating the time to the next transition, given the current number of individuals in each compartment, simply involves simulating from an exponential distribution. Theorem A.3 states that given that a transition occurred, the probability it was due to the process $\mathcal{E}_i$ is proportional to its intensity. As soon as the transition occurs, all the intensities for each Poisson process will be updated since the intensities depend on the number of individuals in each compartment.

Doob-Gillespie Algorithm

Algorithm 1 The Doob-Gillespie Algorithm (Gillespie 1977)

Initialise time $t \leftarrow 0$ and initial state of the model $\mathbf{C}(0) := \{C_1(0), C_2(0), \ldots, C_n(0)\}$
while termination condition not met **do**
  Calculate intensities κ_i for all possible events $\mathcal{E}_i$
  Calculate total intensity $\kappa = \sum_i \kappa_i$
  Generate $\Delta t \sim \text{Exp}(\kappa)$
  Choose event E_i with probability $\frac{\kappa_i}{\kappa}$
  Update time $t \leftarrow t + \Delta t$
  Update state of $\mathbf{C}(t + \delta t) \leftarrow \mathbf{C}(t) +$ change in state due to event $\mathcal{E}_i$
end while

This leads naturally to a standard method of simulating the stochastic model through Algorithm 1. The Doob-Gillespie algorithm exploits the local behaviour of the compartments as described, sampling an exponential random variable, choosing an event with probabilities proportional to their intensities, updating the model, and updating the intensities given a set of starting conditions (Gillespie 1977).

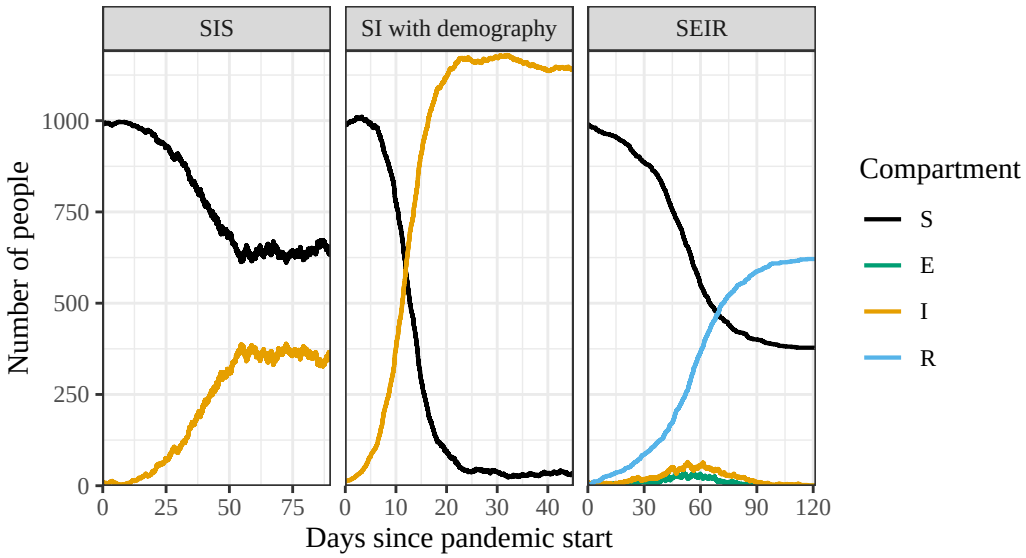

Figure 2.3: Exact stochastic simulations of the three different models using Algorithm 1. The parameters used were identical to those in Figure 2.2

Figure 2.3 demonstrates Doob-Gillespie simulations for the models discussed in this chapter. Compared to the deterministic ODE simulations in Figure 2.2, the stochastic simulations still show variation even near the equilibria.

τ-Leaping

Because the Doob-Gillespie algorithm is an exact simulation method, when the intensities become large, or many people are infected, the time step τ can become increasingly small, resulting in long simulations times.

τ-leaping - Algorithm 2 - further exploits the local Poisson point process-like behaviour of epidemiological models (Gillespie 2001). Consider the SIS model when $S_t = I_t = 10000$. Events happen at a very high rate, meaning the Δt found in each step of the Doob-Gillespie algorithm will be very small, but the rates also change a negligible amount after each event (compare $\gamma \times 10000$ to $\gamma \times 10001$ or $\gamma \times 9999$). Therefore, we can approximate the number of events in a short time period τ as a Poisson point process with the total intensity $\kappa = \sum_i \kappa_i$ at time t, with the probability of any one event having the same probability as above of $\frac{\kappa_i}{\kappa}$. Therefore, we have the following algorithm.

Algorithm 2 τ-Leaping Algorithm Gillespie 2001

Initialise time $t \leftarrow 0$ and initial state of the model $\mathbf{C}(0) := \{C_1(0), C_2(0), \ldots, C_n(0)\}$
while termination condition not met **do**
  Calculate intensities κ_i for all possible events $\mathcal{E}_i$
  Calculate total intensity $\kappa = \sum_i \kappa_i$
  Choose a suitable time step τ (this can be deterministic or adaptive)
  Calculate Poisson random variable $X \sim \text{Poisson}(\kappa\tau)$
  for i in 1 to X **do**
    Choose event E_i with probability $\frac{\kappa_i}{\kappa}$
    Update state of $\mathbf{C}(t+\tau) \leftarrow \mathbf{C}(t) +$ change in state due to event $\mathcal{E}_i$
  end for
  Update time $t \leftarrow t + \tau$
end while

Chapter 3

Malaria and Malaria Models

Malaria as an infectious disease has been the focus of mathematical modelling efforts for over a century (Smith et al. 2012). Despite ongoing eradication efforts, in 2022, malaria killed over 600,000 people, with over 75% of deaths occurring in children under five years old (World Health Organization 2022). Six species of the parasite are able to infect humans (Milner 2018). Although *Plasmodium falciparum* is responsible for around 90% of total human malaria deaths outside of Africa, *Plasmodium vivax* is the leading cause of malaria infection (Zekar and Sharman 2023; Adams and Mueller 2017). Death and severe disease attributable to *P. vivax* have likely been traditionally underestimated. Given recent evidence, the notion that *P. vivax* is benign is unsustainable (Cowman et al. 2016).

The most common symptom of malaria infection in persons without natural or acquired immunity is fever. After treatment, fever usually subsides over a few days. In severe cases, malaria can lead to anemia, cerebral malaria (coma), and respiratory distress (Cowman et al. 2016). However, in a population with stable malarial infection, immunity increases with age, with the proportion of severe cases negligible after age 10, and asymptomatic infection being the dominant infection type beyond age 15 (Cowman et al. 2016).

Lifecycle

Part of the ongoing interest in modelling malaria is its complicated lifecycle. Malaria is a vector borne disease, needing both human (or other vertebrate) and mosquito hosts to complete it's lifecycle. Malaria first enters the human bloodstream via the skin after the female mosquito has a blood meal. From the bloodstream, it proceeds to the liver where it proliferates and is released into the blood, entering the red blood cells and reproducing further. Eventually, the parasites undergo sexual differentiation, maturing in the bone marrow until they are released into the bloodstream to be consumed by a mosquito during a blood feed, where they mature into sporozoites ready to reinfect a new vertebrate host (Cowman et al. 2016).

Figure 3.1 depicts the lifecycle of *P. vivax* malaria, which has an additional lifecycle stage to *P. falciparum*. *P. vivax* malaria can form hypnozoites, a dormant parasite liver-stage. These can remain dormant for weeks and even months, leading to recurrent infections and illness, possibly until the conditions for transmission are more favourable. In subtropical/temperate areas, the incubation periods can be between 8-12 months, compared to 3-4 weeks in tropical regions. Price et al. 2020. *P. vivax* also has lower levels of the blood-stage parasite during infection, which means

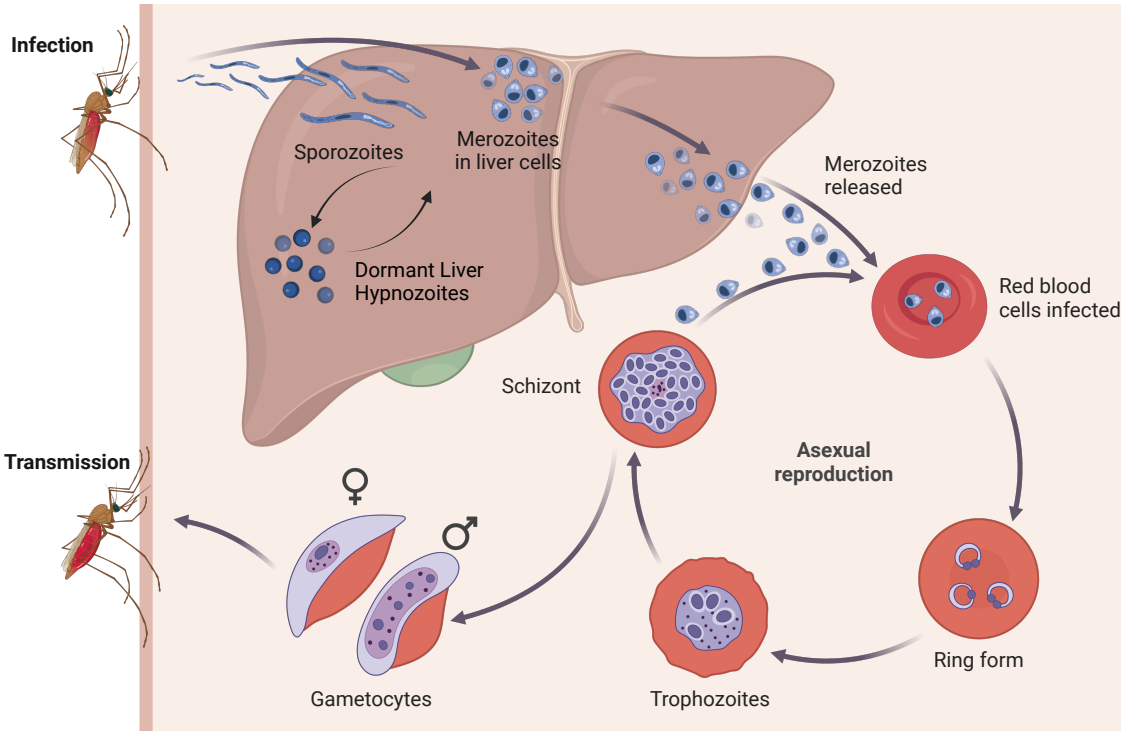

Figure 3.1: The *Plasmodium vivax* (malaria) lifecycle. *P. falciparum* does not have a dormant liver hypnozoite stage. Created with BioRender.com

diagnosis is more difficult and has an increased proportion of asymptomatic cases (Adams and Mueller 2017).

3.1 Mathematical Modelling of Malaria

Levels of asymptomatic cases and dormant parasites (in the case of *P. vivax*) are impossible or difficult to experimentally determine without mass testing. By creating a model of the disease and calibrating the model so that it simulates symptomatic case levels reported by health authorities, it is possible to estimate these previously 'hidden' levels. Furthermore, malaria models allow us to simulate the effects of public health interventions such as mass treatment or testing. Malaria models also allow us to estimate how economical interventions will likely be before large amounts of money are spent on trials.

Ross-Macdonald Models

The most basic model capturing the fundamental lifecycle of malaria is commonly referred to as the Ross-Macdonald model. One example of such a model was used in Aron and May 1982 and is depicted in Figure 3.2. It accounts for human-to-mosquito and mosquito-to-human transmission by having compartments for susceptible and infected humans (S_{H} and I_{H}), as well as susceptible

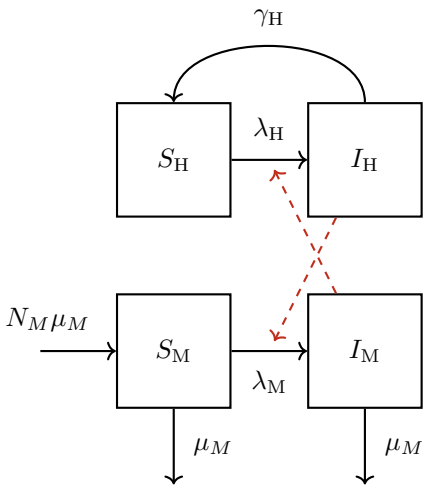

Figure 3.2: A simple Ross-Macdonald malaria model schematic, described in Aron and May 1982. S_{H} and I_{H} are the number of susceptible and infected humans, respectively, and S_{M} and I_{M} are the number of susceptible and infected mosquitos. The rate of human infection (λ_{H}) is dependent on I_{M}, and the rate of human infection (λ_{M}) is dependent on I_{H}.

and infected mosquitos (S_{M} and I_{M}). The ODEs for this model are

$$\begin{aligned}
\frac{\mathrm{d}S_{\mathrm{H}}}{\mathrm{d}t} &= \gamma_{\mathrm{H}} I_{\mathrm{H}} - bT_{\mathrm{HM}} I_{\mathrm{M}} \frac{S_{\mathrm{H}}}{N_{\mathrm{H}}} \\
\frac{\mathrm{d}I_{\mathrm{H}}}{\mathrm{d}t} &= bT_{\mathrm{HM}} I_{\mathrm{M}} \frac{S_{\mathrm{H}}}{N_{\mathrm{H}}} - \gamma I_{\mathrm{H}} \\
\frac{\mathrm{d}S_{\mathrm{M}}}{\mathrm{d}t} &= N_{\mathrm{M}}\mu_M + \gamma_{\mathrm{M}} I_{\mathrm{M}} - bT_{\mathrm{MH}} S_{\mathrm{M}} \frac{I_{\mathrm{H}}}{N_{\mathrm{H}}} - S_{\mathrm{M}}\mu_M \\
\frac{\mathrm{d}I_{\mathrm{M}}}{\mathrm{d}t} &= bT_{\mathrm{MH}} S_{\mathrm{M}} \frac{I_{\mathrm{H}}}{N_{\mathrm{H}}} - \gamma_{\mathrm{M}} I_{\mathrm{M}},
\end{aligned}$$

where b is the biting rate per mosquito, and T_{HM} is the probability of transmission to a human given a bite by an infectious mosquito, with T_{MH} being vice-versa. Note that it is $\frac{I_{\mathrm{H}}}{N_{\mathrm{H}}}$ in the mosquito dynamics. Biologically this is assuming the number of blood meals a mosquito takes per day is invariant to the size of the human population. Mosquitos do not have a possibility of leaving the infected stage apart from death due to their short lifespans. However, the births and deaths are mathematically equivalent to assuming that the rate of 'recovery' amongst mosquitos is $\mu_{\mathrm{M}} I_{\mathrm{M}}$ per unit time, with no population dynamics.

The broader class of Ross-Macdonald style models simplify the lifecycle of malaria to the following four steps (Smith et al. 2012):

1. Malaria is transmitted to humans (or other vertebrates) via a blood feed.

2. Malaria proliferates in the human host until it circulates in the peripheral blood

3. A mosquito then takes a blood feed, ingesting the pathogen

4. Malaria develops within the mosquito host, progressing to its salivary glands, and can infect a human.

Models of *P. vivax* Malaria

The basic Ross-Macdonald model does not sufficiently capture the dynamics of *P. vivax*, since it does not consider relapses. Therefore *P. vivax* specific models have been proposed which introduce compartments for dormant liver-stage infection.

White Model

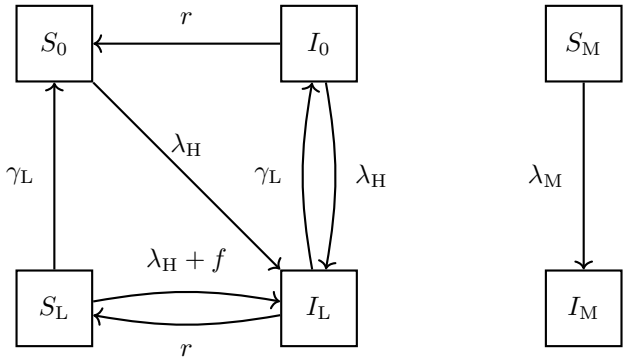

Figure 3.3: Diagram for *P. vivax* model in a tropical setting described by White et al. 2016. S and I are the number of susceptible and infected humans and mosquitos (denoted by subscript M). $\lambda_H = mabI_M$ and $\lambda_M = ac(I_0 + I_L)$

One model incorporating a dormant stage is the White model for *P. vivax* depicted in Figure 3.3 (White et al. 2016, Tropical Model). The model is comprised of six compartments:

1. S_0 **(Susceptible Individuals - No Latent Hypnozoite Liver-Stage Infection)** : People in this compartment have no form of malarial infection. They are susceptible to new malarial infections and are infected into compartment I_L (with both blood and liver-stage parasites) at rate λ_H.

2. I_L **(Infected Individuals - Both Blood-Stage and Latent Hypnozoite Liver-Stage Infection)** : Individuals in this compartment have both an active blood-stage infection, and a latent hypnozoite infection in the liver. Individuals in I_L can progress to either I_0 through the clearance of liver-stage infection with rate γ_L, or to S_L through clearance of blood-stage infection with rate r.

3. I_0 **(Infected Individuals - Blood-Stage Infection Only)** : Individuals in I_0 have a blood-stage infection with no latent hypnozoite infection in the liver. They are be reinfected into I_L with rate λ_H and relapse with rate f. The blood-stage infection is cleared (moving into compartment S_0) with rate r.

4. S_L **(Susceptible Individuals - Blood-Stage Infection Only)** : Individuals in S_L have latent hypnozoite infection in the liver without blood-stage infection. They get novel infection through a mosquito bite into I_L with rate λ_H or hypnozoite activation with rate f. This means those in S_L move to compartment I_L with a total rate $\lambda_H + f$. Alternatively, the hypnozoites are cleared from the liver (moving to compartment S_0) with rate γ_L.

5. S_M **(Susceptible Mosquitoes)** : Suspectable mosquitoes become infectious at rate $\lambda_M p$. They die at rate $g + \lambda_M(1 - p)$. Since there is a constant mosquito population assumption, mosquitoes are born into this state at rate $g + \lambda_M$.

6. I_{M} **(Infectious Mosquitoes)**: Infectious mosquitos die at rate $g + \lambda_{\mathrm{M}}(1-p)$.

The White model is characterised by the following ODEs:

$$\begin{aligned}
\frac{\mathrm{d}S_0}{\mathrm{d}t} &= -\lambda_{\mathrm{H}} S_0 + rI_0 + \gamma_{\mathrm{L}} S_{\mathrm{L}} \\
\frac{\mathrm{d}I_0}{\mathrm{d}t} &= -\lambda_{\mathrm{H}} I_0 - rI_0 + \gamma_{\mathrm{L}} I_{\mathrm{L}} \\
\frac{\mathrm{d}S_{\mathrm{L}}}{\mathrm{d}t} &= -\lambda_{\mathrm{H}} S_{\mathrm{L}} + rI_{\mathrm{L}} - fS_{\mathrm{L}} - \gamma_{\mathrm{L}} S_{\mathrm{L}} \\
\frac{\mathrm{d}I_{\mathrm{L}}}{\mathrm{d}t} &= \lambda_{\mathrm{H}}(S_0 + I_0 + S_{\mathrm{L}}) - rI_{\mathrm{L}} + fS_{\mathrm{L}} - \gamma_{\mathrm{L}} I_{\mathrm{L}} \\
\frac{\mathrm{d}S_{\mathrm{M}}}{\mathrm{d}t} &= g - \lambda_{\mathrm{M}}(pS_{\mathrm{M}} - (1-p)I_{\mathrm{M}}) - gS_{\mathrm{M}} \\
\frac{\mathrm{d}I_{\mathrm{M}}}{\mathrm{d}t} &= \lambda_{\mathrm{M}}(pS_{\mathrm{M}} - (1-p)I_{\mathrm{M}}) - gI_{\mathrm{M}}. \qquad (I_0 + I_{\mathrm{L}} = \text{total number of blood-stage infections})
\end{aligned}$$

In this model, each compartment is expressed as a proportion of the population.

The force of infection for humans is defined as $\lambda_{\mathrm{H}} := mabI_{\mathrm{M}}$ where m is the number of mosquitos per human (held constant since there is no birth or death in the human dynamics), a is the mosquito biting rate, and b is the probability that a human bitten by an infectious mosquito develops an infection.

The force of infection for mosquitos is defined as $\lambda_{\mathrm{M}} := ac(I_0 + I_{\mathrm{L}})$ where a is defined above, and c is the probability that a mosquito bite on an infectious mosquito causes the mosquito to become infectious. g can be interpreted as the natural birth/death rate for mosquitos. p is the proportion of mosquitos that survive long enough after the initial infection, so the parasite matures enough in the mosquito that it can again be transmitted to humans. Under the assumption that the time until parasite transmissibility after infection in a mosquito is a constant of n days and that mosquitoes naturally die at rate g, then $p = e^{-gn}$. To see this, let $V \sim \mathrm{Exp}(g)$ represent the mosquito's lifespan. $\Pr(V > n) = 1 - F_V(n) = 1 - (1 - e^{-gn}) = e^{-gn}$.

$\lambda_{\mathrm{M}}(1-p)$ can be interpreted as an additional rate of death, where of the mosquitos that would develop malaria after a bite, a proportion $1-p$ die instantly. This applies to both the susceptible and infectious mosquitoes. Presumably, this approximates a model where mosquitoes are moved to an 'exposed' compartment for n time, after initial infection. However, no justification is given by White et al. for this additional parameter n. A more straightforward SI model could be constructed that absorbs c and n into the single parameter c^*, such that it becomes the proportion of mosquito bites on blood-stage infectious humans that result in mosquito infection where the mosquito does not die before becoming infectious. With a steady mosquito population, the mosquito dynamics would now be characterised by

$$\frac{\mathrm{d}I_{\mathrm{M}}}{\mathrm{d}t} = \lambda^*_{\mathrm{M}} S_{\mathrm{M}} - gI_{\mathrm{M}} \quad \text{where } \lambda^*_{\mathrm{M}} := ac^*(I_0 + I_{\mathrm{L}}).$$

By modelling both liver-stage and blood-stage infection, blood-stage infections from relapses can be captured in the dynamics, meaning it is possible to analyse case number data that may be confounded by relapses as well as novel infections.

This model does not account for continual depletion of liver-stage parasites, which would vary the rate of relapse over time (through clearance or relapse). It also does not directly model any

interventions or case importations. The lack of population dynamics means the model may only be useful on a small time scale. Finally, it does not account for any importation of disease from an outside area, so if $S_0 = 1$, *P. vivax* is presumed permanently eradicated.

Champagne Model

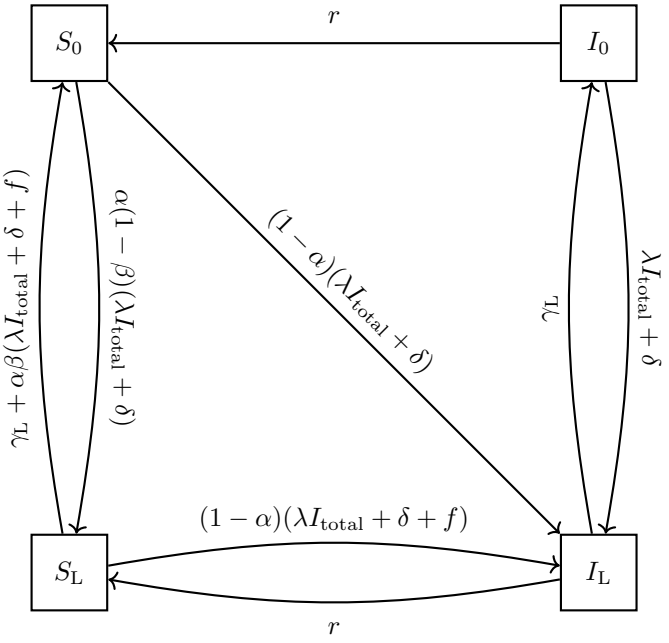

Figure 3.4: Diagram for *P. vivax* model described by Champagne et al. 2022. $I_{\text{total}} = I_0 + I_{\text{L}}$. Since the mosquito dynamics have been removed, λ now has no dependencies on the number of infectious mosquitos.

The Champagne model - described in (Champagne et al. 2022) and diagrammatically depicted in Figure 3.4 - simultaneously simplifies and extends the White model. The model assumes human-to-human transmission, removing mosquito dynamics, and extends it by adding in a rate of imported cases and treatment of malarial infection. It is characterised by the system of ODEs:

$$\begin{aligned}
\frac{\mathrm{d}I_{\text{L}}}{\mathrm{d}t} =& (1-\alpha)(\lambda I_{\text{total}} + \delta)(S_0 + S_{\text{L}}) + (\lambda I_{\text{total}} + \delta)I_0 + (1-\alpha)fS_{\text{L}} - \gamma_{\text{L}} I_{\text{L}} - rI_{\text{L}} \\
\frac{\mathrm{d}I_0}{\mathrm{d}t} =& -(\lambda I_{\text{total}} + \delta)I_0 + \gamma_{\text{L}} I_{\text{L}} - rI_0 \\
\frac{\mathrm{d}S_{\text{L}}}{\mathrm{d}t} =& -(1-\alpha(1-\beta))(\lambda I_{\text{total}} + \delta + f)S_{\text{L}} + \alpha(1-\beta)(\lambda I_{\text{total}} + \delta)S_0 - \gamma_{\text{L}} S_{\text{L}} + rI_{\text{L}} \\
\frac{\mathrm{d}S_0}{\mathrm{d}t} =& -(1-\alpha\beta)(\lambda I_{\text{total}} + \delta)S_0 + (\lambda I_{\text{total}} + \delta)\alpha\beta S_{\text{L}} + \alpha\beta f S_{\text{L}} + \gamma_{\text{L}} S_{\text{L}} + rI_0,
\end{aligned}$$

where $I_{\text{total}} := I_0 + I_{\text{L}}$.

The compartments S_0, I_0, I_{L} and S_{L} have the same interpretation as in the White model, however the rates between compartments are significantly modified.

The new parameters are

- λ : the rate of infection
- δ : importation rate

- α : proportion of those infected who clear blood-stage infections through immediate treatment, and
- β : proportion of those cleared of blood-stage infection who are also cleared of liver-stage parasites (radical cure).

In other words, the proportion $\alpha\beta$ of infected individuals is wholly cured of liver-stage and blood-stage parasites. The model assumes treatment clears the infection instantaneously. Individuals in S_{L} who relapse or get a new infection are assumed to be cured with the same proportions as new infections from S_0. However, individuals in I_0 who are superinfected are assumed not to seek treatment.

In contrast to the White model, the Champagne model allows analysis of potential treatment interventions or how much of an impact limiting the importation rate might have on case numbers (through border control/testing). Although the lack of mosquito dynamics simplifies the model and it's running, it is unrealistic. The model still has some of the same problems as the White model, such as not incorporating hypnozoite depletion rates and a lack of population dynamics, meaning all analytic results are done assuming the system is at equilibrium.

Chapter 4

Parameter Inference

4.1 Motivation

Building mathematical models of real-world phenomena allows us to simulate changes in the world without undertaking large-scale experiments. However, once we have a model that sufficiently approximates *P. vivax* transmission or anything else we are trying to model, we need to estimate the 'true' underlying parameters. We calibrate the model against real-world data such as case counts and prevalence surveys to do this. Under frequentist assumptions, there is a 'true' set of parameters that simulated the observed data. In the Bayesian framework, the parameters are considered to be random, and This chapter explores statistical inference techniques to recover the parameters under both the frequentist and Bayesian frameworks.

4.2 Frequentist Parameter Estimation

Assume the model is parameterised by a set of parameters $\boldsymbol{\theta} \in \boldsymbol{\Theta}$, which we are trying to estimate by considering some observed data $\mathbf{y}^{\text{obs}} = (y_1^{\text{obs}}, \dots, y_n^{\text{obs}})$. Consider $\mathbf{y}(\boldsymbol{\theta}) = (y_1(\boldsymbol{\theta}), \dots, y_n(\boldsymbol{\theta}))$ some model simulation of $\mathbf{y}^{\text{obs}}$. Often, the observed data has some underlying index set $x_1, \dots, x_n$, where x_i might be something like time. In this case, we can also consider the observed data to be $\{(x_1, y_1^{\text{obs}}), \dots, (x_n, y_n^{\text{obs}})\}$, and the model simulated data to be $\{(x_1, y_1(\boldsymbol{\theta})), \dots, (x_n, y_n(\boldsymbol{\theta}))\}$.

Least Squares Estimator

It is common for models to be deterministic, for example, when modelling the mean behaviour of a system. In this case, $\mathbf{y}(\boldsymbol{\theta})$ is not random. Therefore, we can assume that $y_i^{\text{obs}} = y_i(\boldsymbol{\theta}) + \varepsilon_i$, where ε_i is a random variable with some (possibly unknown) distribution and zero mean.

When the distribution of ε_i is unknown, a common approach for estimating $\boldsymbol{\theta}^{\text{LSE}}$ is to take the least squares estimate (although we show in Theorem 4.6 that implicitly normal noise is assumed).

Definition 4.1 (Least Squares Estimate)**.** *The* **least squares estimate** $\boldsymbol{\theta}^{\text{LSE}}$ *for* $\boldsymbol{\theta}$ *is*

$$\boldsymbol{\theta}^{\text{LSE}} := \underset{\boldsymbol{\theta} \in \boldsymbol{\Theta}}{\arg\min} \sum_{i=1}^{n} (y_i(\boldsymbol{\theta}) - y_i^{\text{obs}})^2.$$

Example 4.2. *Consider the observed data* $\{(x_1, y_1^{\text{obs}}), (x_2, y_2^{\text{obs}}), (x_3, y_3^{\text{obs}})\} = \{(1,2),(2,4),(3,4)\}$, *which we assume were generated from the model* $y_i(\boldsymbol{\theta}) + \varepsilon_i$. *Let* $y_i(\boldsymbol{\theta}) = \theta_0 + \theta_1 x_i$ *and* $\mathbb{E}(\varepsilon_i) = 0$. *We derive the least squares estimate of our parameters* $\boldsymbol{\theta} = (\theta_0, \theta_1)$ *by*

$$\begin{aligned}
\boldsymbol{\theta}^{\text{LSE}} &= \arg\min_{\boldsymbol{\theta}} [\sum_{i=1}^{3} (y_i(\boldsymbol{\theta}) - y_i^{\text{obs}})^2] \\
&= \arg\min_{\boldsymbol{\theta}} [\sum_{i=1}^{3} (\theta_0 + \theta_1 x_i - y_i^{\text{obs}})^2] \\
&= \arg\min_{\boldsymbol{\theta}} [(\theta_0 + \theta_1 - 2)^2 + (\theta_0 + 2\theta_1 - 4)^2 + (\theta_0 + 3\theta_1 - 4)^2].
\end{aligned}$$

Since the expanded quadratic will have positive coefficients for θ_0 *and* θ_1, *we can solve for* $\boldsymbol{\theta}^{\text{LSE}}$ *by*

$$\begin{aligned}
\mathbf{0} &= \frac{\partial}{\partial \boldsymbol{\theta}} [(\theta_0^{\text{LSE}} + \theta_1^{\text{LSE}} - 2)^2 + (\theta_0^{\text{LSE}} + 2\theta_1^{\text{LSE}} - 4)^2 + (\theta_0^{\text{LSE}} + 3\theta_1^{\text{LSE}} - 4)^2] \\
&= \begin{bmatrix} 6\theta_0^{\text{LSE}} + 12\theta_1^{\text{LSE}} - 20 \\ 12\theta_0^{\text{LSE}} + 28\theta_1^{\text{LSE}} - 44 \end{bmatrix}.
\end{aligned}$$

Solving these two equations results in $\theta_0^{\text{LSE}} = 4/3$ *and* $\theta_1^{\text{LSE}} = 1$. *This can be visually seen in Figure 4.1 in the red line that minimises the sum of the squares of the difference between the observations (in black dots) and the linear model.*

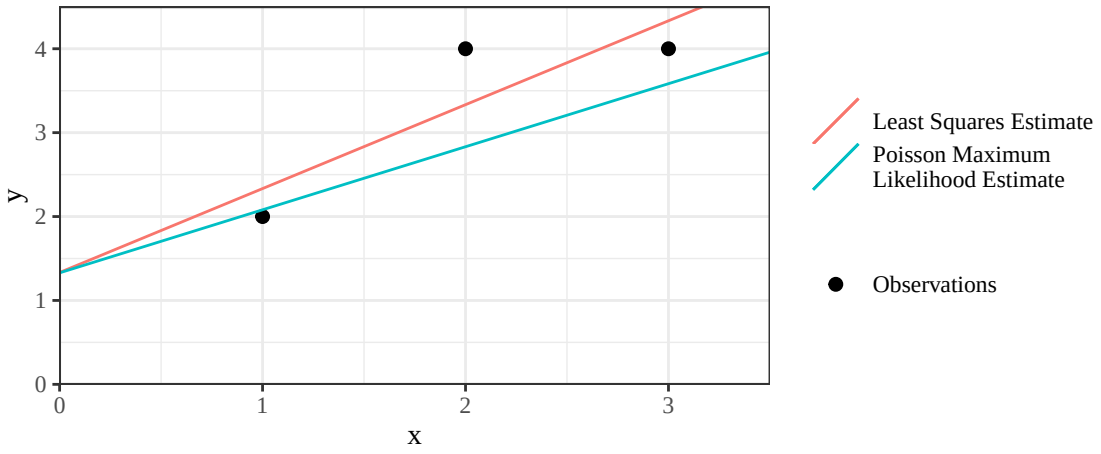

Figure 4.1: Two linear models of the form $y_i(\boldsymbol{\theta}) = \theta_0 + \theta_1 x_i$ fit given the set of observations $\{(1,2),(2,4),(3,4)\}$ using the method of least squares and maximum likelihood under the assumption that the data are independent realisations from a Poisson distribution with mean $y_i(\boldsymbol{\theta})$. The least squares estimates were $\theta_0^{\text{LSE}} = 4/3$ and $\theta_1^{\text{LSE}} = 1$. The maximum likelihood estimates were $\hat{\theta}_0 \approx 1.329$ and $\hat{\theta}_1 \approx 0.751$.

Maximum Likelihood Estimator

The least squares method makes no explicit assumptions about the distribution of the noise ε. However, if the distribution of ε is known (or can be reasonably assumed), we can explicitly calculate the probability of the data given the parameters.

Definition 4.3 (Likelihood function)**.** *With* $\mathbf{y}^{\text{obs}}$ *fixed, the* **likelihood function** *is*

$$\mathcal{L}(\boldsymbol{\theta}) := \Pr(\mathbf{y}(\boldsymbol{\theta}) + \boldsymbol{\varepsilon} = \mathbf{y}^{\text{obs}} | \boldsymbol{\theta}).$$

Particularly, if $y_i(\boldsymbol{\theta}) + \varepsilon_i$ *are independent*

$$\mathcal{L}(\boldsymbol{\theta}) = \prod_{i=1}^{n} \Pr(y_i(\boldsymbol{\theta}) + \varepsilon_i = y_i^{\text{obs}} | \boldsymbol{\theta}).$$

The dependence of the likelihood function on $\mathbf{y}^{\text{obs}}$ is notationally suppressed but can be explicitly written as $\mathcal{L}(\boldsymbol{\theta}|\mathbf{y}^{\text{obs}})$ to avoid confusion. In the continuous (or mixture of discrete and continuous) case, we interpret $\Pr(\mathbf{y}(\boldsymbol{\theta}) + \boldsymbol{\varepsilon} = \mathbf{y}^{\text{obs}}|\boldsymbol{\theta})$ as the density $\Pr(\mathbf{y}(\boldsymbol{\theta}) + \boldsymbol{\varepsilon} \in \mathrm{d}\mathbf{y}^{\text{obs}}|\boldsymbol{\theta})$ with respect to an underlying probability measure.

A natural estimate for $\boldsymbol{\theta}$ is the one that maximises the likelihood function $\mathcal{L}$, as it coincides with the value of $\boldsymbol{\theta}$ that maximises the probability of the data (possibly expressed as a density). Such an estimate is called the maximum likelihood estimate.

Definition 4.4 (Maximum Likelihood Estimate)**.** *The* **maximum likelihood estimate** *of* $\boldsymbol{\theta}$ *is*

$$\hat{\boldsymbol{\theta}} := \arg\max_{\boldsymbol{\theta} \in \boldsymbol{\Theta}} \mathcal{L}(\boldsymbol{\theta}).$$

It is often computationally easier to deal with the log-likelihood $\ell(\boldsymbol{\theta}) := \ln \mathcal{L}(\boldsymbol{\theta})$. Since the natural logarithm is a monotonic function,

$$\arg\max_{\boldsymbol{\theta} \in \boldsymbol{\Theta}} \mathcal{L}(\boldsymbol{\theta}) = \arg\max_{\boldsymbol{\theta} \in \boldsymbol{\Theta}} \ell(\boldsymbol{\theta}).$$

Example 4.5. *Using the same observed data set as Example 4.2, we assume that* y_i^{obs} *were generated independently from* $y_i(\boldsymbol{\theta}) + \varepsilon_i \sim \text{Pois}(y_i(\boldsymbol{\theta}))$*, where* $y_i(\boldsymbol{\theta}) := \theta_0 + \theta_1 x_i$ *as previously defined. Therefore, the maximum likelihood estimate of* $\boldsymbol{\theta}$ *is*

$$\begin{aligned}
\hat{\boldsymbol{\theta}} &= \arg\max \ell(\boldsymbol{\theta}) \\
&= \arg\max_{\boldsymbol{\theta} \in \boldsymbol{\Theta}} \sum_{i=1}^{3} y_i^{\text{obs}} \ln(y_i(\boldsymbol{\theta})) - y_i^{\text{obs}}(\boldsymbol{\theta}) - \ln(y_i^{\text{obs}}!) \\
&= \arg\max_{\boldsymbol{\theta} \in \boldsymbol{\Theta}} \sum_{i=1}^{3} y_i^{\text{obs}} \ln(\theta_0 + \theta_1 x_i) - \theta_0 - \theta_1 x_i - \ln(y_i^{\text{obs}}!) \\
&= \arg\max_{\boldsymbol{\theta} \in \boldsymbol{\Theta}} 2\ln(\theta_0 + \theta_1) - \theta_0 - \theta_1 + 4\ln(\theta_0 + 2\theta_1) - \theta_0 - 2\theta_1 + 4\ln(\theta_0 + 3\theta_1) - \theta_0 - 3\theta_1.
\end{aligned}$$

Numerically solving, we obtain $\hat{\theta}_0 \approx 1.329$*, and* $\hat{\theta}_1 \approx 0.751$*, as seen by the green line in Figure 4.1. This estimate is not the same as the linear model estimate using the least squares estimates for* $\boldsymbol{\theta}$*.*

Relationship of Least Squares and Maximum Likelihood Estimates

Although the least squares estimate does not explicitly assume a distribution, it coincides with the maximum likelihood estimate under the assumption that the y_i^{obs} were generated with i.i.d. normal error.

Theorem 4.6. *If* $y_i(\boldsymbol{\theta}) + \epsilon_i \sim N(y_i(\boldsymbol{\theta}), \sigma^2)$, *then*

$$\hat{\boldsymbol{\theta}} = \boldsymbol{\theta}^{\text{LSE}}.$$

Proof.

$$\begin{aligned}
\hat{\boldsymbol{\theta}} &= \arg\max_{\boldsymbol{\theta}\in\boldsymbol{\Theta}} \ell(\boldsymbol{\theta}) \\
&= \arg\max_{\boldsymbol{\theta}\in\boldsymbol{\Theta}} \sum_{i=1}^{n} \ln(\frac{1}{\sqrt{2\pi}\sigma}) - \frac{(y_i(\boldsymbol{\theta}) - y_i^{\text{obs}})^2}{\sigma^2} \\
&= \arg\max_{\boldsymbol{\theta}\in\boldsymbol{\Theta}} \sum_{i=1}^{n} -\frac{(y_i(\boldsymbol{\theta}) - y_i^{\text{obs}})^2}{\sigma^2} \\
&= \arg\max_{\boldsymbol{\theta}\in\boldsymbol{\Theta}} \sum_{i=1}^{n} -(y_i(\boldsymbol{\theta}) - y_i^{\text{obs}})^2 \\
&= \arg\min_{\boldsymbol{\theta}\in\boldsymbol{\Theta}} \sum_{i=1}^{n} (y_i(\boldsymbol{\theta}) - y_i^{\text{obs}})^2 \\
&= \boldsymbol{\theta}^{\text{LSE}}.
\end{aligned}$$

□

Surprisingly, the proof only requires σ^2 to be a constant but does not require it to be known.

Frequentist Parameter Estimates in Compartmental Models

Various approaches are possible to parameterise compartmental models. If the stochastic compartmental model is simple enough, and the number of people in the model is small enough, then the likelihood for the stochastic model could be calculated directly. However, this is hardly ever the case, and approximations are usually made.

For a model with a single unknown parameter, it is possible to fit a deterministic ODE model to a single data point. For example, Champagne et al. 2022 fits one unknown model parameter to incidence data. Fitting to a single data point is not generally advisable, as the parameter estimates will not be robust to variations in the observation of that data. Alternatively, if the model is fit to multiple observations, parameters can be estimated by finding the ODE model the least squares parameter estimates. Gani and Leach fit part of their modified $SEIR$ smallpox model using least squares estimates. Another approach is to assume that the observed data follow a particular distribution determined by the ODE solution. For example, it is plausible to assume that daily incidence (case counts) in an SIS model, such as described by Equations 2.1 and 2.2, could be distributed according to a Poisson distribution, with a mean number of cases $\beta\frac{I_t}{N}S_t$, where I_t and S_t are solutions of the ODEs at time t. This is because $\beta\frac{I_t}{N}S_t$ describes the rate at which individuals are moving from the susceptible compartment to the infected compartment. Other data, such as samples from the population to estimate the proportion of the population who are infectious, could be distributed according to Binom$(n, \frac{I_t}{N})$, where n is the total number of people sampled.

Figure 4.2 demonstrates the estimation of one unknown parameter β from an $SEIR$ model using prevalence data. Both β^{LSE} in grey and $\hat{\beta}$ in yellow are very close but do not fit the data well, suggesting fitting the ODEs to a stochastic model simulation may be a poor choice. This is

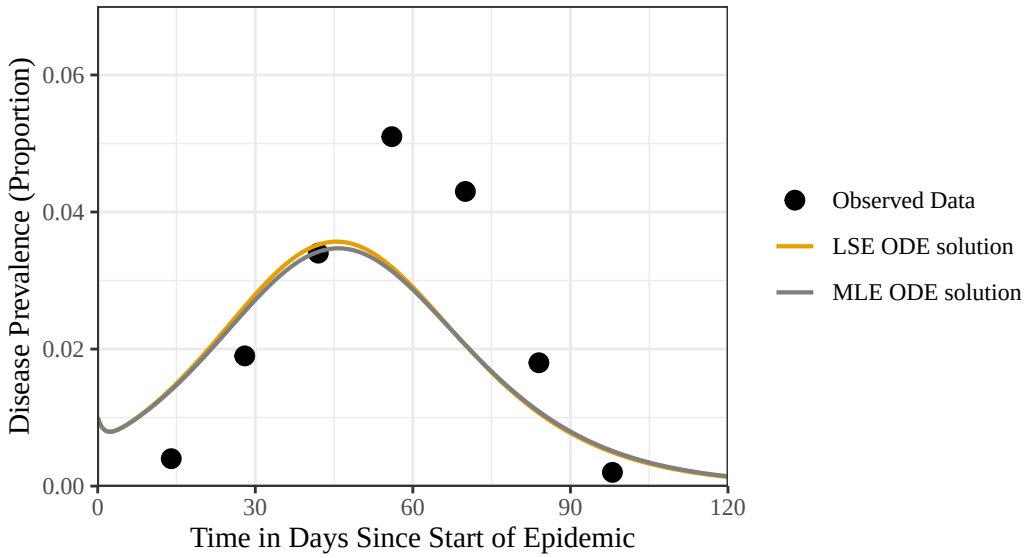

Figure 4.2: An $SEIR$ model calibrated to some observed prevalence data taken every two weeks over a 14-week period, generated as I_t/N from the $SEIR$ simulation in Figure 2.3. All parameters were considered known except for β. The least squares estimate (LSE) $\beta^{\text{LSE}} = 0.3516$ was found by solving the model ODEs and numerically minimising the square differences between observed prevalences and the ODE prevalences (as proportions). Similarly, the maximum likelihood estimate $\hat{\beta} = 0.3493$ was found by assuming the prevalence (times 1000) was binomially distributed from 1000 samples with the probability of being infectious equal to $\frac{I_t}{N}$.

because, at the beginning of an epidemic, the disease dynamics are highly stochastic. Therefore, trying to fit an ODE model to its stochastic analogue is not necessarily a good idea. ODEs are more likely to approximate the stochastic model well when the number of people in each compartment is high.

4.3 Bayesian Parameter Estimation

In frequentist statistical inference, $\boldsymbol{\theta}$ is considered to be fixed, with the observed data $\mathbf{y}^{\text{obs}}$ assumed to be generated from a distribution depending on $\boldsymbol{\theta}$. Although it is possible to quantify the uncertainty in parameter estimates through confidence intervals, frequentist estimates naturally lend themselves to point estimates. In contrast, inference under a Bayesian framework assumes that $\boldsymbol{\theta}$ is also a random variable that, before any observations are made, follows a prior distribution. 'Evidence' from the observed data then updates belief about $\boldsymbol{\theta}$, resulting in a posterior distribution of $\boldsymbol{\theta}$, described by Bayes' theorem, namely

$$\Pr(\boldsymbol{\theta}|\mathbf{y}^{\text{obs}}) \propto \Pr(\mathbf{y}^{\text{obs}}|\boldsymbol{\theta}) \Pr(\boldsymbol{\theta}).$$

Bayesian parameter estimation is still dependent on the likelihood function $\mathcal{L}(\boldsymbol{\theta}) := \Pr(\mathbf{y}^{\text{obs}}|\boldsymbol{\theta})$. By using the posterior estimates of our parameter values, we can generate a posterior predictive distribution of our model. This can be helpful in forecasting, as it can capture uncertainty more robustly (at least than point estimates). For instance, a government may be interested in the number of additional hospital beds that need to be available to cope with an outbreak of a disease. If a disease model can be used to approximate outbreaks of the disease, we can use previous

instances of the disease to calibrate our model parameters. Samples from the posterior parameter distribution allow the model to be run multiple times with varying sets of parameters and provide a range of predicted outcomes for the disease. This allows for confidence in how much investment may be required in the health system. Similarly, samples from the posterior parameter distribution allow for scenario modelling, such as introducing a new vaccine.

If $\Pr(\boldsymbol{\theta}|\mathbf{y}^{\text{obs}})$ is a known distribution with established sampling methods, we can sample directly from the distribution. If not, we have to use other methods to sample from the distribution.

Rejection Sampling

Algorithm 3 Rejection Sampler

Sample $\Theta^* \sim p$
Sample $U \sim \text{Unif}(0,1)$
if $U \leq \frac{g(\Theta^*)}{Mp(\Theta^*)}$ **then**
  return Θ^* as a sample from the distribution of Θ
else
  Reject Θ^* as a sample from the distribution of Θ, and repeat the algorithm
end if

Rejection sampling is not just a method for sampling from a posterior distribution but also a method for sampling from any distribution where the density can be calculated up to a proportionality constant. Algorithm 3 demonstrates how this can be done for Θ with density proportional to g. Given a distribution p and constant M such that $Mp(x) \geq g(x)$, we sample a proposal Θ^* from p. We then accept Θ^* as a sample from g with probability $\frac{g(\Theta^*)}{Mp(\Theta^*)}$ and reject otherwise.

Under this methodology, let Θ^* be the proposed sample. The distribution function of the accepted samples Θ is

$$\begin{aligned}
\Pr(\Theta = \theta) &\propto \Pr\left(\Theta^* = x, U \leq \frac{g(\Theta^*)}{Mp(\Theta^*)}\right) \\
&\qquad \text{(where the probabilities may be interpreted as densities)} \\
&= \Pr\left(U \leq \frac{g(X^*)}{Mp(X^*)} | X^* = x\right) \Pr(X^* = x) \\
&= \frac{g(x)}{Mp(x)} p(x) \\
&= \frac{g(x)}{M}
\end{aligned}$$

as required.

Example 4.7. *Let $g(x) = (x-1)^2$ be an unnormalised density function for $x \in (0,2)$. It can be shown that $g(x) \leq 1$, the density of a* $\text{Unif}(0,1)$ *random variable. Therefore, to generate samples from g we sample uniformly from $X^* \sim \text{Unif}(0,1)$, and accept the sample if a new $U \sim \text{Unif}(0,1)$ is less than $(X^*-2)^2$. This is demonstrated in Figure 4.3, with the black line being the unnormalised density, the green dots being accepted samples, and the red dots being rejected samples. The values along the X^* axis correspond to samples from g.*

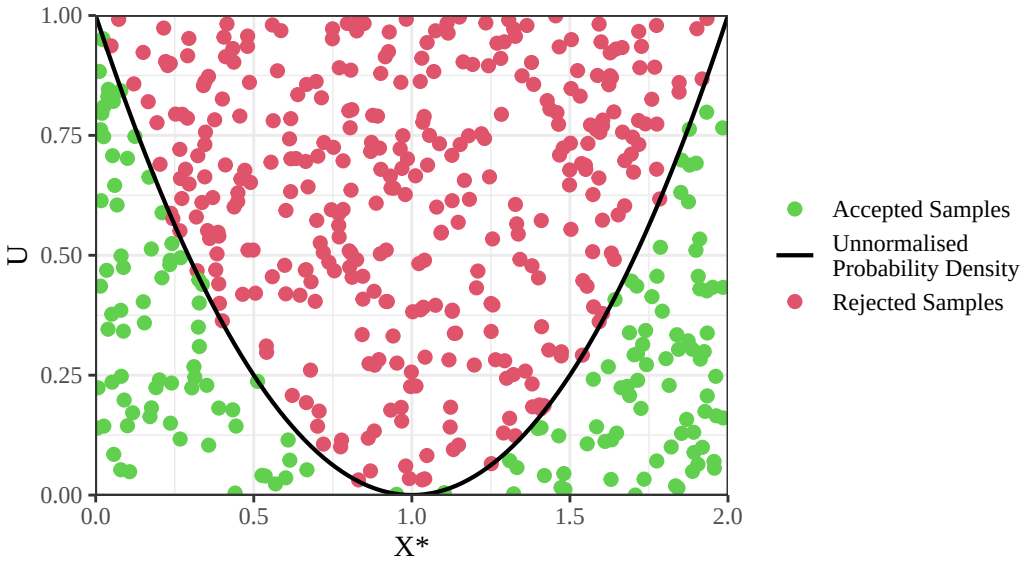

Figure 4.3: Samples of X from the unnormalised density $g(x) = (x-1)^2$ with $x \in (0,2)$ using the rejection sampler. $X^* \sim \text{Unif}(0,2)$ and $M = 1$. Green dots are samples from from X. Of 500 samples of X^*, 157 were accepted as samples of X.

Markov Chain Monte Carlo Methods

Often it is not possible to sample directly from the posterior distribution $\Pr(\boldsymbol{\theta}|\mathbf{y}^{\text{obs}})$ using a rejection sampler, as there is no explicit form proportional to the true density. Therefore, a common way of sampling from a distribution $p(x)$ is to construct a Markov chain with stationary distribution $p(x)$. Hence, eventually each new state the chain moves to will be a (not necessarily independent) sample from $p(x)$, or in our case $\Pr(\boldsymbol{\theta}|\mathbf{y}^{\text{obs}})$.

Definition 4.8 ((Discrete-Time) Markov Chain)**.** *A sequence of random variables $X_0, X_1, \ldots$ is a* **(discrete-time) Markov chain** $\{X_i\}_{i\in\mathbb{N}}$ *if for all $k \in \mathbb{N}$,*

$$\Pr(X_{i+1} \in A | X_0, X_1, \ldots, X_i) = \Pr(X_{i+1} \in A | X_i).$$

If $X_i \in \mathcal{X}$, then $\mathcal{X}$ is the state space of the Markov chain. For example the Markov chain depicted in Figure 4.4, has discrete state space $\mathcal{X} = \{1, 2\}$, and transition probabilities depicted by the numbers on the arrows.

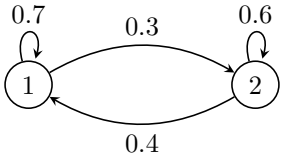

Figure 4.4: A simple time-homogeneous Markov chain, with two states. It is characterised by the transition kernel $K(1,1) = \Pr(X_{i+1} = 1 | X_i = 1) = 0.7$, $K(1,2) = \Pr(X_{i+1} = 2 | X_i = 1) = 0.3$, $K(2,1) = \Pr(X_{i+1} = 1 | X_i = 2) = 0.4$, and $K(2,2) = \Pr(X_{i+1} = 2 | X_i = 2) = 0.6$. The stationary distribution is $\pi(1) = 4/7$ and $\pi(2) = 3/7$.

Markov chains are characterised by a transition kernel K with

$$K(x_i, x_{i+1}) := \Pr(X_{i+1} = x_{i+1} | X_i = x_{i+1}),$$

where this probability is interpreted as a density for continuous random variables. $K(1,1)$ would therefore be the probability of transitioning from state 1 to state 2 in a single discrete time step.

We will restrict our focus to time-homogeneous Markov chains where if the value of X_i is known to be x, the behaviour of the chain from this point on will be identical to the behaviour of the chain from X_j, if this is also observed to be x.

Definition 4.9 (Time-Homogeneous)**.** *A Markov chain is* **time-homogeneous** *if*

$$\{X_i, X_{i+1}, \ldots, X_{i+n}\} \overset{d}{=} \{X_{i'}, X_{i'+1}, \ldots, X_{i'+n}\}$$

for all $i, i', n \in \mathbb{N}$*, given* $X_i = x = X_{i'}$*.*

The Markov chain in Figure 4.4 is time-homogeneous. It does not matter how long it took to get into a state, the Markov chain will behave the same from that point forward.

Definition 4.10 (Stationary Distribution)**.** *A Markov chain has* **stationary distribution** π *if for* $X_i \sim \pi$*, then* $X_{i+1}|X_i \sim \pi$*.*

Example 4.11. *Given the Markov chain in Figure 4.4, the stationary distribution can be calculated by solving the simultaneous equations*

$$\begin{aligned} K(1,1) \times \pi(1) + K(2,1) \times \pi(2) = 0.7 \times \pi(1) + 0.4 \times \pi(2) &= \pi(1) \\ \pi(1) + \pi(2) &= 1. \end{aligned}$$

Therefore, $\pi(1) = 4/7$ *and* $\pi(2) = 3/7$*.*

As stated earlier, to sample from a distribution $p(x)$, we construct a Markov chain with this stationary distribution. A sufficient condition to know that we have achieved this is if our chain satisfies the detailed balance condition.

Theorem 4.12 (Detailed balance condition)**.** *A Markov chain has stationary distribution* $p(x)$*, which it converges to independent of initialisation, if for all* x, x'*,*

$$p(x)K(x, x') = p(x')K(x', x).$$

Proof. More formally this requires the notions of recurrent, non-null, irreducible and aperiodic Markov chains which we do not discuss here. For a full discussion and proof see Robert and Casella 2010, Chapter 6. □

Metropolis-Hastings

The Metropolis-Hastings algorithm is one way of constructing a Markov chain with stationary distribution equal to the target distribution g. We choose a proposal distribution $q(x'|x)$ which given our last sample x, generates a new random variable X'. For example q might be the density of $X' \sim N(x, 1)$, a normal random variable with mean around the previous sample. Then similar to rejection sampling, X' is accepted as the next state in the distribution with some probability α,

chosen in such a way that if the chain is distributed according to a stationary distribution $X_i \sim g$, then the next step will also be distributed according to that stationary distribution $X_{i+1} \sim g$. Formally this is set out in Algorithm 4.

Algorithm 4 Metropolis-Hastings Sampler

Initialise x_0
for $i = 1$ to N **do**
  Sample $X' \sim q(x'|x_{i-1})$
  Compute acceptance ratio $\alpha = \min\left(\frac{g(x')q(x_{i-1}|x')}{g(x_{i-1})q(x'|x_{i-1})}, 1\right)$
  Sample $U \sim \text{Uniform}(0, 1)$
  if $U \leq \alpha$ **then**
    $x_i \leftarrow X'$
  else
    $x_i \leftarrow x_{i-1}$
  end if
end for
return $\{x_0, x_1, \ldots, x_N\}$

Note that for symmetric proposal distributions $q(x'|x) = q(x|x')$, α simplifies to $\min\left(\frac{g(x')}{g(x)}, 1\right)$, in which case the algorithm is simply called a Metropolis sampler.

Theorem 4.13. *The chain produced by Algorithm 4, $\{X_k\}_{k\in\mathbb{N}}$, has stationary distribution g for proposal distributions that cover the support of g.*

Proof. We show that the detailed balance condition

$$g(x)q(x'|x)\alpha(x, x') = g(x')q(x|x')\alpha(x', x)$$

where $\alpha(x, x') = \min\left(\frac{g(x')q(x|x')}{g(x)q(x'|x)}, 1\right)$ is satisfied. Without loss of generality let $g(x')q(x|x') < g(x)q(x'|x)$, so $\alpha(x, x') = \frac{g(x')q(x|x')}{g(x)q(x'|x)}$, and $\alpha(x', x) = 1$.

$$\begin{aligned} g(x)q(x'|x)\alpha(x, x') &= g(x)q(x'|x) \times \frac{g(x')q(x|x')}{g(x)q(x'|x)} \\ &= g(x')q(x|x') \\ &= g(x')q(x|x')\alpha(x', x) \end{aligned}$$

□

As seen empirically in Example 4.14 and Figure 4.5, the proof does not depend on choice of proposal distribution.

Example 4.14 (Coin toss)**.** *Let the probability of tossing heads on a weighted coin be* $\Pr(X = 1) = p$*. Assume that* $p \sim \text{Unif}(0, 1)$*. We observe* $y^{\text{obs}} = 6$ *heads from 10 tosses of the coin. Therefore*

$$\Pr(p|y^{\text{obs}}) \propto \Pr(y^{\text{obs}}|p)\Pr(p) = \binom{n}{y^{\text{obs}}} p^{y^{\text{obs}}}(1-p)^{n-y^{\text{obs}}} \times 1 = 210p^6(1-p)^4.$$

We sample from this distribution using the Metropolis algorithm which becomes

Initialise p_0
for $i = 1$ *to* N ***do***

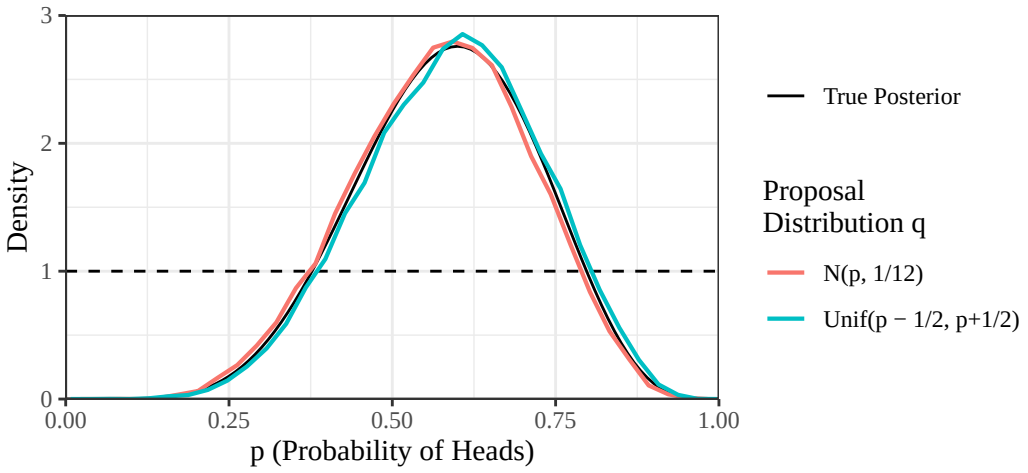

Figure 4.5: Samples from the posterior distribution of p using the Metropolis-Hastings algorithm. p was assumed to have a uniform prior between 0 and 1, with $y^{\text{obs}} = 6$, generated from Binom$(10, p)$, The choice of proposal distribution did not impact the final estimate of $\Pr(p|y^{\text{obs}})$.

Sample $P' \sim q(p'|p_{i-1})$
Compute acceptance ratio $\alpha = \min\left(\frac{(P')^6(1-P')^4}{p_{i-1}^6(1-p_{i-1})^4}, 1\right)$ ▷ *Assuming q symmetric*
Sample $U \sim Uniform(0, 1)$
if $U \leq \alpha$ ***then***
$p_i \leftarrow X'$
else
$p_i \leftarrow x_{i-1}$
end if
end for
return $\{p_0, p_1, \ldots, p_N\}$

We can compare two different proposal distributions for $q(p'|p)$*,* $P' \sim N(p, 1/12)$*, and the second being* $P' \sim \text{Unif}(p - 1/2, p + 1/2)$*. The first 1000 samples were discarded as burn in, and it was thinned to every 5 samples. The resulting distribution of the samples can be seen in Figure 4.5, with both proposal distributions resulting in samples that are good at estimating the true distribution.*

Since the chain converges to the stationary distribution over time, and is highly correlated, a derived chain $\{x_{B+iT}\}_{i\in\mathbb{N}}$ is constructed from the output. The first B samples are discarded as 'burn in' samples to reduce the impact of the initialisation point. The chain is 'thinned' by taking every Tth sample, since X_i and X_{i+1} may also be highly correlated (in samples where the proposed X' is rejected, $X_i = X_{i+1}$). This derived chain is considered a random sample from the target distribution g. In practice, diagnostics such as trace plots and autocorrelation plots are used to determine B and T (see Gelman et al. 2014, Chapter 11).

For disease models, given a prior distribution for the parameter(s) $\boldsymbol{\theta}$, Metropolis-Hastings can be used to produce samples from $\Pr(\boldsymbol{\theta}|y^{\text{obs}}) \propto \mathcal{L}(\boldsymbol{\theta})\Pr(\boldsymbol{\theta})$, where $\mathcal{L}(\boldsymbol{\theta})\Pr(\boldsymbol{\theta})$ can be calculated to a proportionality constant but not directly sampled from. For example given an SIS model described in Equations 2.1 and 2.2 with unknown effective contact rate $\beta \sim \text{Gamma}(2, 6)$ and daily case counts y^{obs}, we can draw samples from $\boldsymbol{\theta}|y^{\text{obs}}$ as in Figure 4.6. This figure demonstrates that the choice of likelihood results in different posterior sample distributions. The samples from Poisson likelihood have greater variance than the samples from the binomial likelihood.

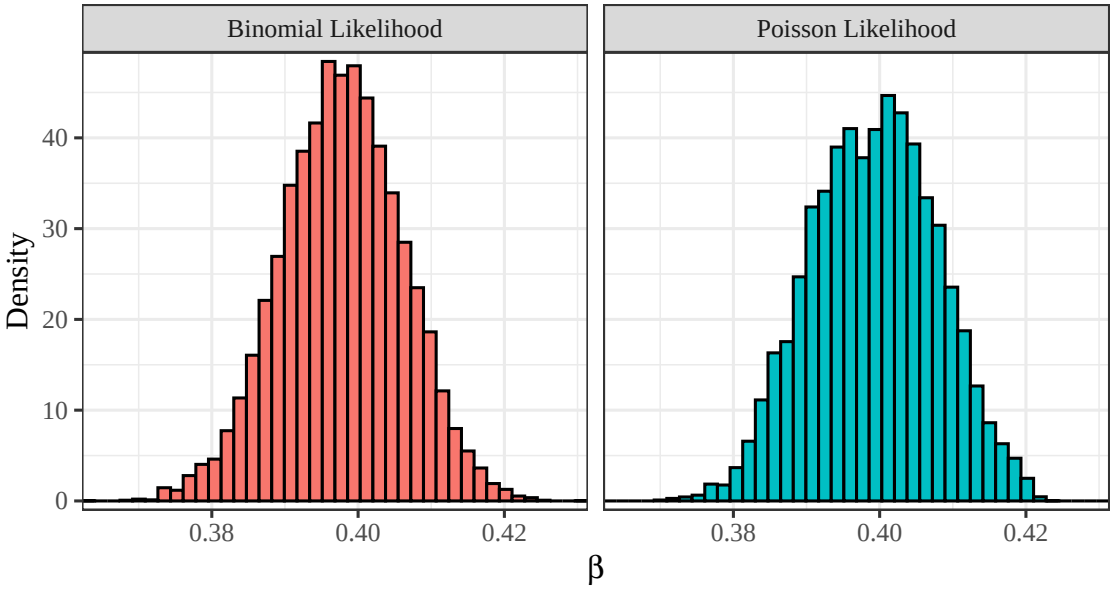

Figure 4.6: Given a daily incidence of $y^{\text{obs}} = 26$ at day 30 of an SIS epidemic, with unknown β, we use Metropolis-Hasting to sample from $\Pr(\beta|y^{\text{obs}})$. $\gamma = 1/4$ was assumed to be correct, and we compared the assumption $y^{\text{obs}} \sim \text{Binom}(\lfloor S_{30} \rfloor, \beta I_{30}/N)$, to the assumption $y^{\text{obs}} \sim \text{Pois}(\frac{\beta I_{30} S_{30}}{N})$ where I_{30}, S_{30} are the ODE solutions to Equations 2.1 and 2.2. We assumed the prior distribution $\beta \sim \text{Gamma}(2, 6)$, where $\mathbb{E}(\beta) = 1/3$. Our proposal density was $N(\beta^*, 1/10)$, where β^* was the previous sample.

Gibbs Sampling

Algorithm 5 Gibbs Sampler

Initialise $\boldsymbol{\theta}^{(0)} = (\theta_1^{(0)}, \theta_2^{(0)}, \ldots, \theta_d^{(0)})$
for $i = 1$ to N **do**
  Sample $\theta_1^{(i)} \sim \Pr(\theta_1 | \theta_2^{(i-1)}, \theta_3^{(i-1)}, \ldots, \theta_d^{(i-1)})$
  Sample $\theta_2^{(i)} \sim \Pr(\theta_2 | \theta_1^{(i)}, \theta_3^{(i-1)}, \ldots, \theta_d^{(i-1)})$
  $\vdots$
  Sample $\theta_d^{(i)} \sim \Pr(\theta_d | \theta_1^{(i)}, \theta_2^{(i)}, \ldots, \theta_{d-1}^{(i)})$
  Save $(\theta_1^{(i)}, \theta_2^{(i)}, \ldots, \theta_d^{(i)})$ as $\boldsymbol{\theta}^{(i)}$
end for
return $\{\boldsymbol{\theta}^{(0)}, \boldsymbol{\theta}^{(1)}, \ldots, \boldsymbol{\theta}^{(N)}\}$

Some models may be structured such that it is possible to sample from the parameters distributions $\theta_1|\theta_2, \mathbf{y}^{\text{obs}}$, and $\theta_2|\theta_1, \mathbf{y}^{\text{obs}}$ but not the joint distribution of $(\theta_1, \theta_2)|\mathbf{y}^{\text{obs}}$. A (multidimensional) Markov chain can be constructed by iteratively updating the parameters. Such a method is called a Gibbs sampler, described in Algorithm 5. The distribution of the Markov chain sampler will eventually converge to the $\Pr(\theta_1, \theta_2|\mathbf{y}^{\text{obs}})$, and for the same reasons as for the Metropolis-Hastings sampler, after thinning and discarding burn in, we consider the resulting chain a sequence of independent samples from our target distribution.

Theorem 4.15 (Gibbs Sampler)**.** *The Markov chain generated by Algorithm 5 converges to the distribution of* $\Pr(\boldsymbol{\theta}|\mathbf{y}^{\text{obs}})$.

Proof. We prove that the Gibbs Sampler satisfies the detailed balance equation for two unknown parameters. The transition kernel of the Markov chain is

$$q(\boldsymbol{\theta}^{(i)}|\boldsymbol{\theta}^{(i-1)}) := \Pr(\theta_1^{(i)}|\theta_2^{(i-1)}, \mathbf{y}) \Pr(\theta_2^{(i)}|\theta_1^{(i)}, \mathbf{y}).$$

To prove the detailed balance condition is satisfied, we need to show that

$$\Pr(\boldsymbol{\theta}^{(i-1)}|\mathbf{y})q(\boldsymbol{\theta}^{(i)}|\boldsymbol{\theta}^{(i-1)}) = \Pr(\boldsymbol{\theta}^{(i)}|\mathbf{y})q(\boldsymbol{\theta}^{(i-1)}|\boldsymbol{\theta}^{(i)}).$$

$$\begin{aligned}
\Pr(\boldsymbol{\theta}^{(t-1)}|\mathbf{y})q(\boldsymbol{\theta}^{(i)}|\boldsymbol{\theta}^{(i-1)}) &= \Pr(\theta_1^{(i-1)}, \theta_2^{(i-1)}|\mathbf{y}) \times \Pr(\theta_1^{(i)}|\theta_2^{(i-1)}, \mathbf{y}) \times \Pr(\theta_2^{(i)}|\theta_1^{(i)}, \mathbf{y}) \\
&= \Pr(\theta_1^{(i-1)}|\theta_2^{(i-1)}, \mathbf{y}) \times \Pr(\theta_2^{(i-1)}|\mathbf{y}) \times \Pr(\theta_1^{(i)}|\theta_2^{(i-1)}, \mathbf{y}) \times \Pr(\theta_2^{(i)}|\theta_1^{(i)}, \mathbf{y}) \\
&= \Pr(\theta_1^{(i-1)}|\theta_2^{(i-1)}, \mathbf{y}) \times \Pr(\theta_1^{(i)}, \theta_2^{(i-1)}|\mathbf{y}) \times \Pr(\theta_2^{(i)}|\theta_1^{(i)}, \mathbf{y}) \\
&= \Pr(\theta_2^{(i)}|\theta_1^{(i)}, \mathbf{y}) \times \Pr(\theta_1^{(i)}, \theta_2^{(i-1)}|\mathbf{y}) \times \Pr(\theta_1^{(i-1)}|\theta_2^{(i-1)}, \mathbf{y}) \\
&= \Pr(\theta_2^{(i)}|\theta_1^{(i)}, \mathbf{y}) \times \Pr(\theta_1^{(i)}|\mathbf{y}) \times \Pr(\theta_2^{(i-1)}|\theta_1^{(i)}, \mathbf{y}) \times \Pr(\theta_1^{(i-1)}|\theta_2^{(i-1)}, \mathbf{y}) \\
&= \Pr(\theta_1^{(i)}, \theta_2^{(i)}|\mathbf{y}) \times \Pr(\theta_2^{(i-1)}|\theta_1^{(i)}, \mathbf{y}) \times \Pr(\theta_1^{(i-1)}|\theta_2^{(i-1)}, \mathbf{y}) \\
&= \Pr(\boldsymbol{\theta}^{(t)}|\mathbf{y})q(\boldsymbol{\theta}^{(i-1)}|\boldsymbol{\theta}^{(i)})
\end{aligned}$$

as required, so the posterior distribution $\Pr(\boldsymbol{\theta}|\mathbf{y})$ is the unique stationary distribution associated with the generated Markov chain. □

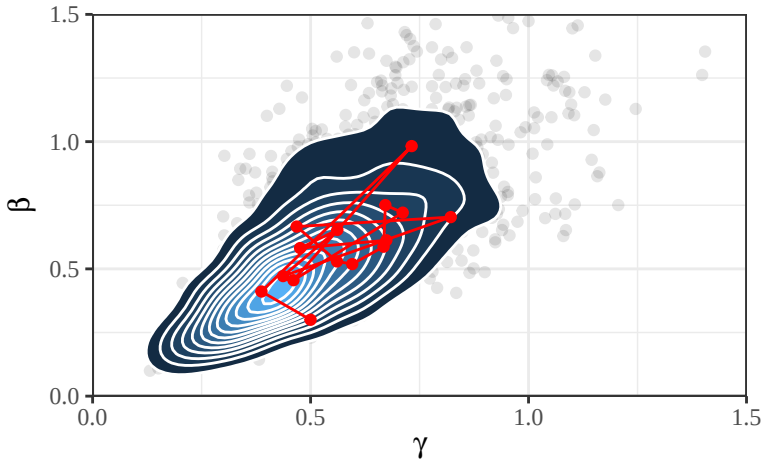

Figure 4.7: 2000 posterior samples from $\Pr(\beta, \gamma|\mathbf{y}^{\text{obs}})$, where $\beta|\gamma, \mathbf{y}^{\text{obs}} \sim \text{Gamma}(9, 4/\gamma + 4 + 8\gamma)$ and $\gamma|\beta, \mathbf{y}^{\text{obs}} \sim \text{InvGamma}(12, 12\beta)$. The samples were obtained using a Gibbs sampler. The red points are the first 15 samples using the Gibbs sampler.

Example 4.16. *Consider the SIS model described by Equations 2.1 and 2.2. Early in an epidemic, the average number of new cases generated from a single infectious individual is known as* R_0*. This can be shown to be* $\frac{\beta}{\gamma}$ *for the SIS model. Let* $\mathbf{y}^{\text{obs}} = \{1, 1, 3, 1\}$ *be the number of people infected by four different individuals at the start of the epidemic. We assume that the number of infections*

are generated from a Poisson distribution with mean $\frac{\beta}{\gamma}$*. Therefore, the likelihood is*

$$\mathcal{L}(\beta,\gamma) := \Pr(\mathbf{y}^{\text{obs}}|\beta,\gamma) = \frac{\left(\frac{\beta}{\gamma}\right)^{1+1+3+1}\exp(-\frac{4\beta}{\gamma})}{1!\times 1!\times 3!\times 1!} \propto \left(\frac{\beta}{\gamma}\right)^{6}\exp(-\frac{4\beta}{\gamma}).$$

Let us assume that from similar previous epidemics we know that $\beta|\gamma \sim \text{Gamma}(3, 4+8\gamma)$*, and* $\gamma|\beta \sim \text{InvGamma}(6, 8\beta)$*. Therefore*

$$\begin{aligned}\Pr(\beta|\gamma,\mathbf{y}^{\text{obs}}) &\propto \Pr(\mathbf{y}^{\text{obs}}|\gamma,\beta)\Pr(\beta|\gamma)\\ &\propto \left(\frac{\beta}{\gamma}\right)^{6}\exp(-\frac{4\beta}{\gamma})\times\beta^{3-1}\exp(-(4+8\gamma)\beta)\\ &\propto \beta^{9-1}\exp(-(4/\gamma+4+8\gamma)\beta),\end{aligned}$$

and so $\beta|\gamma,\mathbf{y}^{\text{obs}} \sim \text{Gamma}(9, 4/\gamma+4+8\gamma)$*. Similarly,*

$$\begin{aligned}\Pr(\gamma|\beta,\mathbf{y}^{\text{obs}}) &\propto \Pr(\mathbf{y}^{\text{obs}}|\gamma,\beta)\Pr(\gamma|\beta)\\ &\propto \left(\frac{\beta}{\gamma}\right)^{6}\exp(-\frac{4\beta}{\gamma})\times\gamma^{-6-1}\exp\left(-\frac{8\beta}{\gamma}\right)\\ &\propto \gamma^{-12-1}\exp\left(-\frac{12\beta}{\gamma}\right),\end{aligned}$$

and so $\gamma|\beta,\mathbf{y}^{\text{obs}} \sim \text{InvGamma}(12, 12\beta)$*. Now we have explicit forms for the conditional probabilities, we generate samples using the Gibbs sampler in Algorithm 5. Samples from the distribution can be seen in Figure 4.7.*

The Gibbs sampler and Metropolis-Hastings sampler are often combined, by using a Metropolis-Hastings sampler for each step of the conditional sampling. This is useful when the conditional distributions $\Pr(\theta_1|\theta_2,\mathbf{y}^{\text{obs}})$ can be calculated up to a proportionality constant, but not directly sampled from.

Approximate Bayesian Computation

So far, under a Bayesian framework, parameter estimation has still been dependent on the likelihood function $\mathcal{L}(\boldsymbol{\theta}) := \Pr(\mathbf{y}^{\text{obs}}|\boldsymbol{\theta})$ through Bayes' theorem. In many cases, such as stochastic disease models and agent based models, the likelihood has no explicit form, or is intractable to calculate. The only option here is to run the model given $\boldsymbol{\theta}$, and sample $\mathbf{y}(\boldsymbol{\theta})$ directly.

Algorithm 6 Naive Bayesian Sampler

Sample $\boldsymbol{\theta}^* \sim \Pr(\boldsymbol{\theta})$
Run model and compute $\mathbf{y}(\boldsymbol{\theta}^*)$
if $\mathbf{y}(\boldsymbol{\theta}^*) = \mathbf{y}^{\text{obs}}$ **then**
  return $\boldsymbol{\theta}^*$ as a sample from $\Pr(\boldsymbol{\theta}|\mathbf{y}^{\text{obs}}$.)
end if

Algorithm 6 outlines a naive method of using such model runs to sample from $\Pr(\boldsymbol{\theta}|\mathbf{y}^{\text{obs}})$ is to sample $\boldsymbol{\theta}^*$ from $\Pr(\boldsymbol{\theta})$, and run the model to obtain $\mathbf{y}(\boldsymbol{\theta}^*)$. For each iteration, $\mathbf{y}(\boldsymbol{\theta}^*)$ will exactly equal $\mathbf{y}^{\text{obs}}$ with probability $\Pr(\mathbf{y}^{\text{obs}}|\boldsymbol{\theta}^*)\Pr(\boldsymbol{\theta}^*) \propto \Pr(\boldsymbol{\theta}^*|\mathbf{y}^{\text{obs}})$, and hence if $\mathbf{y}(\boldsymbol{\theta}^*) = \mathbf{y}^{\text{obs}}$ we can accept $\boldsymbol{\theta}^*$ as a sample from our posterior parameter distribution. When $\mathbf{y}^{\text{obs}}|\boldsymbol{\theta}^*$ does

not have a countable number of non-zero probability outputs, $\mathbf{y}(\boldsymbol{\theta}^*) = \mathbf{y}^{\text{obs}}$ can be exactly zero, and even in the countable case, for higher dimensional $\mathbf{y}(\boldsymbol{\theta})$, the probability of returning exactly $\mathbf{y}^{\text{obs}}$ vanishes. Therefore, we draw inspiration from the continuous interpretation of the likelihood $\mathcal{L}(\boldsymbol{\theta}) := \Pr(\mathbf{y}(\boldsymbol{\theta}) \in \mathrm{d}\mathbf{y}^{\text{obs}}|\boldsymbol{\theta})$. Since

$$\Pr(\mathbf{y}(\boldsymbol{\theta}) \in \mathrm{d}\mathbf{y}^{\text{obs}}|\boldsymbol{\theta}) := \lim_{\epsilon \to 0} \frac{\Pr(\mathbf{y}(\boldsymbol{\theta}) \in B_\epsilon^D(\mathbf{y}^{\text{obs}}))}{\varepsilon}, \tag{4.1}$$

where $B_\epsilon^D(\mathbf{y}^{\text{obs}})$ is a ball of size ϵ around $\mathbf{y}^{\text{obs}}$, with respect to some (unknown) metric D induced by the (unknown) probability distribution of $\mathbf{y}(\boldsymbol{\theta})$. Therefore, $\mathcal{L}(\boldsymbol{\theta})$ is approximately proportional to $\Pr(\mathbf{y}(\boldsymbol{\theta}) \in B_\epsilon^D(\mathbf{y}^{\text{obs}})|\boldsymbol{\theta})$, (as a function of $\boldsymbol{\theta}$).

Hence we construct a new approximate sampling algorithm where rather than rejecting the sample for $\mathbf{y}(\boldsymbol{\theta}) \neq \mathbf{y}^{\text{obs}}$, we accept $\mathbf{y}(\boldsymbol{\theta})$ if it falls within a ball of size ϵ around $\mathbf{y}^{\text{obs}}$. Equivalently we accept samples if $D(\mathbf{y}(\boldsymbol{\theta}), \mathbf{y}^{\text{obs}}) < \epsilon$.

Since the distribution of $\mathbf{y}(\boldsymbol{\theta})$ is unknown, and since the metric required for Equation 4.1 to hold depends on $\boldsymbol{\theta}$, we do not explicitly derive $D(\mathbf{y}(\boldsymbol{\theta}), \mathbf{y}^{\text{obs}})$, we are forced to approximate it with $\tilde{D}(\mathbf{y}(\boldsymbol{\theta}), \mathbf{y}^{\text{obs}})$. The most common choice of $\tilde{D}$ is the L^p norm of $\mathbf{y}(\boldsymbol{\theta}) - \mathbf{y}^{\text{obs}}$

$$\tilde{D}(\mathbf{y}(\boldsymbol{\theta}), \mathbf{y}^{\text{obs}}) = ||\mathbf{y}(\boldsymbol{\theta}) - \mathbf{y}^{\text{obs}}||_p = \left(\sum_{i=1}^{d} \left| y_i(\boldsymbol{\theta}) - y_i^{\text{obs}} \right|^p \right)^{1/p},$$

for $p \geq 1$. For $p = 1$ or 2 this is the Manhattan or Euclidean distance between the two vectors. When the observations in $\mathbf{y}^{\text{obs}}$ are on different scales, or $\mathbf{y}^{\text{obs}}$ are highly correlated between model runs, care needs to be taken to rescale $\mathbf{y}^{\text{obs}}$ and $\mathbf{y}(\boldsymbol{\theta})$ by a covariance matrix to remove correlation, or by rescaling using the relative differences instead of $||\mathbf{y}(\boldsymbol{\theta}) - \mathbf{y}^{\text{obs}}||_p$.

Algorithm 7 Approximate Bayesian Computation Sampler

```
Sample θ* ~ Pr(θ)
Run model and compute 𝒟(θ*)
if 𝒟(θ*) < ε then
    return θ* as a sample from Pr(θ|y^obs.)
end if
```

The full procedure is outlined in Algorithm 7, but since $\mathbf{y}^{\text{obs}}$ is fixed, we consider $\tilde{D}(\mathbf{y}(\boldsymbol{\theta}), \mathbf{y}^{\text{obs}})$ as a function of $\boldsymbol{\theta}$, and we can equivalently write $\mathcal{D}(\boldsymbol{\theta}) := \tilde{D}(\mathbf{y}(\boldsymbol{\theta}), \mathbf{y}^{\text{obs}})$. We call $\mathcal{D}(\boldsymbol{\theta})$ the discrepancy function where in a non-deterministic model, $\mathcal{D}(\boldsymbol{\theta})$ is random.

Chapter 5

Gaussian Processes and Synthetic Likelihoods

If the distribution of $\mathcal{D}(\boldsymbol{\theta})$ was known for all $\boldsymbol{\theta}$, then the need to sample from the model within Algorithm 7 would be redundant since $\mathcal{D}(\boldsymbol{\theta})$ could be sampled directly. Moreover, the probability of drawing and accepting a sample using this algorithm becomes $\Pr(\boldsymbol{\theta})\Pr(\mathcal{D}(\boldsymbol{\theta}) < \epsilon|\boldsymbol{\theta})$. Comparing this to Bayes' theorem, we can see that $\Pr(\mathcal{D}(\boldsymbol{\theta}) < \epsilon|\boldsymbol{\theta})$ plays the role of the likelihood. Therefore, $L(\boldsymbol{\theta}) := \Pr(\mathcal{D}(\boldsymbol{\theta}) < \epsilon|\boldsymbol{\theta})$ is an approximation of $\mathcal{L}(\boldsymbol{\theta})$ (up to some proportionality constant). In reality, we do not know the distribution of $\mathcal{D}(\boldsymbol{\theta})$ for all $\boldsymbol{\theta}$, but we consider methods to construct an approximation $\hat{L}$ of L, which we call the synthetic likelihood. The approximation considered is achieved by modelling $\mathcal{D}(\boldsymbol{\theta})$ using a surrogate model, which we introduce in this chapter.

5.1 Gaussian Processes

For $\boldsymbol{\theta}$ and $\boldsymbol{\theta}'$ that are close to each other, the distribution of $\mathcal{D}(\boldsymbol{\theta})$ will be similar to the distribution of $\mathcal{D}(\boldsymbol{\theta}')$. Therefore sampling from $\mathcal{D}(\boldsymbol{\theta})$ gives information about the distribution of $\mathcal{D}(\boldsymbol{\theta}')$ for $\boldsymbol{\theta}$, $\boldsymbol{\theta}'$ close. A reasonable assumption could be that $\mathbb{E}(\mathcal{D}(\boldsymbol{\theta}_1)), \mathbb{E}(\mathcal{D}(\boldsymbol{\theta}_2)), \ldots, \mathbb{E}(\mathcal{D}(\boldsymbol{\theta}_n))$ are multivariate normally distributed with $\text{cov}(E(\mathcal{D}(\boldsymbol{\theta}_1)), E(\mathcal{D}(\boldsymbol{\theta}_2)))$ large for $\boldsymbol{\theta}_1, \boldsymbol{\theta}_2$ close, and small for $\boldsymbol{\theta}_1, \boldsymbol{\theta}_2$ far apart, so that $\text{cov}(E(\mathcal{D}(\boldsymbol{\theta}_1)), E(\mathcal{D}(\boldsymbol{\theta}_2)))$ is a function of $\boldsymbol{\theta}_1$ and $\boldsymbol{\theta}_2$. Formally, we treat $\mathbb{E}(\mathcal{D}(\beta))$ as a realisation of a Gaussian process.

Definition 5.1 (Gaussian Process)**.** *A collection of random variables $\{f(x)\}_{x\in\mathcal{X}}$ (where x may be a vector) is a* **Gaussian process** *if any finite subset of the collection of random variables is multivariate normal distributed. That is, there is a function $m : \mathcal{X} \to \mathbb{R}$ and symmetric kernel $k : \mathcal{X} \times \mathcal{X} \to \mathbb{R}$ such that for all finite sets $\mathbf{x} := \{x_1, x_2, \ldots, x_n\} \subset \mathcal{J}$, with $f(\mathbf{x}) := [f(x_1), f(x_2), \ldots, f(x_n)]^T$*

$$f(\mathbf{x}) \sim \text{MVN}\left(\begin{bmatrix} m(x_1) \\ m(x_2) \\ \vdots \\ m(x_n) \end{bmatrix}, \mathbf{K} = \begin{bmatrix} k(x_1,x_1) & k(x_1,x_2) & \ldots & k(x_1,x_n) \\ k(x_2,x_1) & \ddots & & \vdots \\ \vdots & & \ddots & \vdots \\ k(x_n,x_1) & \cdots & \cdots & k(x_n,x_n) \end{bmatrix}\right).$$

Definition 5.2 (Mean Function and Covariance Kernel)**.** *The* **mean function** *and* **covariance kernel** *are*

$$m(x_i) := \mathbb{E}\left[f(x_i)\right]$$

and

$$k(x_i, x_{i'}) := \mathrm{cov}\left(f(x_i), f(x_{i'})\right).$$

Gaussian processes are simultaneously realised over the whole space $\mathcal{X}$ (for example $\mathbb{R}^d$) and are hence collections of (uncountably infinite) random variables. However, the covariance function k is always constructed such that $\mathrm{corr}(x, x') \to 1$ as $||x - x'|| \to 0$. This induces a form of continuity in x called mean square continuity which is defined in Definition 5.4 The most famous example of a Gaussian process is Brownian motion.

Definition 5.3 (Brownian Motion)**.** $B(t) : \mathbb{R}^+ \to \mathbb{R}$ *is a* **Brownian motion** *on* $\mathbb{R}$ *if*

1. $B(0) = 0$ *almost surely*
2. $B(t_0), B(t_1) - B(t_0), \ldots, B(t_n - t_{n-1})$ *are independent for all* $t_0 < t_1 < t_2 < \cdots < t_n$
3. $B(t + s) - B(t) \sim N(0, s)$ *for* $s, t \geq 0$
4. $B(t)$ *is continuous almost surely for* $t > 0$.

Brownian motion has zero mean, and covariance kernel $k(s, t) = \min(s, t)$, which implies that $\mathrm{corr}(B_s, B_t) = \frac{\min(s,t)}{\sqrt{st}}$. This is close to 1 as s is close to t, however as $|s - t| \to \infty$, $\mathrm{corr}(B_s, B_t) \to 0$.

Gaussian processes can be considered as giving a probability distribution to functions $f \in \mathcal{F}$, where $\mathcal{F}$ is a class of functions. The properties of the class of functions $\mathcal{F}$ depend on the covariance kernel k. Different k result in very different functions. One such property to consider is the smoothness of the functions, which we describe by mean square differentiability.

Definition 5.4 (Mean Square Continuous)**.** *A function* $f : \mathbb{R}^d \to \mathbb{R}$ *is* **mean square continuous** *at* $\mathbf{x}$ *in the* i*th direction at* $\mathbf{x}$ *if* $\mathbb{E}(|f(\mathbf{x} + h\mathbf{e}_i) - f(\mathbf{x})|^2) \to 0$ *as* $|h| \to 0$*, where* $\mathbf{e}_i$ *is the unit vector with a 1 in the* i*th coordinate.*

Definition 5.5 (Mean Square Differentiable)**.** *A function* $f : \mathbb{R}^d \to \mathbb{R}$ *is* **mean square differentiable** *at* $\mathbf{x}$ *in the* i*th direction with derivative* $\frac{\partial f(\mathbf{x})}{\partial x_i}$ *if*

$$\mathbb{E}\left[\left|\frac{f(\mathbf{x} + h\mathbf{e}_i) - f(\mathbf{x})}{h} - \frac{\partial f(\mathbf{x})}{\partial x_i}\right|^2\right] \to 0$$

as $|h| \to 0$*, where* $\mathbf{e}_i$ *is the unit vector in the direction of the* i*th coordinate.*

The concept of mean square differentiability and continuity are analogous to differentiability and continuity in the non-random function case.

Theorem 5.6. *Brownian motion is mean square continuous, but not mean square differentiable.*

Proof. $(B_{t+h} - B_t)^2 \sim (\sqrt{|h|}Z)^2$ where $Z \sim N(0, 1)$. Therefore $(B_{t+h} - B_t)^2 \sim |h|\chi_1^2 \to 0$ almost surely as $|h| \to 0$, hence $\mathbb{E}[(B_{t+h} - B_t)^2] = 0$, and so Brownian motion is mean square continuous. Since $\frac{B_{t+h} - B_t}{h} \sim N(0, 1/|h|)$, $\frac{B_{t+h} - B_t}{h}$ does not converge to any valid probability distribution as $|h| \to 0$, as the variance approaches $+\infty$, and so Brownian motion is not mean square differentiable. □

Kernels

Matérn Kernel Family

Since we are motivated to consider $\mathbb{E}(\mathcal{D}(\boldsymbol{\theta}))$ as a realisation of a Gaussian process, we consider some common choices of kernel function and their effect on the Gaussian process realisations. The two most common families of kernel functions are the squared exponential and Matérn families (Rasmussen and Williams 2008). The Matérn kernel explicitly allows for adjustment of function smoothness through a hyperparameter ν.

Definition 5.7 (Matérn Kernel)**.** *The* **Matérn kernel** *is covariance kernel function of the form*

$$k_\nu(x, x') = \sigma_k^2 \frac{2^{1-\nu}}{\Gamma(\nu)} \left(\frac{\sqrt{2\nu}||x - x'||}{\ell} \right)^\nu K_\nu \left(-\frac{\sqrt{2\nu}||x - x'||}{\ell} \right),$$

where K_ν is a modified Bessel function (defined in Abramowitz and Stegun 2013, p. 374). ν, ℓ, and σ_k are hyperparameters.

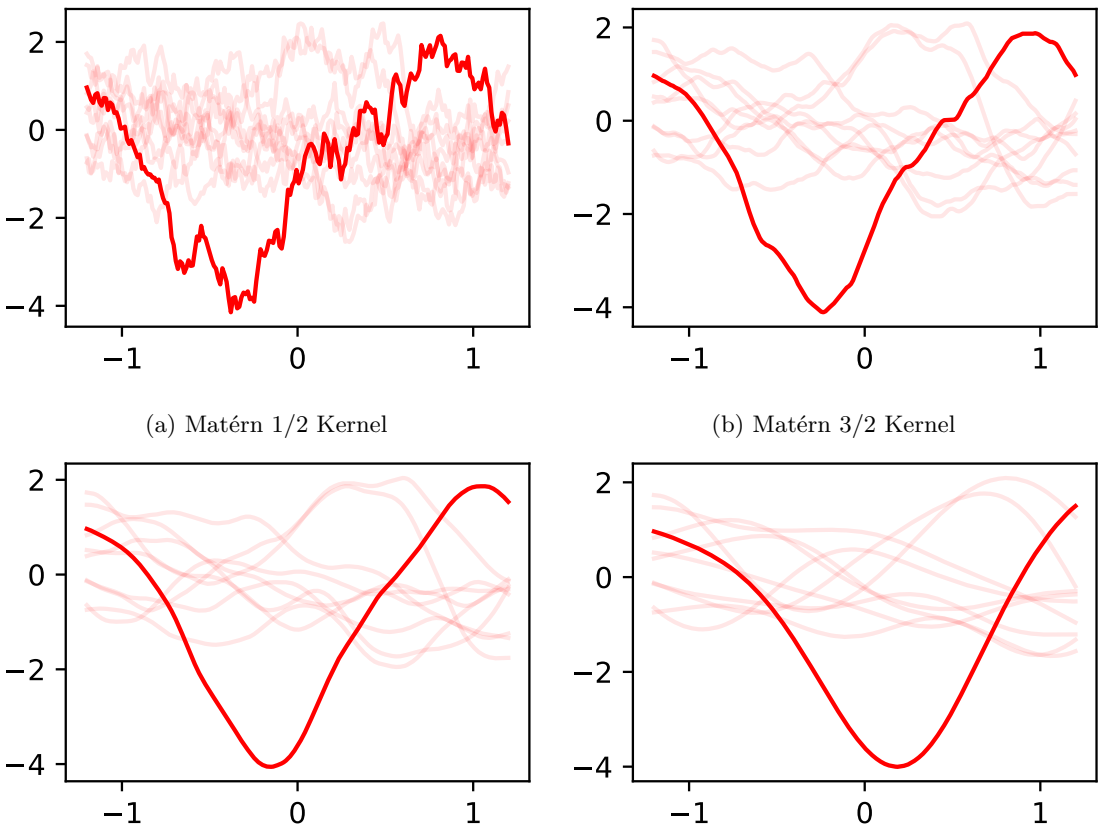

(a) Matérn 1/2 Kernel

(b) Matérn 3/2 Kernel

(c) Matérn 5/2 Kernel

(d) Squared Exponential Kernel

Figure 5.1: Ten sample realisations from 4 different kernels, with one realisation bolded. Samples for each kernel were generated from the same seed and the hyperparameters ℓ, and σ_k were set to 1.

Realisations from zero-mean Gaussian processes with this kernel are $\lfloor \nu \rfloor$ times mean square differentiable (Rasmussen and Williams 2008). The most common values for ν are $1/2, 3/2$ and

5/2, which result in functions that are 0, 1, and 2 times mean square differentiable. In these cases the kernel can be slightly simplified to:

$$k_{1/2}(x, x') = \sigma_k^2 \exp\left(-\frac{||x - x'||}{\ell}\right),$$

$$k_{3/2}(x, x') = \sigma_k^2 \left(1 + \frac{\sqrt{3}||x - x'||}{\ell}\right) \exp\left(-\frac{\sqrt{3}||x - x'||}{\ell}\right),$$

and

$$k_{5/2}(x, x') = \sigma_k^2 \left(1 + \frac{\sqrt{5}||x - x'||}{\ell} + \frac{5||x - x'||}{3\ell^2}\right) \exp\left(-\frac{||x - x'||^2}{2 * \ell^2}\right).$$

The increasing smoothness of these kernels can be see in Figures 5.1a, 5.1b, and 5.1c.

Zero-mean Gaussian processes with a Matérn kernel are n times mean square differentiable, for all $n < \nu$. As seen in Figure 5.1, this means that this kernel allows for flexibility in how smooth realised functions are.

Squared Exponential Kernel

As $\nu \to \infty$, the Matérn kernel converges to a kernel which we call the squared exponential kernel (Rasmussen and Williams 2008, p. 85).

Definition 5.8 (Squared Exponential Kernel)**.** *The* **squared exponential kernel** *is a covariance kernel with the form*

$$k(x, x') = \sigma_k^2 \exp\left(-\frac{||x - x'||^2}{2\ell^2}\right).$$

σ_k^2 and ℓ are hyperparameters.

By construction, the squared exponential kernel is infinitely mean square differentiable, which can visually be seen in 5.1d. Despite this being the 'default' kernel in much of the literature (for example Gutmann and Cor 2016), infinite differentiability is a very strong condition that may not be appropriate in all circumstances.

Length and Amplitude Hyperparameters

In both the Matérn and squared exponential kernels (as well as most other common kernel choices), there are two hyperparameters ℓ and σ_k^2, which are referred to as length and amplitude hyperparameters. ℓ determines how close two points need to be to be highly correlated. Larger values of ℓ generates functions with higher correlation within a larger neighbourhood, as seen in Figure 5.2. σ_k^2 does not impact the correlation between x and x', but scales the correlation matrix. In other words, larger σ_k^2 increases the size but not the rate of fluctuations. This can be seen comparing Figure 5.2a to Figure 5.2b.

Other kernels exist and are used in the literature. Here we briefly discuss when $k(x, x')$ is a valid kernel. We need the formal notions of symmetry and positive semi-definite.

Definition 5.9 (Symmetric)**.** *A (square) matrix* $\mathbf{A}$ *is* **symmetric** *if* $A = A^T$.

Definition 5.10 (Positive Semi-Definite)**.** *An* $n \times n$ *matrix* $\mathbf{A}$ *is* **positive semi-definite** *if* $\mathbf{v}^T\mathbf{A}\mathbf{v} \geq 0$ *for all* $\mathbf{v} \in \mathbb{R}^n$.

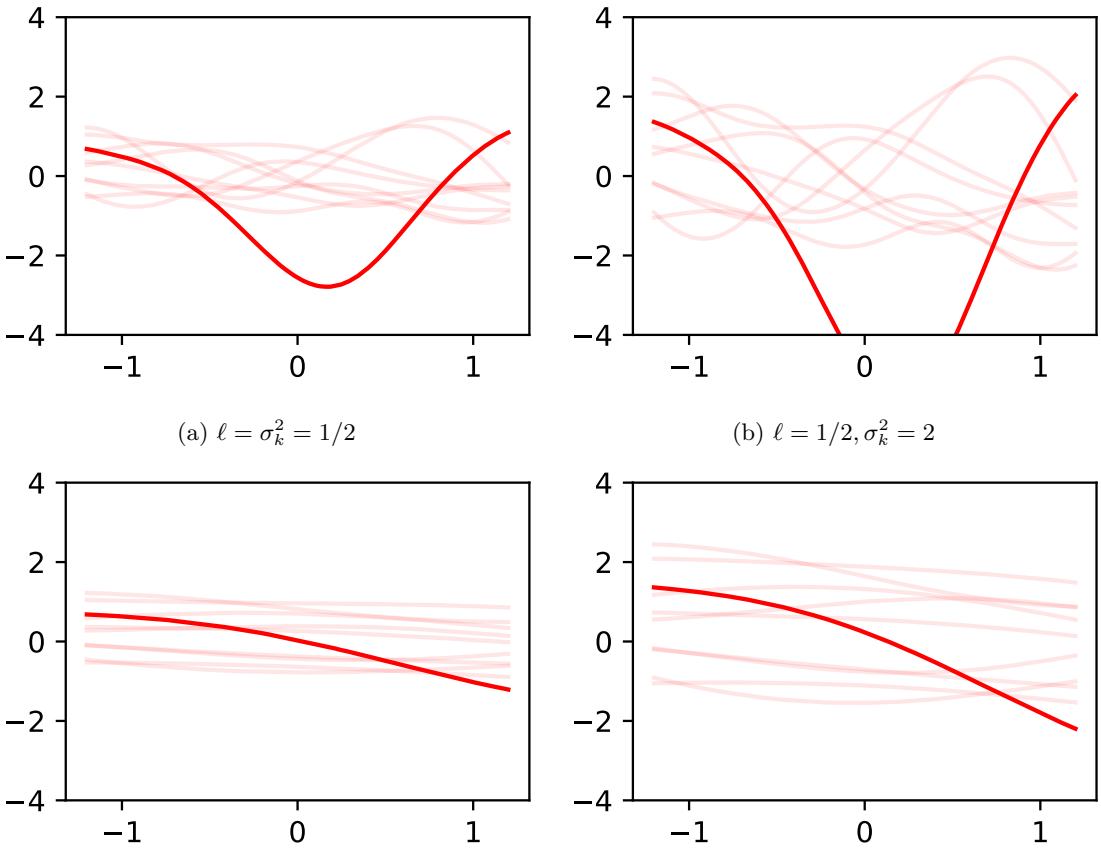

(a) $\ell = \sigma_k^2 = 1/2$

(b) $\ell = 1/2, \sigma_k^2 = 2$

(c) $\ell = 2, \sigma_k^2 = 1/2$

(d) $\ell = \sigma_k^2 = 2$

Figure 5.2: Ten realisations of zero-mean Gaussian processes with the squared exponential kernel, varying the length and amplitude parameters. The samples were generated using the same seed

Theorem 5.11. *Any kernel k is admissible if the gram matrix*

$$\mathbf{K} = \begin{bmatrix} k(x_1, x_1) & k(x_1, x_2) & \dots & k(x_1, x_n) \\ k(x_2, x_1) & \ddots & & \vdots \\ \vdots & & \ddots & \vdots \\ k(x_n, x_1) & \cdots & \cdots & k(x_n, x_n) \end{bmatrix}$$

associated with k is symmetric and positive semi-definite for all choices of $(x_1, \dots, x_n)$, for finite n.

Theorem 5.12. *The Matérn kernel and squared exponential kernels are admissible.*

Proof. The proof of the above two theorems are beyond the scope of this thesis, and involves analysis of spectral densities. See Rasmussen and Williams 2008, chapter 4 for more details. □

5.2 Gaussian Process Regression

Given a realisation of a Gaussian process f, observed at the set of indices $\mathbf{x}^*$, we can make inferences on unobserved indices $\mathbf{x}$ by considering the Gaussian process conditioned on $f(\mathbf{x}^*)$. Since f is a realisation of a Gaussian process, the distribution of $f(\mathbf{x})|f(\mathbf{x}^*)$ reduces to linear algebra and has a multivariate normal distribution.

Theorem 5.13 (Conditional Multivariate Normal Distribution is Multivariate Normal)**.** *If*

$$\begin{bmatrix} f(\mathbf{x}) \\ f(\mathbf{x}^*) \end{bmatrix} \sim \text{MVN}\left(\begin{bmatrix} m(\mathbf{x}) \\ m(\mathbf{x}^*) \end{bmatrix}, \begin{bmatrix} K & K^* \\ (K^*)^T & K^{**} \end{bmatrix} \right),$$

then

$$f(\mathbf{x})|f(\mathbf{x}^*) \sim \text{MVN}\left(m(\mathbf{x}) + K^*(K^{**})^{-1}(f(\mathbf{x}^*) - m(\mathbf{x}^*)),\ K - K^*(K^{**})^{-1}(K^*)^T\right).$$

Proof. Since marginal distribution of the multivariate normal distribution, is also multivariate normal, $f(\mathbf{x}^*) \sim \text{MVN}(m(\mathbf{x}^*), K)$. Let the inverse of $\begin{bmatrix} K & K^* \\ (K^*)^T & K^{**} \end{bmatrix}$ be

$$\begin{bmatrix} \tilde{K} & \tilde{K}^* \\ (\tilde{K}^*)^T & \tilde{K}^{**} \end{bmatrix}$$

where

$$\begin{aligned} \tilde{K} &:= (K - K^*(K^{**})^{-1}(K^*)^T)^{-1} \\ \tilde{K}^* &:= -(K - K^*(K^{**})^{-1}(K^*)^T)^{-1}K^*(K^{**})^{-1} \\ \tilde{K}^{**} &:= (K^{**})^{-1} + (K^{**})^{-1}(K^*)^T(K - K^*(K^{**})^{-1}(K^*)^T)^{-1}K^*(K^{**})^{-1} \end{aligned}$$

by the inverse of a block matrix. Therefore

$$\begin{aligned}
p(f(\mathbf{x})|f(\mathbf{x}^*)) =& \frac{p(f(\mathbf{x}), f(\mathbf{x}^*))}{p(f(\mathbf{x}^*))} \\
\propto& \frac{\exp\left[-\frac{1}{2}\left(\begin{bmatrix} f(\mathbf{x}) \\ f(\mathbf{x}^*) \end{bmatrix} - \begin{bmatrix} m(\mathbf{x}) \\ m(\mathbf{x}^*) \end{bmatrix}\right)^{\mathrm{T}} \begin{bmatrix} K & K^* \\ (K^*)^T & K \end{bmatrix}^{-1} \left(\begin{bmatrix} f(\mathbf{x}) \\ f(\mathbf{x}^*) \end{bmatrix} - \begin{bmatrix} m(\mathbf{x}) \\ m(\mathbf{x}^*) \end{bmatrix}\right)\right]}{\exp\left[-\frac{1}{2}(f(\mathbf{x}^*) - m(\mathbf{x}^*))^{\mathrm{T}}(K^{**})^{-1}(f(\mathbf{x}^*) - m(\mathbf{x}^*))\right]} \\
=& \exp\left[-\frac{1}{2}\left(\begin{bmatrix} f(\mathbf{x}) \\ f(\mathbf{x}^*) \end{bmatrix} - \begin{bmatrix} m(\mathbf{x}) \\ m(\mathbf{x}^*) \end{bmatrix}\right)^{\mathrm{T}} \begin{bmatrix} K & K^* \\ (K^*)^T & K^{**} \end{bmatrix}^{-1} \left(\begin{bmatrix} f(\mathbf{x}) \\ f(\mathbf{x}^*) \end{bmatrix} - \begin{bmatrix} m(\mathbf{x}) \\ m(\mathbf{x}^*) \end{bmatrix}\right)\right. \\
& \left. + \frac{1}{2}(f(\mathbf{x}^*) - m(\mathbf{x}^*))^{\mathrm{T}}(K^{**})^{-1}(f(\mathbf{x}^*) - m(\mathbf{x}^*))\right] \\
=& \exp\left[-\frac{1}{2}\left((f(\mathbf{x}) - m(\mathbf{x}))^{\mathrm{T}}\tilde{K}(f(\mathbf{x}) - m(\mathbf{x}))\right.\right. \\
& + 2(f(\mathbf{x}) - m(\mathbf{x}))^{\mathrm{T}}\tilde{K}^*(f(\mathbf{x}^*) - m(\mathbf{x}^*)) \\
& \left.\left. + (f(\mathbf{x}^*) - m(\mathbf{x}^*))^{\mathrm{T}}\tilde{K}^{**}(f(\mathbf{x}^*) - m(\mathbf{x}^*))\right) \right. \\
& \left. + \frac{1}{2}(f(\mathbf{x}^*) - m(\mathbf{x}^*))^{\mathrm{T}}(K^{**})^{-1}(f(\mathbf{x}^*) - m(\mathbf{x}^*))\right] \\
\propto& \exp\left[-\frac{1}{2}(f(\mathbf{x}) - m(\mathbf{x}))^{\mathrm{T}}\tilde{K}(f(\mathbf{x}) - m(\mathbf{x}))\right. \\
& \left. - (f(\mathbf{x}) - m(\mathbf{x}))^{\mathrm{T}}\tilde{K}^*(f(\mathbf{x}^*) - m(\mathbf{x}^*))\right]. \\
& \qquad \text{(by removing the terms independent of } f(\mathbf{x}))
\end{aligned}$$

Since

$$p(\mathbf{z}) \propto \exp\left(-\frac{1}{2}\mathbf{z}^T\Sigma^{-1}\mathbf{z} + \mathbf{z}^T\mathbf{c}\right) \implies \mathbf{z} \sim \mathrm{MVN}\left(\Sigma\mathbf{c}, \Sigma\right),$$

$f(\mathbf{x}) - m(\mathbf{x})|f(\mathbf{x}^*)$ is multivariate normal with mean

$$\begin{aligned}
-\tilde{K}^{-1}\tilde{K}^*(f(\mathbf{x}^*) - m(\mathbf{x}^*)) =& (K - K^*(K^{**})^{-1}(K^*)^T) \\
& \times (K - K^*(K^{**})^{-1}(K^*)^T)^{-1}K^*(K^{**})^{-1}(f(\mathbf{x}^*) - m(\mathbf{x}^*)) \\
=& K^*(K^{**})^{-1}(f(\mathbf{x}^*) - m(\mathbf{x}^*))
\end{aligned}$$

and covariance matrix

$$\tilde{K}^{-1} = K - K^*(K^{**})^{-1}(K^*)^T$$

by the alternative parameterisation of the multivariate normal distribution as a member of the exponential family of distributions (see Wikipedia contributors 2024, Table of Distributions). Finally, by the linearity of the multivariate normal mean,

$$f(\mathbf{x})|f(\mathbf{x}^*) \sim \mathrm{MVN}\left(m(\mathbf{x}) + K^*(K^{**})^{-1}(f(\mathbf{x}^*) - m(\mathbf{x}^*)),\ K - K^*(K^{**})^{-1}(K^*)^T\right).$$

□

We can use this to fit a Gaussian process to set of indices $\mathbf{x}^*$ with observations $f(\mathbf{x}^*)$. This can be used in an iterative process where $f(x)$ may be expensive to compute and by treating f as a Gaussian process realisation, the function can be probabilistically interpolated for unobserved

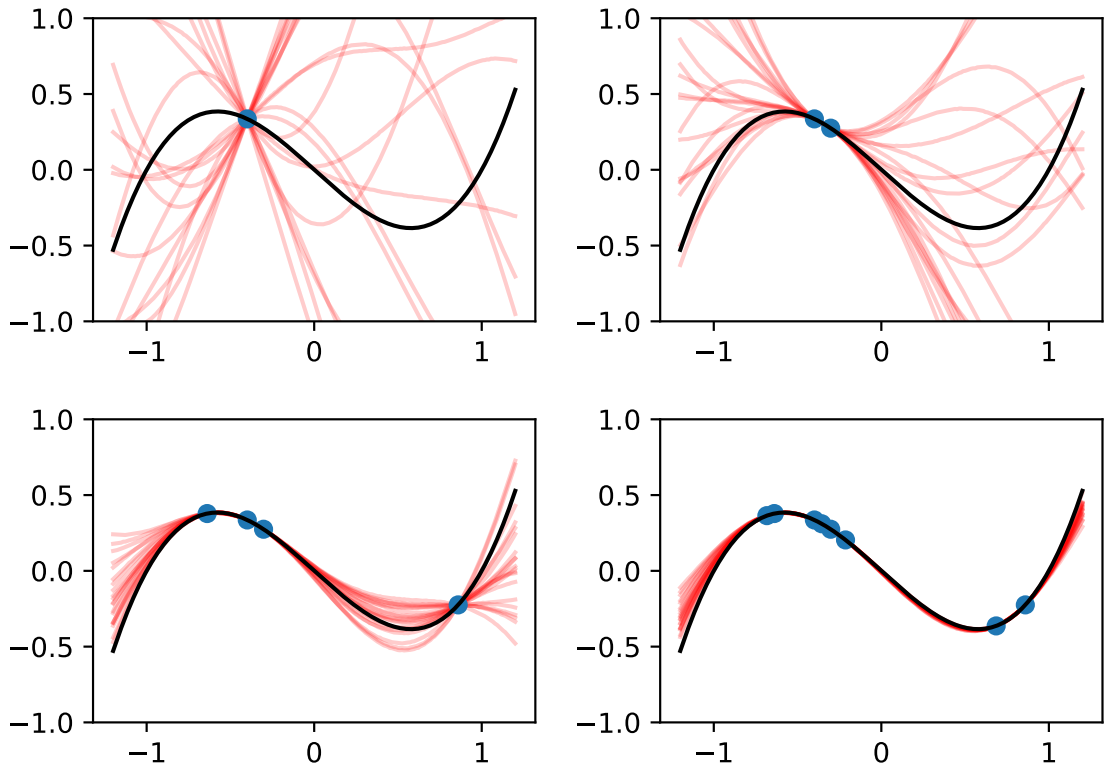

Figure 5.3: Sequence of Gaussian process regressions on the target function (black) $f(x) = x(x-1)(x+1)$, after 1, 2, 4, and 8 observations in blue. The red lines are new realisations from the conditioned Gaussian process. The Gaussian process was zero-mean and had a squared exponential kernel. The hyperparameters were fixed with $\ell = 2.7$ and $\sigma_k^2 = 1.1$.

$f(x)$. Figure 5.3 empirically demonstrates that as the number of points that the Gaussian process is conditioned on increases, the variance in the sample paths decreases.

Observation Variance

For most functions, model outputs, or processes desirable for approximating through Gaussian process regression, it may not be possible to observe $f(\mathbf{x})$ directly, but observations may be noisy. The simplest assumption is that the observations are of the form

$$f_o(\mathbf{x}^*) = f(\mathbf{x}^*) + \varepsilon$$

where $\varepsilon \sim \text{MVN}(\mathbf{0}, \sigma_o^2 I)$. Under these assumptions, $\text{Cov}(f_o(\mathbf{x}^*), f_o(\mathbf{x}^*)) = K^{**} + \sigma_o^2 I$, where $K^{**} = \text{Cov}(f(\mathbf{x}^*), f(\mathbf{x}^*))$ matrix of $f(\mathbf{x}^*)$ without noise. Therefore the conditional distribution of our unobserved function outputs given noisy observations

$$f(\mathbf{x})|f_o(\mathbf{x}^*) \sim \text{MVN}\left(m(\mathbf{x}) + K^*(K^{**} + \sigma_o^2 I)^{-1}(f(\mathbf{x}^*) - m(\mathbf{x}^*)),\ K - K^*(K^{**} + \sigma_o^2 I)^{-1}(K^*)^T\right).$$

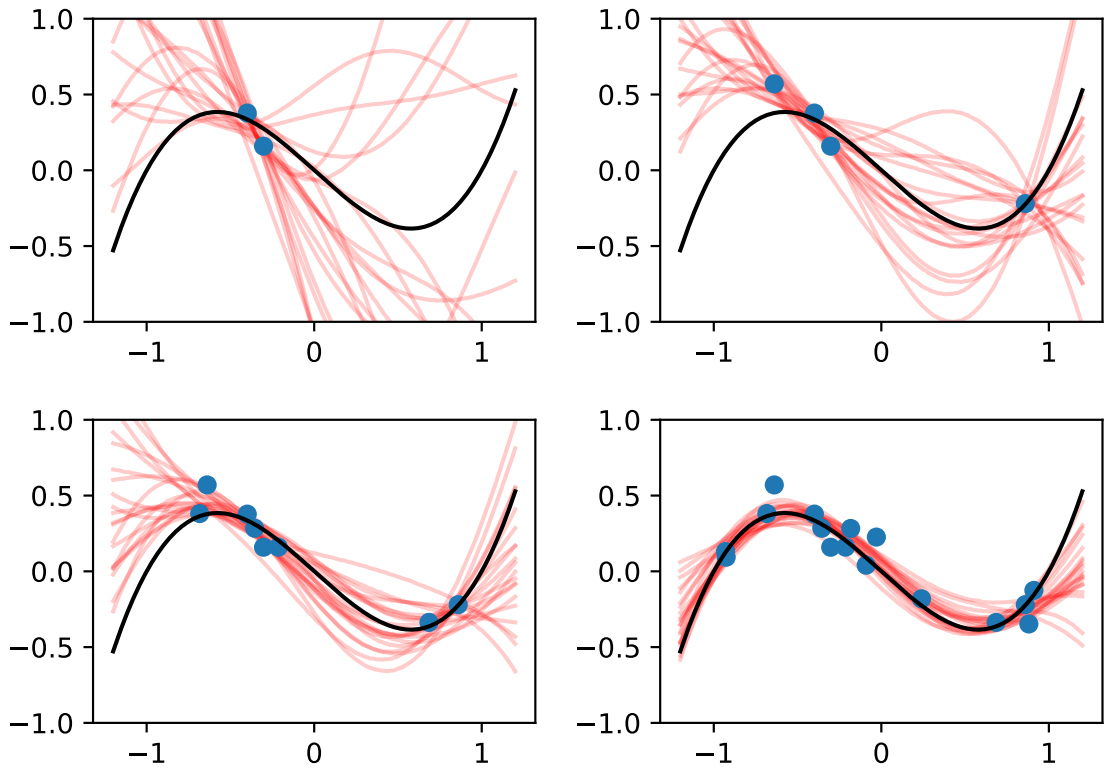

Figure 5.4: Sequence of Gaussian process regressions on the target function (black) $f(x) = x(x-1)(x+1)$, after 2, 4, 8, and 16 observations of $f(x_i)+\varepsilon_i$, where ε_i is i.i.d. $\text{MVN}(0, \sigma_o^2)$ with $\sigma_o^2 = 0.01$ in blue. The red lines are new realisations from the conditioned Gaussian process. The Gaussian process was 0 mean and had a squared exponential kernel. The hyperparameters were fixed with $\ell = 2.7$ and $\sigma_k^2 = 1.1$.

The observations $f_o(\mathbf{x}^*)$ contain less information than when $f(\mathbf{x}^*)$ is directly observed, and hence interpolating to $\mathbf{x}$ or even $\mathbf{x}^*$ naturally has a greater degree of uncertainty as seen in Figure 5.4.

5.3 Model Selection

After deciding to use a Gaussian process to approximate a function, there is still a variety of choices that need to be made, particularly regarding the covariance kernel. The first choice needs to be the class of kernel used.

Kernel

The appropriate choice of kernel will depend on the properties of the target function f to be regressed to. In the case of estimating an extremely stochastic distribution (such as the price of a stock over time), a kernel with a high degree of mean square differentiability would be inappropriate. On the other hand a Matérn 1/2 kernel may be appropriate, since it is not mean square differentiable. If it is known that the target function is smooth, such as a polynomial function or $\sin(x)$, then the choice of squared exponential kernel is the most appropriate kernel.

Hyperparameters

The kernel hyperparameters ℓ and σ_k^2 are generally not fixed *a priori*. Similarly, the observation variance σ_o^2 may not be known. There are two main (frequentist) ways to fit these hyperparameters: maximum likelihood estimation, and leave-one-out cross validation.

Defining the likelihood $\mathcal{L}(\ell, \sigma_k^2, \sigma_o^2) := p(f(\mathbf{x}^*)|\ell, \sigma_k^2, \sigma_o^2)$ in the usual way, the maximum likelihood estimates are

$$\{\hat{\ell}, \hat{\sigma}_k^2, \hat{\sigma}_o^2\} := \underset{\{\ell, \sigma_k^2, \sigma_o^2\}}{\arg\max}\, \mathcal{L}(\ell, \sigma_k^2, \sigma_o^2) \tag{5.1}$$

which is equivalent to minimising

$$-\ln(\mathcal{L}) = \frac{1}{2}\left[\ln(|K^{**}(\ell, \sigma_k^2) + \sigma_o^2|\,) + (f(\mathbf{x}^*) - m(\mathbf{x}^*))^T (K^{**}(\ell, \sigma_k^2) + \sigma_o^2)^{-1} (f(\mathbf{x}^*) - m(\mathbf{x}^*)) + c\right].$$

The covariance matrix generated by the choice of kernel K^{**} is explicitly written with its dependence on ℓ and σ_k^2. Here c is a constant.

Leave-one-out cross validation aims to maximise the predictive log probability:

$$\{\tilde{\ell}, \tilde{\sigma}_k^2, \tilde{\sigma}_o^2\} := \underset{\ell, \sigma_k^2, \sigma_o^2}{\arg\max} \sum_i \ln p(f_i(\mathbf{x}^*)|f_{-i}(\mathbf{x}^*), \ell, \sigma_k^2, \sigma_o^2), \tag{5.2}$$

where $f_i(\mathbf{x}^*)|f_{-i}(\mathbf{x}^*)$ is the distribution of the ith element of $f(\mathbf{x}^*)$ conditioned on the rest of the observed data excluding that element (represented by $f_{-i}(\mathbf{x}^*)$). $f_i(\mathbf{x}^*)|f_{-i}(\mathbf{x}^*)$ can be found by Theorem 5.13. Computationally efficient methods for calculating the predictive log probability (Equation 5.2) that avoid having to invert the covariance matrix for every summand element exist. In particular it can be shown that $f_i(\mathbf{x}^*)|f_{-i}(\mathbf{x}^*)$ has mean

$$f_i(\mathbf{x}^*) - m_i(\mathbf{x}^*) - [(K^{**} + \sigma_o^2 I)^{-1}(f(\mathbf{x}^*) - m(\mathbf{x}^*))]_i / [(K^{**} + \sigma_o^2 I)^{-1}]_{ii}$$

and variance $1/[(K^{**} + \sigma_o^2 I)^{-1}]_{ii}$, where both the mean and covariance are (surprisingly) independent of $f_i(\mathbf{x}^*)$ (Rasmussen and Williams 2008, p. 116).

Recent work has shown that at least under specific conditions, the leave-one-out estimates for the scale hyperparameter are more robust to a larger family of target functions (Naslidnyk et al.

2024), and the broader literature seems to favor leave-one-out cross validation (for example see Gutmann and Cor 2016).

Finally there is scope for a Bayesian approach to model selection. By setting priors on the hyperparameters (sometimes called hyper-priors) and using the likelihood as described in the maximum likelihood estimation approach (Equation 5.1), a posterior distribution can be contrived. Samples could then be taken from the posterior density of the hyperparameters. Alternatively a point estimate could be drawn by choosing the maximum a posteriori estimate (i.e. the mode of the posterior density). Posterior samples of the hyperparameters, can then capture some of the model fit uncertainty, unlike in a point estimate.

Mean Functions

Although in the majority of use cases for Gaussian processes, the mean function is assumed to be zero, it is not necessary for this to be the case. In cases where the discrepancy function has been estimated by a Gaussian process, the mean function has been assumed to be quadratic, such as in (Gutmann and Cor 2016). Gaussian process regression is relatively resilient to misspecified mean function in areas with samples. However, the regression will return to the behaviour of the mean function where there are no points to regress to.

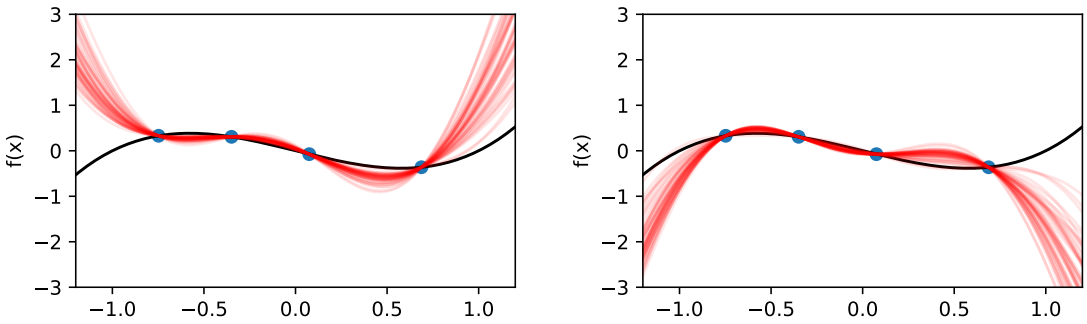

Figure 5.5: Gaussian process regressions on the target function (black) $f(x) = x(x-1)(x+1)$, 4, observations of $f(x_i)$ in blue. The left Gaussian process had mean function $3x^2$, and the right Gaussian process had mean function $-3x^2$. The red lines are new realisations from the conditioned Gaussian process.

This can be seen in Figure 5.5. Around the observed data in blue, the processes have similar predictions for the function, however outside of where the function has been observed, both Gaussian processes return to their quadratic mean functions. Specifying a mean for the Gaussian process may be appropriate, but it must be done with caution.

5.4 Bayesian Acquisition Functions

Gaussian processes may be a useful approximation of $\mathbb{E}[\mathcal{D}(\boldsymbol{\theta})]$. We can express the Gaussian process surrogate model as $\mathcal{D}_{\mathcal{GP}}(\boldsymbol{\theta})$, trained on samples of $\mathcal{D}(\boldsymbol{\theta})$. Considering the approximate Bayesian computation described in Algorithm 7, samples are only accepted when $\mathcal{D}(\boldsymbol{\theta})$ is small. Therefore we care most about accurately approximating $\mathcal{D}(\boldsymbol{\theta})$ where $\mathbb{E}[\mathcal{D}(\boldsymbol{\theta})]$ is small since the probability of acceptance elsewhere is negligible. Therefore we focus our model sampling where we predict the Gaussian process is small, or where the variance of the Gaussian process is large (hence the

true values are highly uncertain), to avoid unnecessary model runs that may be extremely time-consuming.

These ideas are formalised by Bayesian acquisition functions $\mathcal{A}(\boldsymbol{\theta})$ which describe the desirability of sampling from $\boldsymbol{\theta}$ as a combination of low posterior mean and uncertainty.

Lower Confidence Bound

The lower confidence bound acquisition function is a calculation of the lower bound of the confidence interval of the regressed Gaussian process. It is a function of both the posterior mean and variance, weighted according to a constant η.

Definition 5.14 (Lower Confidence Bound)**.** *The* **lower confidence bound** *of a Gaussian process f at x given some observations $\mathbf{x}^*$ is*

$$\mathcal{A}_{\text{LCB}}(x) := \mathbb{E}[f(x)|f(\mathbf{x}^*)] - \eta\sqrt{\text{Var}[f(x)|f(\mathbf{x}^*)]}.$$

For example, when $\eta = 1.96$, $\mathcal{A}_{\text{LCB}}(x)$ returns the lower bound of the 95% confidence interval at x. In problems where a global minimum is to be estimated, and where f is regressed on realisations of a model, the next point to sample from the model would then be chosen $\arg\min_x A_{\text{LCB}}(x)$. Larger η will prioritise exploration of the space of x, whereas small η will continue to sample around areas of confirmed low mean.

η can also be replaced by $\eta(t)$, where t is the number of points that have been regressed on. Generally $\eta(t)$ is chosen to be an increasing function, so that exploration is given more weight over time. Some theoretical results regarding optimal choice of $\eta(t)$ are given in Srinivas et al. 2010, and are highly dependent on the choice of covariance function and dimensionality of the parameter space.

Probability of Improvement

The probability of improvement is simply a measure of how probable it is that an observation at x is better than the previous best observation.

Definition 5.15. *The* **probability of improvement** *of a Gaussian process f at x given some observations $\mathbf{x}^*$ is*

$$\mathcal{A}_{\text{PI}}(x) := \Pr(f(x) < \mu^*),$$

where $\mu^* := \min_{x^* \in \mathbf{x}^*} f(x^*)$.

Unlike the lower confidence bound, we choose $\arg\max_x A_{\text{PI}}(x)$, as the point which is most likely to better than our current best.

The probability of improvement can also be expressed as

$$\mathcal{A}_{\text{PI}}(x) = \Pr(\min(f(x) - \mu^*, 0) < 0),$$

which motivates the form of the next acquisition function.

Expected Improvement

A similar acquisition function to the probability of improvement is the expected improvement function. Rather than returning a the probability that $f(x)$ is better (lower) than the current

best, it also takes into account how large that improvement is likely to be.

Definition 5.16. *The* **expected improvement** *of a Gaussian process f at x given some observations $\mathbf{x}^*$ is*

$$\mathcal{A}_{\mathrm{EI}}(x) := \mathbb{E}[\min(f(x) - \mu^*, 0)],$$

where $\mu^* := \min_{x^* \in \mathbf{x}^*} f(x^*)$.

The next point to be sampled from $\arg\min_x A_{\mathrm{EI}}(x)$ is the point where we expect μ^* to have the largest improvement, if it is indeed improved. [1] Both the probability of improvement and expected improvement do not require a choice of hyperparameter such as η, but more exploration can be encouraged by slightly altering the probability of improvement to $\Pr(f(x) < \mu^* + \epsilon)$, and the expected improvement to $\mathbb{E}[\min(f(x) - (\mu^* + \epsilon), 0)]$. ϵ allows for new samples to be ϵ worse (larger) than the current best sample. This is beneficial in the case where finding the exact global minimum may not be the target, but rather exploring areas close to the minimum.

[1] Bayesian acquisition functions are conventionally employed to find the maximum of an unknown function, and so generally, the expected improvement is maximised. However, in the context of $\mathcal{D}_{\mathcal{GP}}(\boldsymbol{\theta})$, we want to find the minimum. Therefore we have reframed the expected improvement as a function to be minimised.

Part II

Calibrating Parameters for a *P. vivax* Model

Chapter 6

Methods

We now develop a method for calibrating model parameters for a *P. vivax* model. In order to validate the method, we will create a simulation study. This is where we simulate our observed data from the model and then use that data to recover the parameters used in creating our observed data.

6.1 Creation of Simulated Data

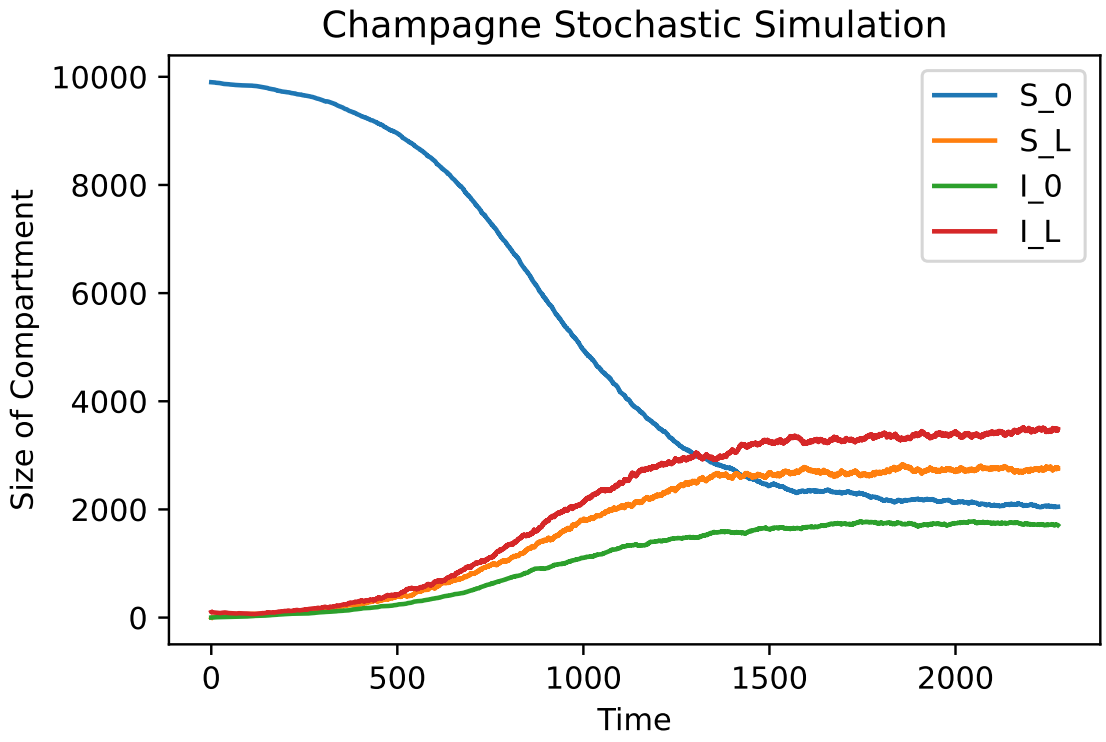

Figure 6.1: A Doob-Gillespie simulation of the model described by Champagne et al. 2022 with $\alpha = 0.4$, $\beta = 0.4$, $\gamma_L = 1/223$, $\lambda = 0.04$, $f = 1/72$, $r = 1/60$, and $\delta = 0$. The population was 10000, with 100 initial infections (both blood-stage and liver-stage I_L).

We investigated the model by Champagne et al. 2022, as described in Section 3.1. A malaria

Table 6.1: The parameters used to simulate a *P. vivax* outbreak using the model described by Champagne et al. 2022

Parameter description	Parameter	Value	Units
effective blood-stage treatment proportion	α	0.1235	None
effective liver-stage treatment proportion	β	0.429	None
rate of liver-stage disease clearance	γ_L	1/383	1/days
rate of infection	λ	0.01	1/days
rate of relapse	f	1/69	1/days
rate of blood-stage disease clearance	r	1/60	1/days.

epidemic was simulated using the Doob-Gillespie algorithm shown in Figure 6.1, using a population size of 10,000 and an initial infected population of 100 (with both liver-stage and blood-stage infection). The parameters used closely followed those reported in Champagne et al. 2022, with the exact parameters reported in Table 6.1. To simplify our analysis, we have assumed that case importation is negligible, so we have set $\delta = 0$. From initialisation, the simulation was run for 200,000 time steps, after which the model was assumed to have reached steady state behaviour. The number of time steps was chosen as the stopping criteria because the time the model takes to reach a steady state is highly dependent on the scales of the parameters. Time steps adapt to the scale of the parameters.

Table 6.2: Observed simulated data $\mathbf{y}^{\text{obs}} := \{\iota_{\text{obs}}, \pi_{\text{obs}}, i_{\text{obs}}, p_{obs}\}$ from the simulation in Figure 6.1.

Parameter Description	Parameter	Observed Value
Weekly incidence at epidemic steady state	ι_{obs}	461
Prevalence at epidemic steady state	π_{obs}	5205
Incidence in the first month of the epidemic	i_{obs}	42
Prevalence after one month of the epidemic	p_{obs}	87

Within our assumed model framework, new infections that instantly undergo radical cure do not change the size of each compartment. These infections should contribute to our incidence, even though they are not calculated. To account for these silent infections, we calculated the number of additional infections to be Poisson distribution with rate $\Delta t \times \alpha\beta\lambda(I_L + I_0)S_0/N$, where Δt is the time between events (one time step). The (simulated) observed data was taken as the simulated case counts (incidence) and prevalence (as the absolute number of people infected) of the simulated epidemic, described in Table 6.2.

6.2 Model Simulations and Discrepancy Function

New epidemics were simulated as above, with 200,000 events and at least 30 days (to allow for calculation of incidence in the first month of the epidemic), with parameters $\boldsymbol{\theta} = \{\alpha, \beta, \gamma_L, \lambda, f, r\}$. For each model $y(\boldsymbol{\theta}) = \{\iota, \pi, i, p\}$ was calculated with the same method as $\mathbf{y}^{\text{obs}}$, where the interpretation of each parameter is described in Table 6.2.

We defined the discrepancy function to be the L_2 norm of the relative differences

$$\mathcal{D}(\boldsymbol{\theta}) = \mathcal{D}(\alpha, \beta, \gamma_L, \lambda, f, r) := \sqrt{\left(\frac{\iota - \iota_{\text{obs}}}{\iota_{\text{obs}}}\right)^2 + \left(\frac{\pi - \pi_{\text{obs}}}{\pi_{\text{obs}}}\right)^2 + \left(\frac{i - i_{\text{obs}}}{i_{\text{obs}}}\right)^2 + \left(\frac{p - p_{\text{obs}}}{p_{\text{obs}}}\right)^2}.$$

Relative difference was chosen to limit the impact between the scale differences of the summary statistics.

6.3 Gaussian Process Model Selection and Initialisation

We approximated $\mathbb{E}[\ln \mathcal{D}(\boldsymbol{\theta})]$ with a Gaussian process $d_{\mathcal{GP}}(\boldsymbol{\theta})$ surrogate model. $d_{\mathcal{GP}}(\boldsymbol{\theta})$ was regressed on sample means

$$\overline{\ln \mathcal{D}(\boldsymbol{\theta})} := \frac{1}{30} \sum_{j=1}^{30} \ln \mathcal{D}_j(\boldsymbol{\theta})$$

where the $\ln \mathcal{D}_j(\boldsymbol{\theta})$s are i.i.d. samples generated by model runs. Each evaluation of the discrepancy function was run in parallel using a supercomputer. The samples $\overline{\ln \mathcal{D}(\boldsymbol{\theta})}$ were assumed to be noisy observations of $\mathbb{E}[\ln \mathcal{D}(\boldsymbol{\theta})] + \varepsilon$, where $\varepsilon \sim N(0, \sigma_o^2)$, by the central limit theorem. σ_o^2 was assumed to be independent of $\boldsymbol{\theta}$ and has the natural interpretation as the variance of the sample mean. $d_{\mathcal{GP}}(\boldsymbol{\theta})$ was assumed to have an unknown constant mean $m_{\mathcal{GP}}$, and kernel

$$k(\boldsymbol{\theta}_i, \boldsymbol{\theta}_i') = \sigma_k^2 (1 + z_i + \frac{z_i^2}{3}) \exp(-z_i)$$

where

$$z_i = \sqrt{5 \sum_{\theta \in \boldsymbol{\theta}} \left(\frac{\theta_i - \theta_i'}{\ell_\theta} \right)^2}.$$

This kernel is a Matérn kernel with $\nu = 5/2$ and automatic relevance determination - i.e. each parameter $\theta \in \boldsymbol{\theta}$ was scaled by ℓ_θ. In effect, this assigns each parameter its own length hyperparameter. It is important that each parameter has its own length scale because each parameter has different scales and has varying degrees of impact on the mean of the log discrepancy.

Table 6.3: Conservative upper bounds for parameters to be calibrated. Values were informed by Champagne et al. 2022; White et al. 2016. All lower bounds were zero.

Parameter	Upper Bound	Unit
The proportion of treatment clearing blood stage disease α	1	
The proportion of treatment clearing liver stage disease β	1	
Rate of liver stage disease clearance γ_L	1/30	1/days
Rate of infection λ	1/10	1/days
Rate of relapse f	1/14	1/days
Rate of blood stage disease clearance r	1/14	1/days

All parameters to be calibrated were given conservative upper bounds after considering values reported in the literature. $d_{\mathcal{GP}}(\boldsymbol{\theta})$ was fit over this compact subspace of the whole parameter space.

Latin hypercube sampling was used to initialise 50 samples of the parameter space (scaled to be between zero and the upper bounds described in Table 6.3). For each set of parameters, $\overline{\ln \mathcal{D}(\boldsymbol{\theta})}$ was generated. The hyperparameters described in Table 6.4 were optimised using leave-one-out cross-validation of the log predictive likelihood described in Equation 5.2, and $d_{\mathcal{GP}}^{(0)}(\boldsymbol{\theta})$ was fit to the samples.

Table 6.4: Hyperparameters used in training $d_{\mathcal{GP}}(\boldsymbol{\theta})$.

Hyperparameter	Description
σ_k^2	Matérn kernel amplitude
σ_o^2	Observation variance ($\text{var}(\overline{\ln \mathcal{D}(\boldsymbol{\theta})})$)
ℓ_α	Length parameter associated with α
ℓ_β	Length parameter associated with β
ℓ_{γ_L}	Length parameter associated with γ_L
ℓ_λ	Length parameter associated with λ
ℓ_f	Length parameter associated with f
ℓ_r	Length parameter associated with r
$m_{\mathcal{GP}}$	Gaussian process mean

Algorithm 8 ABC-like synthetic likelihood

Input: Initial values for $\boldsymbol{\theta}$, lower and upper bounds for $\boldsymbol{\theta}$, initial Gaussian process model $d_{\mathcal{GP}}^{(0)}(\boldsymbol{\theta})$
Output: Synthetic likelihood $\hat{L}(\boldsymbol{\theta})$
for $t = 1$ to 500 **do**
  $\boldsymbol{\theta}^{(t)} \leftarrow \arg\min_{\boldsymbol{\theta}} \mathcal{A}_{\text{EI}}(\boldsymbol{\theta})$
  Sample $\overline{\ln \mathcal{D}(\boldsymbol{\theta}^{(t)})}$
  if $t \leq 6$ **then** ▷ Once per parameter
    $j \leftarrow t$
    Create $\mathbf{s}_j$, 15 evenly spaced values from 0 to the upper bound of θ_j in Table 6.3
    for k in 1 to 15 **do**
      $\theta_j^{(t)} \leftarrow s_{jk}$
      Sample $\overline{\ln \mathcal{D}(\boldsymbol{\theta}^{(t)})}$
    end for
  else
    $j \leftarrow t \mod 6$ ▷ Iterating over $\boldsymbol{\theta}$
    for 4 repeats **do**
      Sample $U_j \sim \text{Unif}(0, m_j)$, with m_j being θ_j's upper bound
      $\theta_j^{(t)} \leftarrow U_j$
      Sample $\overline{\ln \mathcal{D}(\boldsymbol{\theta}^{(t)})}$
    end for
  end if
  if $t \mod 50 == 0$ **then** ▷ Every 50 iterations
    Reoptimise the Gaussian process hyperparameters using leave-one-out cross-validation
  end if
  Update $d_{\mathcal{GP}}^{(t)}(\boldsymbol{\theta})$ on the new samples
end for
return $d_{\mathcal{GP}}^{(500)}(\boldsymbol{\theta})$

6.4 Bayesian Acquisition and Parameter Updates

The Gaussian process was optimised over 500 iterations. Each iteration minimises the expected improvement and obtains a new sample $\overline{\ln \mathcal{D}(\boldsymbol{\theta})}$. For each iteration, one of the variables $\theta_j \in \boldsymbol{\theta}$ was chosen, and multiple samples of $\overline{\ln \mathcal{D}(\boldsymbol{\theta})}$ were taken using multiple values for θ_j. This was done to improve the values for the length parameters and explore the parameter space more widely. This step is highly parallelisable. The hyperparameters were reoptimised every 50 iterations as the number of samples increased. The full procedure is specified in Algorithm 8.

Given the set of previously sampled parameters $\boldsymbol{\theta}^*$, and $\mu_* := \min_{\boldsymbol{\theta}^* \in \boldsymbol{\theta}^*} \mathbb{E}(d_{\mathcal{GP}}(\boldsymbol{\theta}_*))$, the expected improvement with exploration

$$\mathcal{A}_{\text{EI}}(\boldsymbol{\theta}) := \mathbb{E}[\min(d_{\mathcal{GP}}(\boldsymbol{\theta}) - (\mu^* + 0.1), 0)],$$

was minimised using a gradient descent algorithm. The gradient descent was initialised at $\boldsymbol{\theta}^\dagger$, where $\boldsymbol{\theta}^\dagger$ was a combination of the best parameters yet observed $\boldsymbol{\theta}^{**} := \arg\min_{\boldsymbol{\theta}^* \in \boldsymbol{\Theta}^*} d_{\mathcal{GP}}(\boldsymbol{\theta}^*)$, and values between 0 and the upper bounds described in 6.3 distributed uniformly at random. Each $\theta_j^\dagger$ was set independently, with

$$\Pr(\theta_j^\dagger = \theta_j^{**}) = 1/2 = \Pr(\theta_j^\dagger \text{ uniformly distributed}).$$

We could have chosen random initialisation, but we do not expect it to improve the success of the gradient descent algorithm, because for samples where $\mathcal{A}_{\text{EI}}(\boldsymbol{\theta})$ is very small, particularly if $d_{\mathcal{GP}}(\boldsymbol{\theta}^*)$ is large, the gradient of $\mathcal{A}$ can be negligible, causing the convergence criteria to be met prematurely. Furthermore, starting only at the current minimum will increase the possibility of being stuck in local minima.

The final fitted Gaussian process $d_{\mathcal{GP}}^{(500)}(\boldsymbol{\theta})$ approximates $\mathbb{E}(\ln \mathcal{D}(\boldsymbol{\theta}))$. Since the variance of the sample mean $\text{var}(\overline{\ln \mathcal{D}(\boldsymbol{\theta})})$ is estimated by σ_o^2, the variance of the the log discrepancy function $\ln \mathcal{D}(\boldsymbol{\theta})$ is approximately $30\sigma_o^2$. We then used moment matching assuming that $\mathcal{D}(\boldsymbol{\theta})$ is approximately log-normally distributed distribution, and hence can be approximated by

$$\hat{\mathcal{D}}(\boldsymbol{\theta}) \sim \text{LN}\left(\mathbb{E}[d_{\mathcal{GP}}^{(500)}(\boldsymbol{\theta})], 30\sigma^2\right).$$

Therefore using approximate Bayesian computation described in Algorithm 7, the probability of sampling and accepting a $\boldsymbol{\theta}$ is $\Pr(\boldsymbol{\theta}) \Pr(\mathcal{D}(\boldsymbol{\theta}) < \epsilon | \boldsymbol{\theta})$, where $L(\boldsymbol{\theta}) := \Pr(\mathcal{D}(\boldsymbol{\theta}) < \epsilon | \boldsymbol{\theta})$ approximates the true likelihood $\mathcal{L}(\boldsymbol{\theta})$. Finally, we substitute in our approximation $\hat{\mathcal{D}}$ for $\mathcal{D}$, to create our synthetic likelihood

$$\hat{L}(\boldsymbol{\theta}) := \Pr(\hat{\mathcal{D}}(\boldsymbol{\theta}) < \epsilon | \boldsymbol{\theta}). \tag{6.1}$$

Since

$$\ln \hat{\mathcal{D}}(\boldsymbol{\theta}) \sim N\left(\mathbb{E}[d_{\mathcal{GP}}^{(500)}(\boldsymbol{\theta})], 30\sigma^2\right),$$

we can express $\hat{L}$ as

$$\hat{L}(\boldsymbol{\theta}) = \Pr(\ln \hat{\mathcal{D}}(\boldsymbol{\theta}) < \ln \epsilon | \boldsymbol{\theta}).$$

This final step is the crux of our methodology. By recovering a likelihood, the standard frequentist and Bayesian parameter estimation methods will be usable.

The all Gaussian processes and Gaussian process regression models were implemented using TensorFlow (Martín Abadi et al. 2015). All code is available at `https://github.com/jaycrick/masters_project`.

Chapter 7

Results

We outline the results of the method first by validating that each step of the method had plausible outputs, and then by reporting the estimated parameters based on the observed data.

7.1 Validation

Table 7.1: Final optimised Gaussian process hyperparameters

Hyperparameter	Final value
σ_o^2	0.064
σ_k^2	0.762
ℓ_α	0.362
ℓ_β	1.229
ℓ_{γ_L}	0.009
ℓ_λ	0.006
ℓ_f	0.016
ℓ_r	0.017
$m_{\mathcal{GP}}$	0.881

The final hyperparameters are reported in Table 7.1. To ensure that our expected improvement and hyperparameter optimisation functions converged, we plotted the initial training in Figures 7.2 and 7.3. The plots have a smooth curve, demonstrating that both algorithms converged at a reasonable rate.

The violin plot of discrepancy function in Figure 7.1 is well dispersed suggesting a good amount of exploration of the parameter space has been done. A large number of samples were in areas of low mean log discrepancy, and so this suggests a good exploration exploitation trade-off.

Figure 7.4 suggests that after 400 iterations $d_{\mathcal{GP}}(\boldsymbol{\theta})$ fits to $\mathbb{E}(\ln \mathcal{D}(\boldsymbol{\theta}))$ well. The λ slice has the sharpest minimum, whereas β does not appear to have much impact on the discrepancy. As the number of iterations increased, the Gaussian process visibly improved at fitting to the mean. Interim iterations of $d^{(t)}_{\mathcal{GP}}(\boldsymbol{\theta})$ can be seen in the appendix.

7.2 Parameter Estimates and Synthetic Likelihoods

For parameter estimation, we typically look at likelihood instead of discrepancy. This is done by inverting that distribution function (see Equation 6.1). In Table 7.2 we present the global

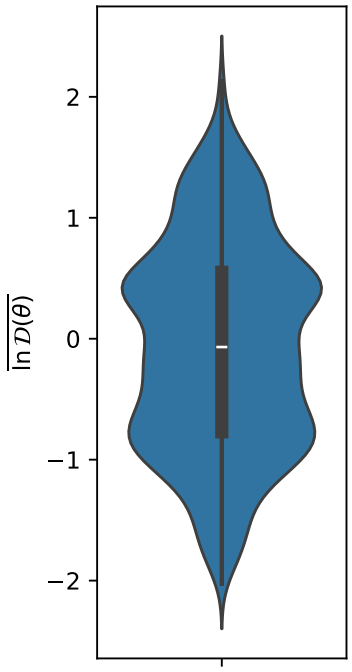

Figure 7.1: Sampled $\overline{\ln \mathcal{D}(\boldsymbol{\theta})}$ violin plot

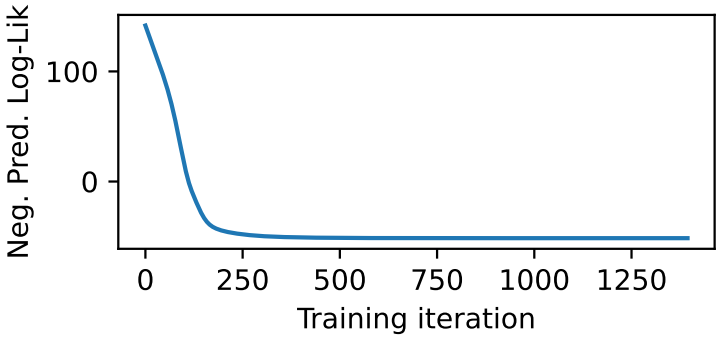

Figure 7.2: A plot showing the value of the leave-one-out cross-validation log predictive likelihood for each gradient descent iteration.

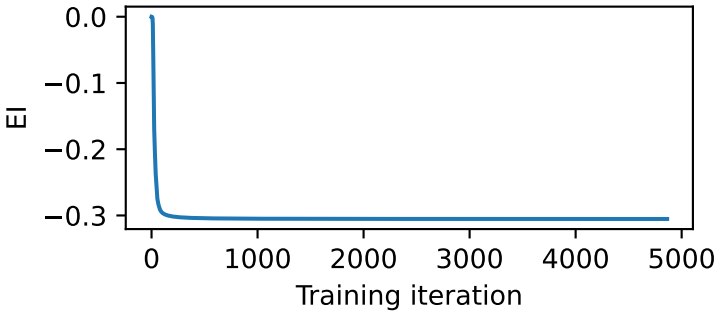

Figure 7.3: A plot showing the value of $\arg\min_{\boldsymbol{\theta}} \mathcal{A}_{\mathrm{EI}}(\boldsymbol{\theta})$ for each gradient descent iteration.

Table 7.2: Estimates of our model parameters. The maximum likelihood estimate (MLE) of the true parameters using $\hat{L}$. The maximum slice estimate was the one-dimensional maximum likelihood estimate where all other parameters are held constant at the true value.

Parameter	True	MLE	ML Slice Estimate
α	0.124	0.049	0.02
β	0.43	0.42	0.64
γ_L	0.0026	0.006	0.005
λ	0.01	0.01	0.01
f	0.014	0.018	0.017
r	0.017	0.024	0.022

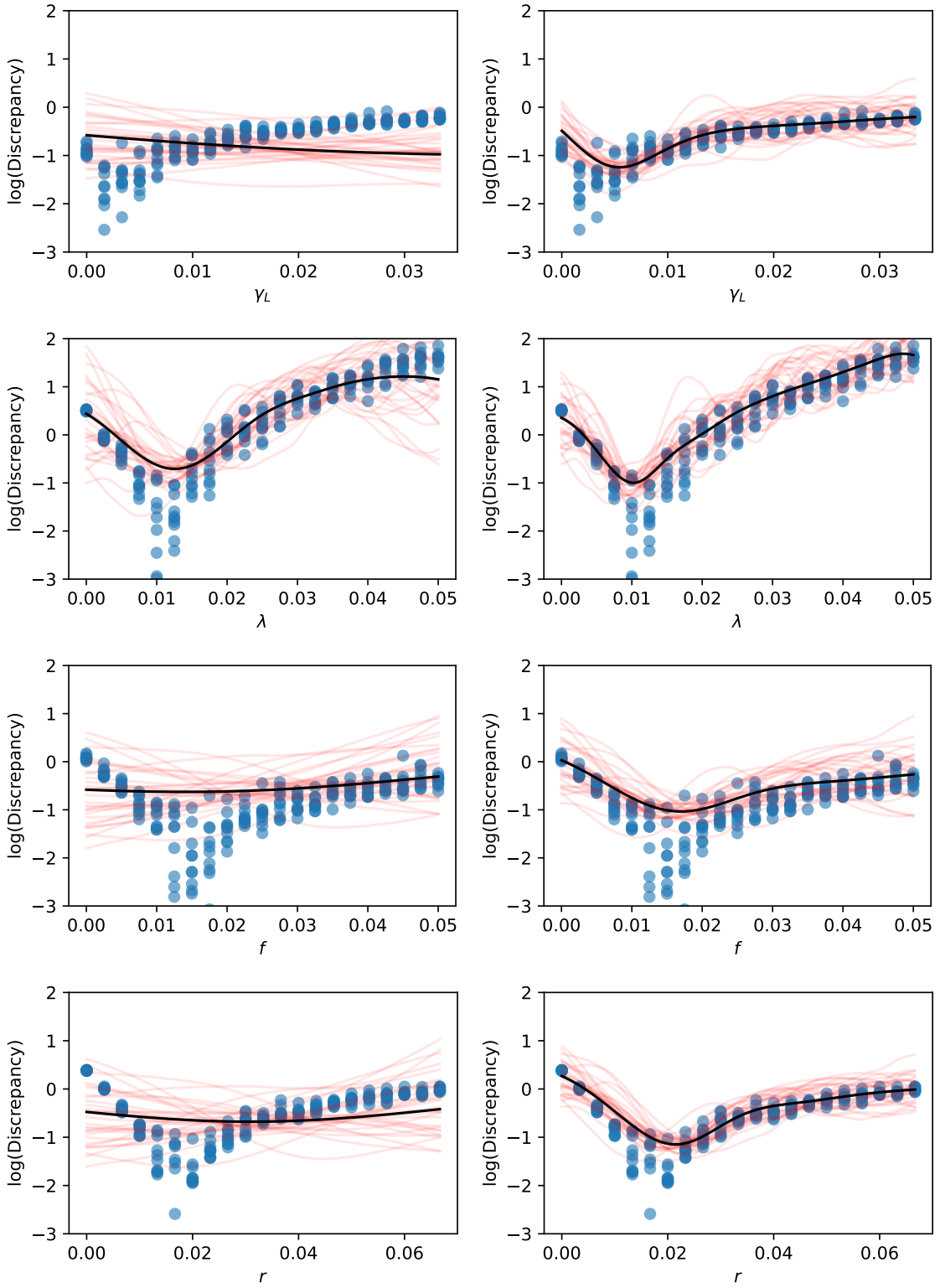

Figure 7.4: The left column of figures is the Gaussian process after initialisation $d^{(0)}_{\mathcal{GP}}(\boldsymbol{\theta})$. The black line is $\mathbb{E}(d^{(0)}_{\mathcal{GP}}(\boldsymbol{\theta}))$, and the red lines are multiple realisations of $d^{(0)}_{\mathcal{GP}}(\boldsymbol{\theta})$. The right column of figures is after 400 sampling iterations, with the black line being $\mathbb{E}(d^{(400)}_{\mathcal{GP}}(\boldsymbol{\theta}))$. The blue dots are realisations of $\ln \mathcal{D}(\boldsymbol{\theta})$. $d_{\mathcal{GP}}$ has not been trained on these realisations. The parameters are varied univariately, with all other parameters fixed at the true parameters.

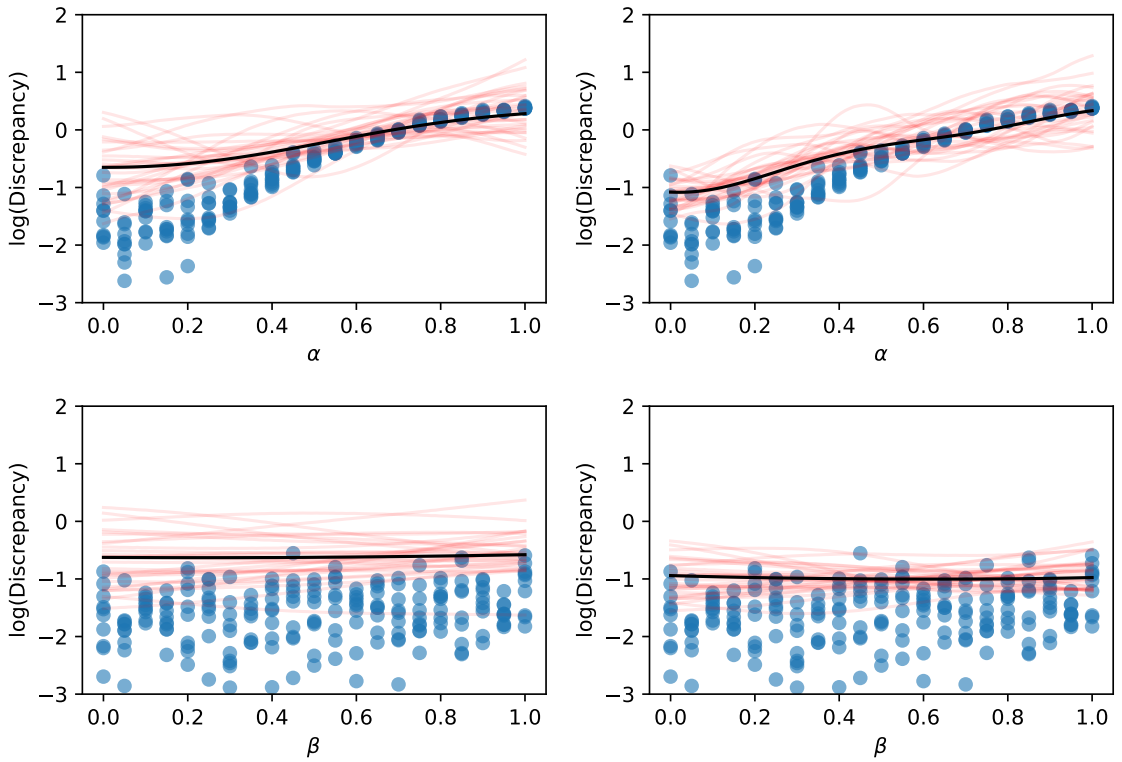

Figure 7.5: Gaussian process approximations of the treatment parameters, as with Figure 7.4

maximum likelihood estimate found by finding the maximum synthetic likelihood $\arg\max_{\boldsymbol{\theta}} \hat{L}(\boldsymbol{\theta})$.

In Figure 7.6 we show our final likelihood function estimate from the trained Gaussian process. For simplicity we only present the likelihood across parameter slices, where the parameter of interest is allowed to vary, while all other parameters are held constant at their true values. The maximum likelihood values for each parameter slice are also presented in Table 7.2 but do are very similar to the maximum likelihood estimates and the true values. For this reason, we can be confident that our synthetic likelihood is a good approximation of the true likelihood, despite the true likelihood being infeasible to compare to. Certain parameters such as λ, r, and γ_L have sharper likelihood peaks than parameters such as α and β, suggesting the data we used may lend itself to estimating parameters such as λ over the treatment parameters, although all likelihood slices calculated were unimodal.

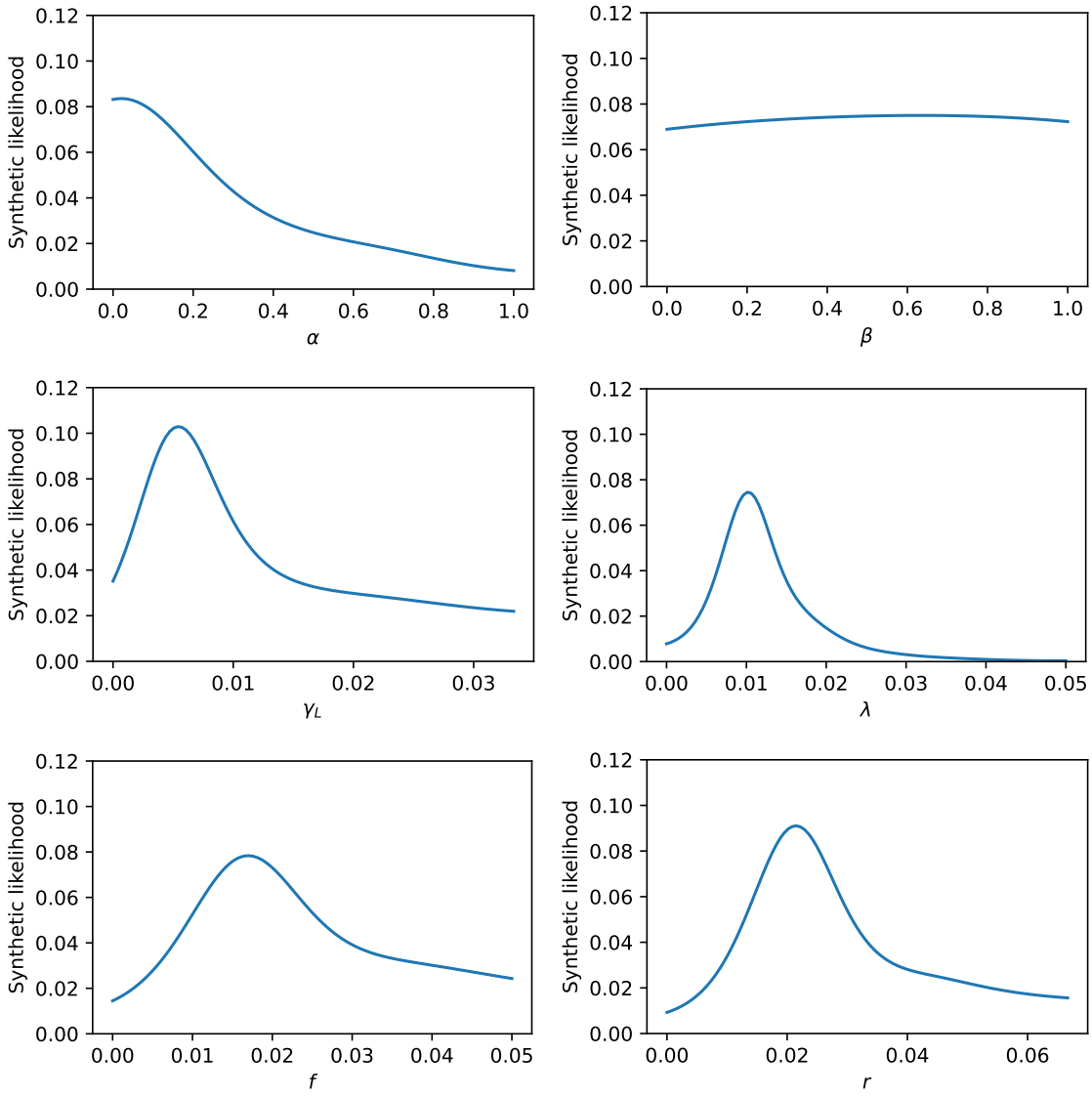

Figure 7.6: Final univariate synthetic likelihoods $\hat{L}(\boldsymbol{\theta})$ after 400 sampling iterations. All values not shown were fixed at the true parameters.

Chapter 8

Discussion

To our knowledge, the synthetic likelihood described above has not been used to calibrate a malaria model before. Champagne et al. calibrate the model we use by finding the ODE equilibrium and fitting a single parameter λ to incidence data. Note that this comes with limitations. For example, it relies on data being observed when the disease is roughly at equilibrum in the population. This is not desirable for modelling outbreaks or seasonality effects. Champagne et al.'s approach to parameter calibration does not work in these scenarios.

In comparison, not only were we able to effectively recover the true λ from a synthetic run, we were able to recover all model parameters simultaneously.

This methodology is very robust to both frequentist and Bayesian inference. Under a Bayesian framework, since we can evaluate the synthetic likelihood for any $\boldsymbol{\theta}$, we can use a Metropolis Hasting sampler to obtain samples from a distribution approximately equal to the posterior distribution $\Pr(\boldsymbol{\theta}|\mathbf{y}^{\text{obs}})$. Alternatively, standard frequentist inference can also be used on our synthetic likelihood $\hat{L}$. For example, numerically approximating the observed Fisher information matrix

$$F(\hat{\theta}) = -\frac{\partial \ln \hat{L}}{\partial \boldsymbol{\theta} \partial \boldsymbol{\theta}^T}(\hat{\boldsymbol{\theta}})$$

allows us to do hypothesis testing and construct confidence intervals since asymptotically $\hat{\boldsymbol{\theta}} \sim N(\boldsymbol{\theta}, F^{-1}(\hat{\boldsymbol{\theta}}))$ (see Fahrmeir, Hennevogl, and Tutz 2013).

Although the likelihood-free procedure we outlined for this model closely resembles Gutmann and Cor 2016, a few significant changes improve on the method outlined in that manuscript.

The most significant change is the choice to model the sample mean as a noisy Gaussian process rather than modelling the discrepancy function as a noisy Gaussian process. Changing this assumption means that we are not subject to the distributional assumption of normal noise and constant variance with respect to $\mathcal{D}(\boldsymbol{\theta})$. Once we have an approximation for the mean as a function of $\boldsymbol{\theta}$, we could choose a distribution that scales with the mean. This is analogous to the generalised linear modelling framework. For example, assuming that $\mathcal{D}(\boldsymbol{\theta})$ follows a Gamma distribution may be reasonable. Letting $\mu(\boldsymbol{\theta}) := \mathbb{E}[\mathcal{D}(\boldsymbol{\theta})]$, we can approximate $\mathcal{D}(\boldsymbol{\theta})$ with $\hat{\mathcal{D}}(\boldsymbol{\theta}) \sim \text{Gamma}\left(\frac{\mu(\boldsymbol{\theta})}{\phi}, \frac{1}{\phi}\right)$, where $\frac{\mu(\boldsymbol{\theta})}{\phi}, \frac{1}{\phi}$ are the shape and rate parameters. Trivially,

$$\mathbb{E}[\hat{\mathcal{D}}(\boldsymbol{\theta})] = \frac{\mu(\boldsymbol{\theta})}{\phi} / \frac{1}{\phi} = \mu(\boldsymbol{\theta}),$$

and for a fixed ϕ, $\text{var}[\mathcal{D}(\boldsymbol{\theta})] = \phi\mu(\boldsymbol{\theta})$, so the variance scales linearly with the mean. If this behaviour is observed empirically, then such a choice will be preferable since then $\hat{L}(\boldsymbol{\theta})$ will better approximate the true likelihood. This can be done with any individual parameter distribution with a fixed variance structure.

Alternatively, the sample variance could be modelled with a different Gaussian process $s^2_{\mathcal{GP}}(\boldsymbol{\theta})$ along with the sample mean. Any two-parameter distribution could be moment matched by the two Gaussian processes to get a more accurate $\hat{L}(\boldsymbol{\theta})$. Therefore, if empirically we observe that $\mathcal{D}(\boldsymbol{\theta})$ is approximately Gamma distributed, then we could approximate $\mathcal{D}(\boldsymbol{\theta})$ with

$$\hat{\mathcal{D}}(\boldsymbol{\theta}) \sim \text{Gamma}\left(\frac{\mu^2(\boldsymbol{\theta})}{\sigma^2(\boldsymbol{\theta})}, \frac{\mu(\boldsymbol{\theta})}{\sigma^2(\boldsymbol{\theta})}\right),$$

where $\text{var}[\hat{\mathcal{D}}(\boldsymbol{\theta})] = \sigma^2(\boldsymbol{\theta})$ and $\mathbb{E}(\hat{\mathcal{D}}(\boldsymbol{\theta})) = \mu(\boldsymbol{\theta})$ as required.

The mean and variance do not have a linked structure in the discrepancy function we used for the Champagne model. This can be seen particularly in the λ slice in Figure 7.4. For $\boldsymbol{\theta}$ with $\lambda < 0.03$, $\text{var}(\ln \mathcal{D}(\boldsymbol{\theta}))$, is small, and $\mathbb{E}(\ln \mathcal{D}(\theta)) \approx 0$. However, for $\lambda \approx 0.02$, we also have $\mathbb{E}[\ln \mathcal{D}(\theta)] \approx 0$, but the variance is observably larger. Therefore, if we had modelled the sample variance of our log discrepancy as a noisy Gaussian process $s^2_{\mathcal{GP}}(\boldsymbol{\theta})$, then we could have approximated $\mathcal{D}(\boldsymbol{\theta})$ with $\hat{\mathcal{D}}(\theta) \sim \text{LN}\left(\mathbb{E}(d_{\mathcal{GP}}(\boldsymbol{\theta})), \sigma^2(\boldsymbol{\theta})\right)$, where $\mu(\boldsymbol{\theta}) := \mathbb{E}(d_{\mathcal{GP}}(\boldsymbol{\theta}))$ and $\sigma^2(\boldsymbol{\theta}) := \mathbb{E}(s^2_{\mathcal{GP}}(\boldsymbol{\theta}))$.

Empirically, it is not surprising that the variance is not constant across the parameter space or even mean dependent. Disease model behaviour is heavily dependent on the values of the parameters. For example, around bifurcation points, a slight change in parameters may lead to a disease model that dies out sometimes but reaches equilibrium in other runs. Here, we expect $\text{var}[\mathcal{D}(\boldsymbol{\theta})]$ to be large. This threshold is important in disease modelling and is called R_0 : the expected number of secondary cases a single infectious individual causes in a completely susceptible population. But when $\boldsymbol{\theta}$ is changed only a small amount such that $R_0 < 1$, and so the disease consistently dies out, the $\text{var}[\mathcal{D}(\boldsymbol{\theta})]$ will be close to 0. Since the model run will always end with a disease-free population, the summary statistics, such as incidence or prevalence, will always be 0. This is likely what happens for very small λ in Figure 7.4.

This highlights another problem. Around bifurcation points, such as near where $R_0 = 1$, $\mathbb{E}(\mathcal{D}(\boldsymbol{\theta}))$ is expected to behave erratically. Gutmann and Cor use a squared exponential kernel for their Gaussian process approximation, which cannot capture this behaviour without making any length scales very large. On the other hand, a Matérn 5/2 kernel, as we used, is still smooth but allows enough flexibility that sharp changes in the target function do not require overcompensation in the length scales. For an example demonstrating the utility of the Matérn kernel over the squared exponential in the case of a non-smooth function, see Jones 2021. Another possible solution is to use a Student-t process to approximate the discrepancy, as it has heavier tails, so it is more forgiving to sudden jumps. The multivariate Student-t distribution has some properties analogous to the multivariate normal distribution. This includes an analytic solution to the conditional distribution, similar to Theorem 5.13; for more details, see Shah, Wilson, and Ghahramani 2014.

Gutmann and Cor 2016 use the lower confidence bound acquisition function, where the exploration parameter is the slowly increasing function

$$\eta_t := \sqrt{2 \ln\left(\frac{t^{2/d+2}\pi^2}{3\varepsilon}\right)}.$$

This is chosen because, under the squared exponential kernel and compact support, the lower confidence bound samples are shown to be no regret with high probability. There are multiple issues with this. The first is that Gutmann and Cor seem to have inherited this form from Brochu, Cora, and Freitas 2010. However, the citation in Brochu, Cora, and Freitas 2010 wrongly reproduces the result in Srinivas et al. 2010, [1] which should be

$$\eta_t := \sqrt{2 \ln \left(\frac{t^{2d+2}\pi^2}{3\varepsilon} \right)}.$$

When we tried these exploration parameters, the choice of ε between $(0, 1)$ largely led to repeated sampling from the same set of parameters, even for very small ε. This is similar to the behaviour reported in Gutmann and Cor 2016. Secondly, Gelman et al. do not restrict the parameter space to a compact subset of the space, so theoretical guarantees of no regret are not valid. Finally, Srinivas et al. find this assuming zero mean Gaussian processes. Gutmann and Cor assume a quadratic mean prior.

Even though we consider a compact subset of the parameter space, we did not use a zero-mean Gaussian process, and we used the Matérn kernel, Therefore, we did not want to use this formulation of the lower confidence bound, and instead chose expected improvement.

The quadratic mean assumption in Gutmann and Cor 2016 is also problematic. Suppose the mean of the Gaussian process is trained on a set of concave data near a local minimum. In that case, no matter which acquisition function is chosen, areas away from the local minimum may not be sampled since the mean function will dominate the predicted behaviour of $\mathcal{D}(\boldsymbol{\theta})$, so exploration will be minimal. This also may explain the behaviour of the acquisition function sampling close to the same point repeatedly.

Although we have validated this method on a relatively low dimensional $\boldsymbol{\theta}$, for models with high dimensionality, the construction of a synthetic likelihood will likely have greater comparative benefits than other methods, such as approximate Bayesian computation. This is because as the dimensionality increases, the curse of dimensionality means that randomly drawn points will be increasingly further away on average. Therefore, many more samples from the prior distribution function are likely to produce $\mathcal{D}(\boldsymbol{\theta}) > \epsilon$, particularly if $\mathcal{D}(\boldsymbol{\theta})$ is small in a small region. Optimising the acquisition function each time encourages efficient sampling from areas likely to be beneficial to sample from.

One way to reduce the computational overhead of this method would be to reduce the number of samples used to calculate the sample mean. Our method used 30 samples to ensure convergence to the normal distribution. However, less could be taken with the trade-off of a larger observation variance. The sample mean can be calculated in parallel, so the rate-limiting step minimises the acquisition function in each iteration. Rather than uniformly sampling a single parameter, multivariate noise could be added to $\boldsymbol{\theta}$ to sample multiple sample means simultaneously. Resources should be maximally allocated to calculate as many $\mathcal{D}(\boldsymbol{\theta})$ as feasible in one step, split between multiple repeats for the sample mean, and multiple $\boldsymbol{\theta}$s for better training of the Gaussian process approximation.

[1] One Python package that implements the methodology in Gutmann and Cor 2016 notes this error; see `https://github.com/elfi-dev/elfi/blob/dev/elfi/methods/bo/acquisition.py`

Chapter 9

Conclusion

Malaria, a significant global health challenge, continues to burden the global health system. Mathematical disease models are increasingly being harnessed to alleviate this burden. This thesis explores ways to maximise the impact of epidemiological models by ensuring they accurately simulate public health scenarios, with a specific focus on the complex issue of *P. vivax* malaria.

The complicated lifecycle of *P. vivax* poses a tough hurdle in disease modelling, particularly with respect to asymptomatic cases and relapses. This complexity is problematic during the parameter calibration stage, where traditional methods that rely on being about to compute a likelihood are not viable. Likelihood-free methods, while effective, come with a high computational cost due to repeated and inefficient model runs. This has led some researchers to calibrate models using deterministic approximations, failing to capture the stochastic models' uncertainty. There is an obvious need for a better calibration methodology.

This research used Gaussian processes to approximate the distribution of the discrepancy function used in approximate Bayesian computation for any set of parameters. The true likelihood function was approximated by using the Gaussian process to create a synthetic likelihood. Empirical evidence demonstrated that this methodology successfully recovered parameters of a *P. vivax* model given simulated data while mitigating the computational overhead. Additionally, this thesis laid out possible further extensions to the methodology.

In conclusion, this thesis has demonstrated the plausibility of a new, more robust method of calibrating malaria models, particularly for *P. vivax.* The use of Gaussian processes and synthetic likelihoods has proven effective in overcoming the infeasibility of traditional calibration methods and the computational cost of likelihood-free calibration methods. Future research should focus on refining these techniques and exploring their application to other infectious diseases. These advancements are crucial for developing more effective interventions and ultimately to help support achieving malaria eradication.

Bibliography

Abramowitz, Milton and Irene A. Stegun, eds. (2013). *Handbook of mathematical functions: with formulas, graphs, and mathematical tables*. 9. Dover print.; [Nachdr. der Ausg. von 1972]. Dover books on mathematics. New York, NY: Dover Publ. 1046 pp. ISBN: 978-0-486-61272-0.

Acuña-Zegarra, Manuel Adrian et al. (July 2021). "COVID-19 optimal vaccination policies: A modeling study on efficacy, natural and vaccine-induced immunity responses". In: *Mathematical Biosciences* 337. Publisher: Elsevier, p. 108614. DOI: 10.1016/j.mbs.2021.108614. URL: https://www.ncbi.nlm.nih.gov/pmc/articles/PMC8095066/ (visited on 06/19/2024).

Adams, John H. and Ivo Mueller (Sept. 2017). "The Biology of Plasmodium vivax". In: *Cold Spring Harbor Perspectives in Medicine* 7.9, a025585. ISSN: 2157-1422. DOI: 10.1101/cshperspect.a025585. URL: https://www.ncbi.nlm.nih.gov/pmc/articles/PMC5580510/ (visited on 03/24/2023).

Aron, Joan L. and Robert M. May (1982). "The population dynamics of malaria". In: *The Population Dynamics of Infectious Diseases: Theory and Applications*. Ed. by Roy M. Anderson. Boston, MA: Springer US, pp. 139–179. ISBN: 978-1-4899-2901-3. DOI: 10.1007/978-1-4899-2901-3_5. URL: https://doi.org/10.1007/978-1-4899-2901-3_5.

Brochu, Eric, Vlad M. Cora, and Nando de Freitas (2010). *A Tutorial on Bayesian Optimization of Expensive Cost Functions, with Application to Active User Modeling and Hierarchical Reinforcement Learning*. arXiv: 1012.2599 [cs.LG].

Champagne, Clara et al. (Jan. 2022). "Using observed incidence to calibrate the transmission level of a mathematical model for Plasmodium vivax dynamics including case management and importation". In: *Mathematical Biosciences* 343, p. 108750. ISSN: 00255564. DOI: 10.1016/j.mbs.2021.108750. URL: https://linkinghub.elsevier.com/retrieve/pii/S0025556421001541 (visited on 08/22/2023).

Cowman, Alan F. et al. (2016). "Malaria: Biology and Disease". In: *Cell* 167.3. Type: Review, pp. 610–624. DOI: 10.1016/j.cell.2016.07.055. URL: https://www.scopus.com/inward/record.uri?eid=2-s2.0-84994000411&doi=10.1016%2fj.cell.2016.07.055&partnerID=40&md5=81d9b4c51fe738ac66e0c8561b12c5bf.

Diggle, Peter, Kung-Yee Liang, and Scott L. Zeger (1994). *Analysis of longitudinal data*. Oxford statistical science series 13. Oxford : New York: Clarendon Press ; Oxford University Press. 253 pp. ISBN: 978-0-19-852284-3.

Fahrmeir, Ludwig, W. Hennevogl, and Gerhard Tutz (2013). *Multivariate Statistical Modelling Based on Generalized Linear Models*. OCLC: 1066189579. New York, NY: Springer. ISBN: 978-1-4899-0010-4.

Gani, Raymond and Steve Leach (Dec. 13, 2001). "Transmission potential of smallpox in contemporary populations". In: *Nature* 414.6865, pp. 748–751. ISSN: 0028-0836, 1476-4687. DOI: 10.1038/414748a. URL: https://www.nature.com/articles/414748a (visited on 06/10/2024).

Gelman, Andrew et al. (2014). *Bayesian data analysis*. Third edition. Texts in statistical science series. Boca Raton London New York: CRC Press, Taylor and Francis Group. 667 pp. ISBN: 978-1-4398-4095-5.

Gillespie, Daniel T. (Dec. 1977). "Exact stochastic simulation of coupled chemical reactions". In: *The Journal of Physical Chemistry* 81.25, pp. 2340–2361. ISSN: 0022-3654, 1541-5740. DOI: 10.1021/j100540a008. URL: https://pubs.acs.org/doi/abs/10.1021/j100540a008 (visited on 06/19/2024).

— (July 22, 2001). "Approximate accelerated stochastic simulation of chemically reacting systems". In: *The Journal of Chemical Physics* 115.4, pp. 1716–1733. ISSN: 0021-9606, 1089-7690. DOI: 10.1063/1.1378322. URL: https://pubs.aip.org/jcp/article/115/4/1716/451187/Approximate-accelerated-stochastic-simulation-of (visited on 06/19/2024).

Gutmann, Michael U. and Jukka Cor (2016). "Bayesian Optimization for Likelihood-Free Inference of Simulator-Based Statistical Models". In: *Journal of Machine Learning Research* 17.125, pp. 1–47. ISSN: 1533-7928. URL: http://jmlr.org/papers/v17/15-017.html (visited on 04/28/2024).

Hagenaars, T. J., C. A. Donnelly, and N. M. Ferguson (Apr. 2006). "Epidemiological analysis of data for scrapie in Great Britain". en. In: *Epidemiology and Infection* 134.2, pp. 359–367. ISSN: 0950-2688, 1469-4409. DOI: 10.1017/S0950268805004966. URL: https://www.cambridge.org/core/product/identifier/S0950268805004966/type/journal_article (visited on 03/26/2024).

Jones, Andy (July 31, 2021). *The Matérn class of covariance functions*. Andy Jones. URL: https://andrewcharlesjones.github.io/journal/matern-kernels.html (visited on 06/18/2024).

Keeling, Matthew James and Pejman Rohani (2008). *Modeling infectious diseases in humans and animals*. OCLC: ocn163616681. Princeton: Princeton University Press. 366 pp. ISBN: 978-0-691-11617-4.

Kerr, Cliff C. et al. (July 26, 2021). "Covasim: An agent-based model of COVID-19 dynamics and interventions". In: *PLOS Computational Biology* 17.7. Ed. by Manja Marz, e1009149. ISSN: 1553-7358. DOI: 10.1371/journal.pcbi.1009149. URL: https://dx.plos.org/10.1371/journal.pcbi.1009149 (visited on 06/19/2024).

Martín Abadi et al. (2015). *TensorFlow: Large-Scale Machine Learning on Heterogeneous Systems*. Software available from tensorflow.org. URL: https://www.tensorflow.org/.

Milner, Danny A. (Jan. 2018). "Malaria Pathogenesis". en. In: *Cold Spring Harbor Perspectives in Medicine* 8.1, a025569. ISSN: 2157-1422. DOI: 10.1101/cshperspect.a025569. URL: http://perspectivesinmedicine.cshlp.org/lookup/doi/10.1101/cshperspect.a025569 (visited on 03/24/2023).

Naslidnyk, Masha et al. (2024). *Comparing Scale Parameter Estimators for Gaussian Process Interpolation with the Brownian Motion Prior: Leave-One-Out Cross Validation and Maximum Likelihood*. arXiv: 2307.07466 [math.ST].

Price, R.N. et al. (2020). "Plasmodium vivax in the Era of the Shrinking P. falciparum Map". English. In: *Trends in Parasitology* 36.6, pp. 560–570. ISSN: 1471-4922. DOI: 10.1016/j.pt.2020.03.009.

Rasmussen, Carl Edward and Christopher K. I. Williams (2008). *Gaussian processes for machine learning*. 3. print. Adaptive computation and machine learning. Cambridge, Mass.: MIT Press. 248 pp. ISBN: 978-0-262-18253-9.

Robert, Christian P. and George Casella (2010). *Monte Carlo statistical methods*. 2. ed., softcover reprint of the hardcover 2. ed. 2004. Springer texts in statistics. New York, NY: Springer New York. 645 pp. ISBN: 978-1-4757-4145-2 978-1-4419-1939-7. DOI: 10.1007/978-1-4757-4145-2.

Shah, Amar, Andrew Gordon Wilson, and Zoubin Ghahramani (2014). *Student-t Processes as Alternatives to Gaussian Processes*. arXiv: 1402.4306.

Smith, David L. et al. (Apr. 2012). "Ross, Macdonald, and a Theory for the Dynamics and Control of Mosquito-Transmitted Pathogens". en. In: *PLOS Pathogens* 8.4. Publisher: Public Library of Science, e1002588. ISSN: 1553-7374. DOI: 10.1371/journal.ppat.1002588. URL: https://journals.plos.org/plospathogens/article?id=10.1371/journal.ppat.1002588 (visited on 03/28/2023).

Srinivas, Niranjan et al. (2010). "Gaussian process optimization in the bandit setting: no regret and experimental design". In: *Proceedings of the 27th International Conference on International Conference on Machine Learning*. ICML'10. Haifa, Israel: Omnipress, pp. 1015–1022. ISBN: 9781605589077.

White, Michael T. et al. (Mar. 30, 2016). "Variation in relapse frequency and the transmission potential of *Plasmodium vivax* malaria". In: *Proceedings of the Royal Society B: Biological Sciences* 283.1827, p. 20160048. ISSN: 0962-8452, 1471-2954. DOI: 10.1098/rspb.2016.0048. URL: https://royalsocietypublishing.org/doi/10.1098/rspb.2016.0048 (visited on 08/22/2023).

Wikipedia contributors (2024). *Exponential family — Wikipedia, The Free Encyclopedia*. [Online; accessed 16-May-2024]. URL: https://en.wikipedia.org/w/index.php?title=Exponential_family&oldid=1202463189.

World Health Organization (Dec. 2022). *World malaria report 2022*. en. Tech. rep. Geneva: World Health Organization.

Zekar, Lara and Tariq Sharman (2023). "Plasmodium Falciparum Malaria". eng. In: *StatPearls*. Treasure Island (FL): StatPearls Publishing. URL: http://www.ncbi.nlm.nih.gov/books/NBK555962/ (visited on 03/24/2023).

Zha, Wen-ting et al. (2020). "Research about the optimal strategies for prevention and control of varicella outbreak in a school in a central city of China: based on an SEIR dynamic model". en. In: *Epidemiology and Infection* 148, e56. ISSN: 0950-2688, 1469-4409. DOI: 10.1017/S0950268819002188. URL: https://www.cambridge.org/core/product/identifier/S0950268819002188/type/journal_article (visited on 03/26/2024).

Part III

Appendices

Appendix A

Additional Theorems and Proofs

Theorem A.1 (Sums of Independent Poisson Point Processes)**.** *Given independent Poisson point processes* $\{\mathcal{N}_1(t)\}_{t\geq 0}, \{\mathcal{N}_2(t)\}_{t\geq 0}, \ldots, \{\mathcal{N}_n(t)\}_{t\geq 0}$*, with intensities* $\lambda_1, \lambda_2, \ldots, \lambda_n$*,*

$$\{\mathcal{N}(t)\}_{t\geq 0} := \{\mathcal{N}_1(t) + \mathcal{N}_2(t) + \cdots + \mathcal{N}_n(t)\}_{t\geq 0}$$

is a Poisson point process with intensity $\lambda_1 + \lambda_2 + \cdots + \lambda_n$*.*

Proof. We show that $\{\mathcal{N}(t) := \{\mathcal{N}_1(t)+\mathcal{N}_2(t)+\cdots+\mathcal{N}_n(t)\}_{t\geq 0}\}$ meets each component of Definition 2.1.

1. $\mathcal{N}(0) := \mathcal{N}_1(0) + \mathcal{N}_2(0) + \cdots + \mathcal{N}_n(0) = 0$ since $\mathcal{N}_i(0) = 0$ by definition of a Poisson point process.

2. We show that $\mathcal{N}(t_1)-\mathcal{N}(t_0), \mathcal{N}(t_2)-\mathcal{N}(t_1), \ldots, \mathcal{N}(t_n)-\mathcal{N}(t_{n-1})$ with $0 \leq t_0 < t_1 < \cdots < t_n$ are independent.

   $$\mathcal{N}(t_i) - \mathcal{N}(t_{i-1}) = \underbrace{[\mathcal{N}_1(t_i) - \mathcal{N}_1(t_{i-1})]}_{X_{i1}} + \underbrace{[\mathcal{N}_2(t_i) - \mathcal{N}_2(t_{i-1})]}_{X_{i2}} + \cdots + \underbrace{[\mathcal{N}_n(t_i) - \mathcal{N}_n(t_{i-1})]}_{X_{in}}$$

   X_{ik} is independent of $X_{j\ell}$ for $k \neq \ell$ since $\mathcal{N}_k$ and $\mathcal{N}_\ell$ are independent processes. X_{ik} is independent of X_{jk} for $i \neq j$ by the second property of Definition 2.1. Therefore all X_{ik} are independent of $X_{j\ell}$ for $i \neq j$, and all j, k. Hence $\mathcal{N}(t_1) - \mathcal{N}(t_0), \mathcal{N}(t_2) - \mathcal{N}(t_1), \ldots, \mathcal{N}(t_n) - \mathcal{N}(t_{n-1})$ with $0 \leq t_0 < t_1 < \cdots < t_n$ are independent.

3. For fixed $t_1 < t_2$, and $i \in \{1, 2, \ldots, n\}$,

   $$\mathcal{N}_i(t_2) - \mathcal{N}_i(t_1) \sim \text{Pois}((t_2 - t_1)\lambda_i).$$

   Consider the associated moment generating function of $\mathcal{N}_i(t_2) - \mathcal{N}_i(t_1)$,

   $$M_i(z) := \exp(\lambda_i(t_2 - t_1)(\exp(z) - 1)).$$

   Therefore the moment generating function of

   $$\mathcal{N}(t_2) - \mathcal{N}(t_1) = [\mathcal{N}_1(t_2) - \mathcal{N}_1(t_1)] + [\mathcal{N}_2(t_2) - \mathcal{N}_2(t_1)] + \cdots + [\mathcal{N}_n(t_2) - \mathcal{N}_n(t_1)]$$

is

$$M(z) := \prod_{i=1}^{n} M_i(z) = \exp[(\lambda_1(t_2 - t_1) + \lambda_2(t_2 - t_1) + \cdots + \lambda_n(t_2 - t_1))(\exp(z) - 1)].$$

Therefore $\mathcal{N}_1(t) + \mathcal{N}_2(t) + \cdots + \mathcal{N}_n(t) \sim \text{Pois}((\lambda_1 + \lambda_2 + \cdots + \lambda_n)t)$ by the uniqueness of the moment generating function.

□

Theorem A.2 (Time to First Event in Poisson Point Process)**.** *Given a Poisson point process* $\{\mathcal{N}(t)\}_{t\geq 0}$ *with intensity* λ*, let* $\tau = \inf\{t|\mathcal{N}(t_0 + t) - \mathcal{N}(t_0) = 1, t > 0\}$*.* $\tau \sim \text{Exp}(\lambda)$ *for* $t_0 \geq 0$

Proof.

$$\Pr(\tau > x) = \Pr(\mathcal{N}(t_0 + x) - \mathcal{N}(t_0) = 0) = \frac{(\lambda x)^0 e^{-\lambda x}}{0!} = e^{-\lambda x}$$

□

Theorem A.3 (Probability of ith Poisson Process Generating the Next Event)**.** *Consider independent Poisson point processes*

$$\{\mathcal{N}_1(t)\}_{t\geq 0}, \{\mathcal{N}_2(t)\}_{t\geq 0}, \ldots, \{\mathcal{N}_n(t)\}_{t\geq 0}$$

having intensities $\lambda_1, \lambda_2, \ldots, \lambda_n$*. For fixed* t_0*, let* $\tau_i := \inf\{t|\mathcal{N}(t_0 + t) - \mathcal{N}(t_0) = 1\}$*. Then*

$$\Pr(\min_i \tau_i = \tau_j) = \frac{\lambda_j}{\sum_{i=1}^{n} \lambda_i}.$$

Proof. By Theorem A.2, $\tau_i \sim \text{Exp}(\lambda_i)$. Therefore

$$\begin{aligned}
\Pr(\min_i \tau_i = \tau_j) &= \int_0^\infty \Pr(\{\tau_i = x\} \cup \bigcup_{j\neq i} \{\tau_j > x\})\, \mathrm{d}x \\
&= \int_0^\infty \Pr(\{\tau_i = x\} \cup \bigcup_{j\neq i} \{\tau_j > x\})\, \mathrm{d}x \\
&= \int_0^\infty \Pr(\tau_i = x) \times \prod_{j\neq i} \Pr(\tau_j > x)\, \mathrm{d}x && \text{(by independence)} \\
&= \int_0^\infty \lambda_i \exp(-\lambda_i x) \times \prod_{j\neq i} \exp(-\lambda_j x)\, \mathrm{d}x \\
&= \lambda_i \int_0^\infty \exp(-(\sum_{i=1}^{n} \lambda_j)x)\, \mathrm{d}x \\
&= \lambda_i \left[\frac{\exp(-(\sum_{i=1}^{n} \lambda_j)x)}{\sum_{i=1}^{n} \lambda_j}\right]_0^\infty \\
&= \frac{\lambda_i}{\sum_{i=1}^{n} \lambda_j}
\end{aligned}$$

□

Appendix B

Additional Results

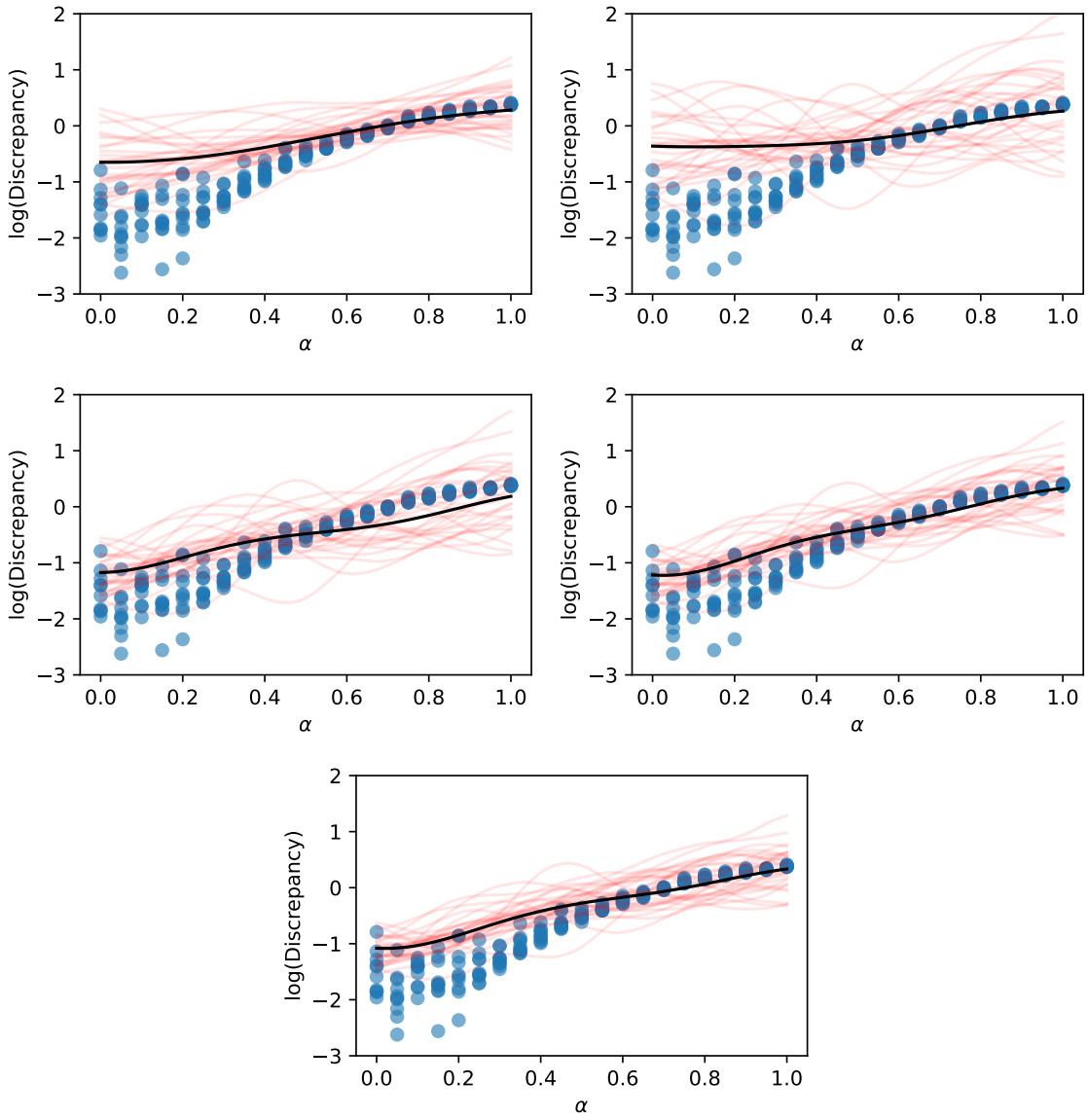

Figure B.1: $d^{(t)}_{\mathcal{GP}}(\boldsymbol{\theta})$ approximation of $\mathbb{E}(\ln \mathcal{D}(\boldsymbol{\theta}))$, for $t = 0$, 100, 200, 300, and 400. Only α was varied. All other parameters were fixed at the true values. Black line is $\mathbb{E}(d^{(i)}(\boldsymbol{\theta}))$. Blue dots are realisations from $\ln \mathcal{D}(\boldsymbol{\theta})$.

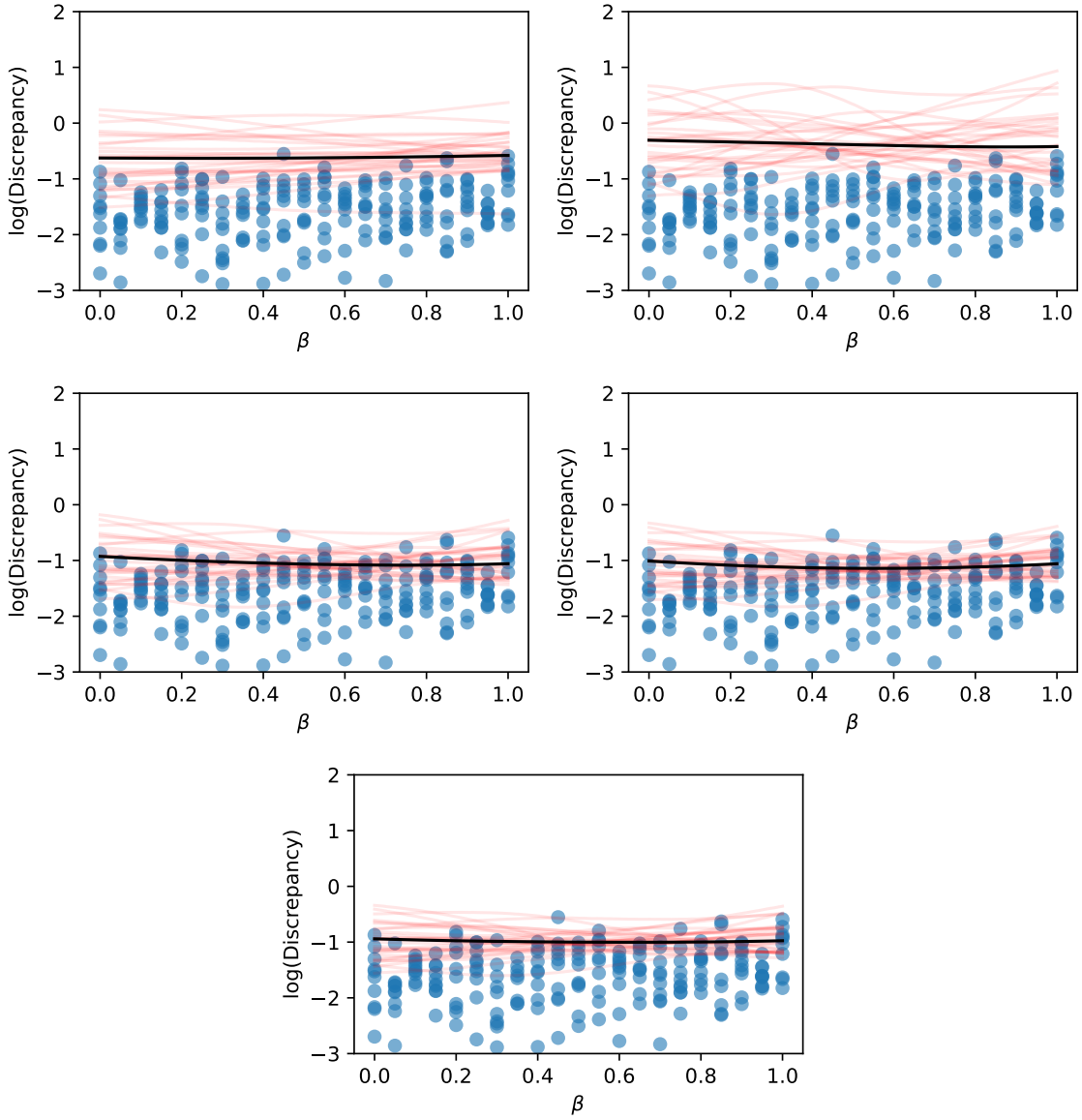

Figure B.2: $d^{(t)}_{\mathcal{GP}}(\boldsymbol{\theta})$ approximation of $\mathbb{E}(\ln \mathcal{D}(\boldsymbol{\theta}))$, for $t = 0$, 100, 200, 300, and 400. Only β was varied. All other parameters were fixed at the true values. Black line is $\mathbb{E}(d^{(i)}(\boldsymbol{\theta}))$. Blue dots are realisations from $\ln \mathcal{D}(\boldsymbol{\theta})$.

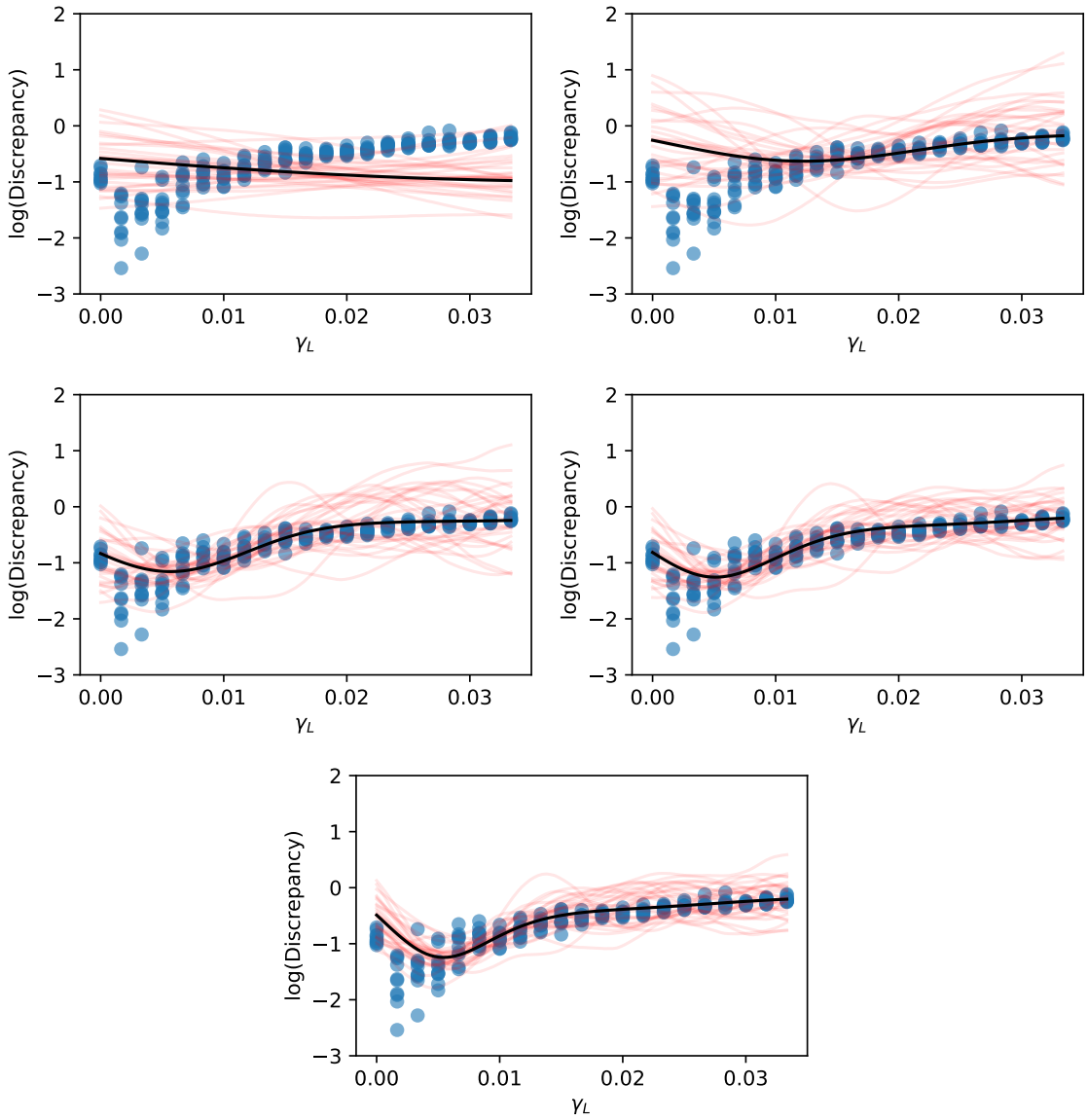

Figure B.3: $d^{(t)}_{\mathcal{GP}}(\boldsymbol{\theta})$ approximation of $\mathbb{E}(\ln \mathcal{D}(\boldsymbol{\theta}))$, for $t = 0$, 100, 200, 300, and 400. Only γ_L was varied. All other parameters were fixed at the true values. Black line is $\mathbb{E}(d^{(i)}(\boldsymbol{\theta}))$. Blue dots are realisations from $\ln \mathcal{D}(\boldsymbol{\theta})$.

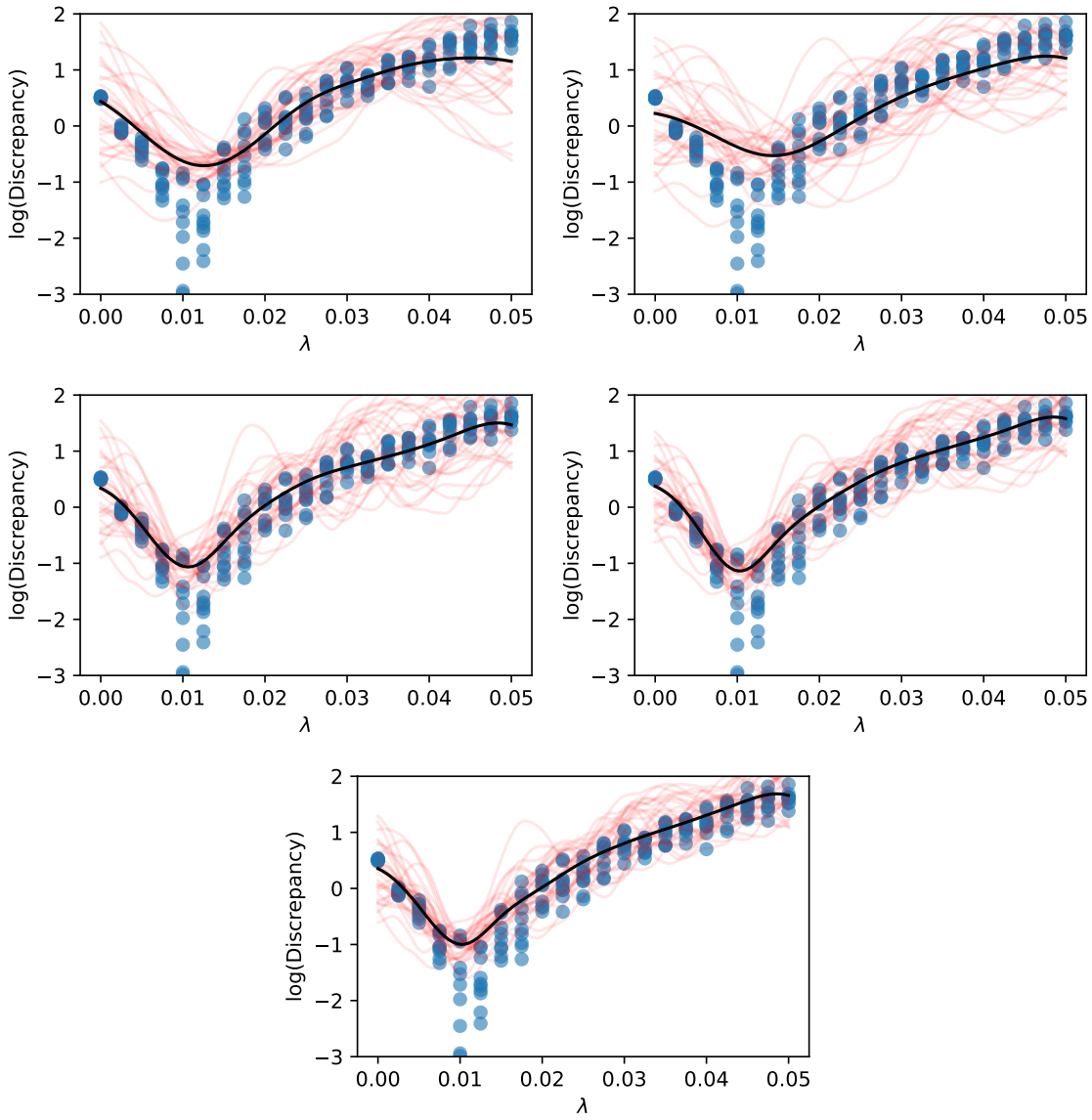

Figure B.4: $d^{(t)}_{\mathcal{GP}}(\boldsymbol{\theta})$ approximation of $\mathbb{E}(\ln \mathcal{D}(\boldsymbol{\theta}))$, for $t = 0$, 100, 200, 300, and 400. Only λ was varied. All other parameters were fixed at the true values. Black line is $\mathbb{E}(d^{(i)}(\boldsymbol{\theta}))$. Blue dots are realisations from $\ln \mathcal{D}(\boldsymbol{\theta})$.

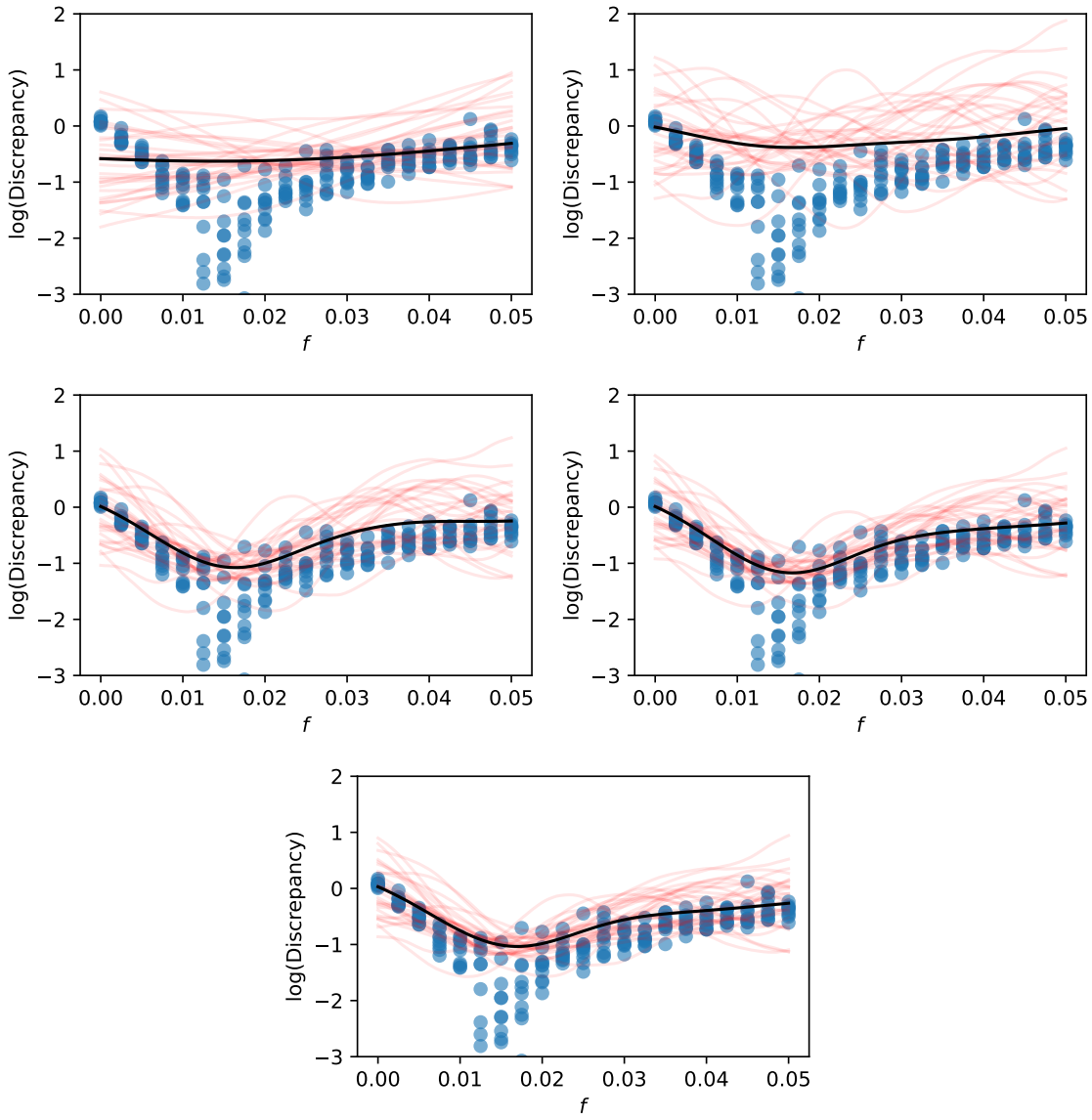

Figure B.5: $d^{(t)}_{\mathcal{GP}}(\boldsymbol{\theta})$ approximation of $\mathbb{E}(\ln \mathcal{D}(\boldsymbol{\theta}))$, for $t = 0$, 100, 200, 300, and 400. Only f was varied. All other parameters were fixed at the true values. Black line is $\mathbb{E}(d^{(i)}(\boldsymbol{\theta}))$. Blue dots are realisations from $\ln \mathcal{D}(\boldsymbol{\theta})$.

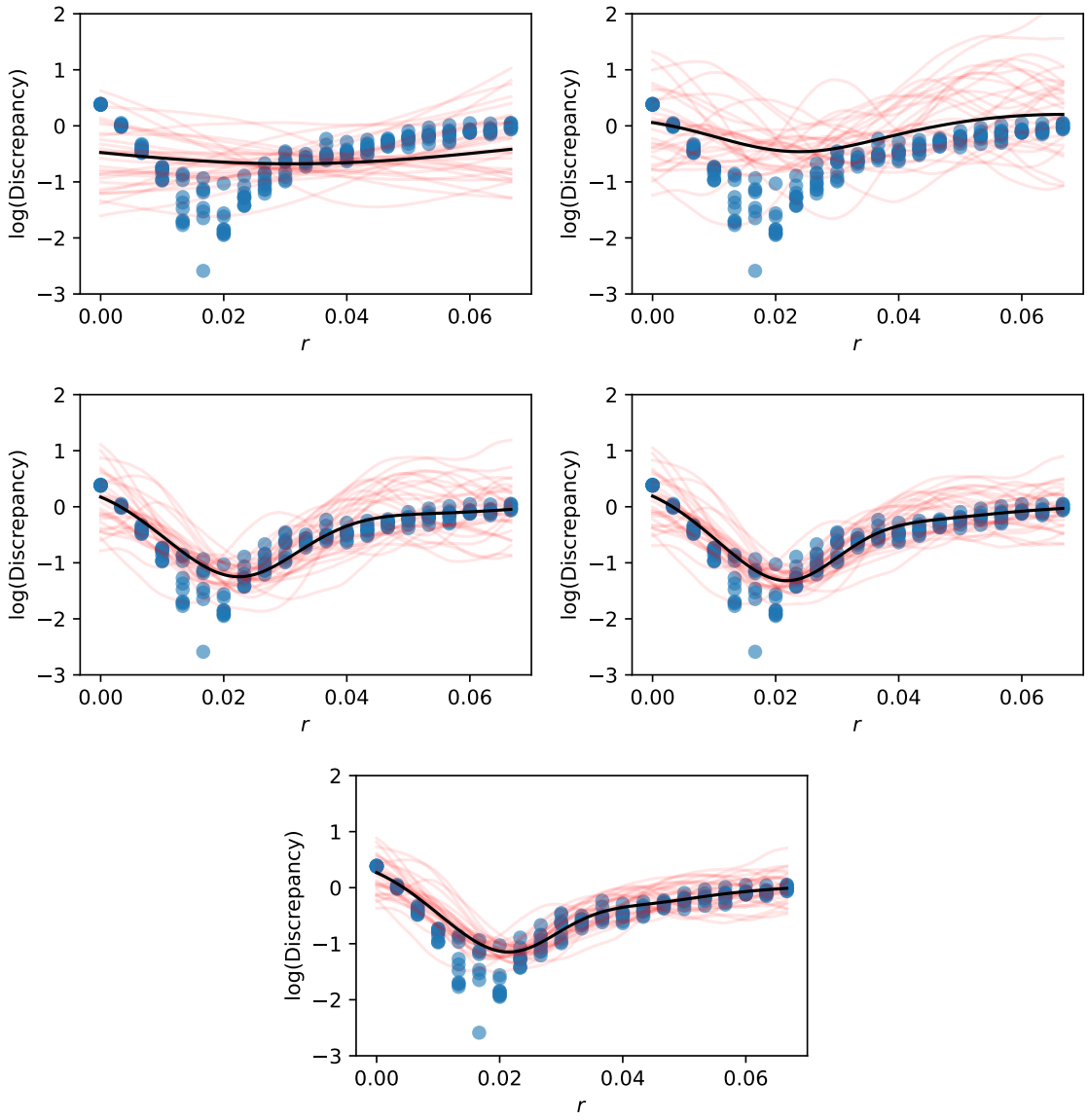

Figure B.6: $d^{(t)}_{\mathcal{GP}}(\boldsymbol{\theta})$ approximation of $\mathbb{E}(\ln \mathcal{D}(\boldsymbol{\theta}))$, for $t = 0$, 100, 200, 300, and 400. Only r was varied. All other parameters were fixed at the true values. Black line is $\mathbb{E}(d^{(i)}(\boldsymbol{\theta}))$. Blue dots are realisations from $\ln \mathcal{D}(\boldsymbol{\theta})$.